



Pilkington Library

Author/Filing Title CASWELL

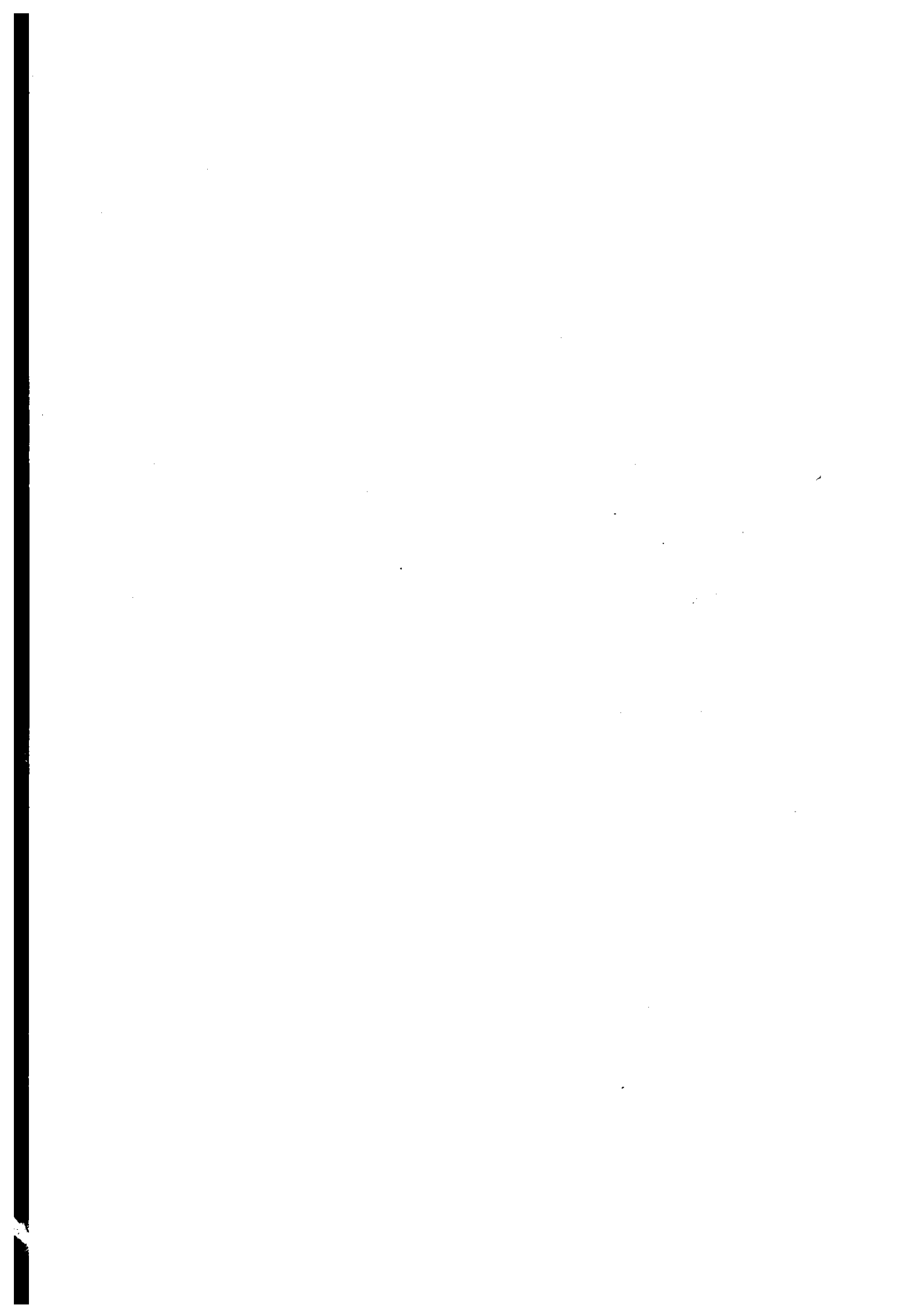
Vol. No. Class Mark T

**Please note that fines are charged on ALL
overdue items.**

FOR REFERENCE ONLY

0402508718





Thermal Welding of an Unstable Thermoplastic
Facilitated by a Diffusion-promoting Interlayer.

By

Andrew Caswell.


Supervisors: Dr Richard J. Heath, Dr. Ian Sutherland,

A Doctoral Thesis.

Submitted in partial fulfilment of the requirements for the award of Doctor of
Philosophy of Loughborough University.

September 2000.

Institute of Polymer Technology and Materials Engineering.

 Loughborough University Physical Library
Date Apr 02
Class
Acc No. 040250871

Acknowledgements

The author would like to thank Drs. Heath and Sutherland for their help and support throughout this research. Drs Friend and Bowman for their many discussions and the development section of Uponor Hilcote for their help and equipment. Thanks also go to Ray Owens and Dave Wilson, technical staff at the IPTME and department of Chemistry respectively, for assistance with the practical aspects of the project. I would also like to thank my colleagues in the IPTME and department of Chemistry, particularly Mark Simmons and Dr. Matthew Ward for many enlightening discussions. Thanks also to Claire Madden of the department of Chemistry for her help with the derivatisation and FTIR analysis.

Special thank to Nadège: je ne saurais assez vous remercier.

ABSTRACT

A study into the feasibility of thermal welding of an unstable thermoplastic has been undertaken. A heater wire embedded in a diffusion promoting interlayer has been used to accelerate interdiffusion between two poly(vinylchloride) (PVC) plaques. Interlayers consisted of a compatible vinyl resin and a plasticiser. Both normal resistance and an isothermal induction process were used as heat sources, with lap shear testing used to determine the strength of such systems. Vickers hardness testing has been used to ascertain the extent of diffusion and immersion diffusion testing was used to find the activation energy for the process. Micro thermal analysis (μ TA) in conjunction with laser induced mass analysis (LIMA), ultra-violet fluorescence microscopy and microscopic infrared techniques were used to study degradation. It has been found that the use of an interlayer allows thermal welding of PVC without deleterious degradation. The concentration and type of plasticiser was found critical in producing a strong weld. Low concentrations of plasticiser did not cause sufficient diffusion and high concentrations of plasticiser in the interlayer produced a weak interface; the optimum amount was dependent on the diffusion coefficient of the plasticiser. Fast fusing plasticisers resulted in higher lap shear strength because they cause a greater extent of diffusion during a constant welding time than slower fusing plasticisers. Degradation products were detected in proximity to the heater wire. Resistance heating was found to cause an exponential increase in degradation closer to the wire while isothermal heating produced a degradation profile with a plateau region next to the heater wire.

CONTENTS

CONTENTS	I
LIST OF FIGURES.....	VI
LIST OF GRAPHS.....	VIII
LIST OF MICROGRAPHS.....	X
LIST OF SYMBOLS.....	XI
1.0 INTRODUCTION	1
1.1 General Background.....	1
1.2 Objectives.....	2
2.0 LITERATURE REVIEW.....	3
2.1 Introduction.....	3
2.2 General	6
2.2.1 A Short History	6
2.2.2 Chemical Structure.....	6
2.2.3 Fusion of PVC Particles.....	7
2.2.4 Production of PVC.....	9
2.2.5 Processing of PVC Compounds.....	11
2.3 The Electrofusion Process.....	14
2.3.1 Electrofusion by Induction: The Smartheat Process.....	18
2.4 Adhesion.....	21
2.4.1 Theories of Adhesion.....	21
2.4.2 Thermodynamics of Adhesion.....	22
2.4.3 Thermodynamics of Wetting	23
2.4.4 Acid Base Interactions	28

2.5 Joining of Amorphous Polymers.....	30
2.5.1 Reptation.....	30
2.5.2 Healing.....	31
2.5.3 Welding.....	32
2.6 Plasticisation of PVC	35
2.6.1 Plasticisation Mechanism.....	35
2.6.2 Function of a Plasticiser.....	36
2.6.3 Types of Plasticisers	38
2.6.4 Anti-plasticisation.....	40
2.7 Degradation and Stabilisation of PVC	42
2.7.1 Degradation of PVC.....	42
2.7.2 Stabilisation of PVC	43
2.8 Test Methods.....	45
2.8.1 Mechanical Tests	45
2.8.2 Spectroscopic Techniques.....	48
2.8.3 Microscopic Techniques	53
3.0 EXPERIMENTAL.....	60
3.1 Introduction	60
3.2 Materials.....	62
3.3 Sample Preparation	64
3.3.1 Compression Moulding.....	64
3.3.2 Interlayer Preparation.....	67
3.4 Welding of Plaques	69
3.5 Lap Shear Testing.....	71
3.6 Optical Microscopy	72
3.7 Hardness Testing.....	73

3.7.1 Vickers Hardness.....	73
3.7.2 Shore A Hardness.....	75
3.8 Immersion Diffusion Testing.....	76
3.9 Atomic Force Microscopy.....	77
3.10 Laser Induced Mass Analysis.....	79
3.11 Ultra-violet Fluorescence Microscopy.....	80
3.12 Infrared Spectroscopy.....	81
3.12.1 Sample Preparation.....	81
3.12.2 Derivatisation.....	81
3.12.3 IR Analysis.....	83
4.0 RESULTS AND DISCUSSION.....	84
4.1 Introduction.....	84
4.2 Welding.....	86
4.3 Tensile Lap Shear Testing.....	89
4.3.1 GA6015.....	89
4.3.2 GA7701H.....	90
4.3.3 GA9028.....	92
4.3.4 Homopolymers.....	94
4.3.5 Lap Shear Strength of Isothermally Welded Specimens.....	96
4.4 Microscopy.....	98
4.4.1 Introduction.....	98
4.4.2 Resistance Heating.....	98
4.4.3 Induction Heating.....	102
4.4.3 Fracture Surfaces.....	104
4.5 Hardness Testing.....	107
4.5.1 Introduction.....	107
4.5.2 Vickers Hardness.....	107

4.5.3 Interlayer Hardness	112
4.6 Diffusion Testing.....	114
4.6.1 Introduction.....	114
4.6.2 Immersion Diffusion.....	114
4.6.3 Activation Energy of Diffusion	117
4.7 Atomic Force Microscopy.....	119
4.7.1 Introduction.....	119
4.7.2 Topography Scan	119
4.7.3 μ TA Scans.....	120
4.8 Laser Induced Mass Analysis.....	121
4.8.1 Introduction.....	121
4.8.2 LIMA Spectra	121
4.9 Ultraviolet Fluorescence Microscopy	124
4.10 Microscopic Infrared Spectroscopy.....	125
4.10.1 Introduction.....	125
4.10.2 Infrared Spectra.....	125
4.10.3 Degradation Profiles.	130
5.0 GENERAL DISCUSSION.....	133
5.1 Introduction	133
5.2 Interlayers.....	133
5.3 Welding	133
5.4 Lap Shear Testing.....	134
5.5 Hardness Testing	134
5.6 Diffusion Testing.....	135
5.7 Microscopy.....	136
5.8 Degradation Analysis	136

5.8.1 Atomic Force Microscopy and LIMA	136
5.8.2 Fluorescence Microscopy	137
5.8.3 Infrared Spectroscopy	137
5.9 Summary	138
6.0 CONCLUSIONS AND FURTHER WORK.....	140
6.1 Conclusions	140
6.2 Further Work.....	142
7.0 REFERENCES.	143
APPENDICES.....	151
Appendix 1 Detailed Interlayer Compositions.....	151
1.1 Copolymers	151
1.2 Homopolymers.....	152
Appendix 2 Infra-red Spectra Frequency-Structure Correlation Chart (after ¹⁵⁵)..	153
Appendix 3 Selected Lap Shear Data and Treatment of Results	154
3.1 Typical Force-Extension Plots.....	154
3.2 Lap Shear Data.....	155
Appendix 4	164
Research Papers Resulting from this Work	164

LIST OF FIGURES

Figure 2.1: Schematic of PVC grain structure.....	7
Figure 2.2: Schematic of typical DSC trace for uPVC.....	9
Figure 2.3: Schematic of electrofusion socket.....	14
Figure 2.4: Cold zones in electrofusion.....	15
Figure 2.5: The control box	16
Figure 2.6: Schematic profile of resistance wire heating	17
Figure 2.7: <i>Smartheat</i> wire	18
Figure 2.8: Self-regulation process in <i>Smartheat</i>	19
Figure 2.9: Time/temperature profile for <i>Smartheat</i> heating.	20
Figure 2.10: Diagram of liquid in contact with solid	24
Figure 2.11: Schematic of contact angle measurement methods.....	26
Figure 2.12: The single lap shear tensile test.....	46
Figure 2.13: Schematic of the FTIR spectrometer	52
Figure 2.14: Schematic of the optical microscope	54
Figure 2.15: Schematic of the TEM	55
Figure 2.16: Schematic of the SEM.....	56
Figure 2.17: Diagram of AFM operating principles.....	58
Figure 3.1: Compression moulding feedstock.....	64
Figure 3.2: Plaque after compression moulding.....	65
Figure 3.3: Schematic of compression moulding pressure cycle	66
Figure 3.4: Completed plaque	67
Figure 3.5: Schematic of heater jig.....	69
Figure 3.6: Assembly of component before welding	69
Figure 3.7: Lap shear testing schematic showing spacers	71

Figure 3.8: Diagram of Vickers hardness testing	73
Figure 3.9: Vickers hardness indentation track	74
Figure 3.9: The three types of indentation observed	75
Figure 3.10: Schematic of immersion diffusion test.....	76
Figure 3.11: Schematic of degradation profiling using UV fluorescence	80
Figure 3.12: Schematic of bromination sub-frame	82
Figure 4.1: Composite topography image	119

LIST OF GRAPHS

Graph 4.2.i: Resistance welding temperature profile	86
Graph 4.2.ii: <i>Smarteat</i> welding temperature profile.....	86
Graph 4.2.iii: <i>Smarteat</i> welding power consumption.....	87
Graph 4.3.1.i: GA6015H with Benzoflex 2088.....	89
Graph 4.3.1.ii: GA6015H with DOP	89
Graph 4.3.1.iii: GA6015H with Admex 523	90
Graph 4.3.2.i: GA7701H with Benzoflex 2088.....	90
Graph 4.3.2.ii: GA7701H with DOP	91
Graph 4.3.2.iii: GA7701H with Admex 523	91
Graph 4.3.3.i: GA9028 with Benzoflex 2088.....	92
Graph 4.3.3.ii: GA9028 with DOP.....	92
Graph 4.3.3.iii: GA9028 with Admex 523	93
Graph 4.3.4 i: A K57 Resin with Benzoflex 2088.....	94
Graph 4.3.4 ii: A K60 Resin with Benzoflex2088	94
Graph 4.3.4 iii: A K74 Resin with Benzoflex 2088	95
Graph 4.3.4.iv: A K80 Resin with Benzoflex 2088.....	95
Graph 4.3.5.i: Effect of welding time on lap shear strength.....	97
Graph 4.5.2.i: Hardness variation across interface at various welding times (sample 9/40B)	108
Graph 4.5.3.i: Shore A hardness of interlayers prepared with copolymer resins compared with average lap shear strength values.....	112
Graph 4.5.3.ii: Shore A hardness of interlayers prepared with homopolymer resins compared with average lap shear strength values.....	113
Graph 4.6.2.i: Mass uptake plots for all plasticisers into PVC at 50°C	114
Graph 4.6.2.ii: Mass uptake plots for all plasticisers into PVC at 60°C	115

Graph 4.6.2.iii: Mass uptake plots for all plasticisers into PVC at 70°C	115
Graph 4.6.2.iv: Mass uptake plots for all plasticisers into PVC at 80°C	116
Graph 4.6.3.i: Arrhenius plots for diffusion of plasticiser into PVC.....	117
Graph 4.7.3.i: μ TA results corresponding to marked points on Figure 4.1	120
Graph 4.8.2.i: Blue bulk positive spectrum	121
Graph 4.8.2.ii: Blue bulk negative spectrum	122
Graph 4.8.2.iii: Brown bulk positive spectrum	122
Graph 4.8.2.3.iv: Brown bulk negative spectrum.....	123
Graph 4.8.2.v: Edge positive spectrum.....	123
Graph 4.8.2.vi: Edge negative spectrum.....	124
Graph 4.10.2.i: Bulk PVC pre-bromination, control spectrum	125
Graph 4.10.2.ii: Bulk PVC post-bromination, control spectrum.....	126
Graph 4.10.2.iii: Spectrum taken next to heater wire	126
Graph 4.10.2.iv: Spectrum taken 0.09mm from heater wire	127
Graph 4.10.2.v: Spectrum taken 0.18mm from heater wire	127
Graph 4.10.2.vi: Spectrum taken 0.27mm from heater wire	128
Graph 4.10.2.vii: Spectrum taken 0.36mm from heater wire	128
Graph 4.10.2.viii: Spectrum taken 0.45mm from heater wire	129
Graph 4.10.2.ix: Spectrum taken 0.54mm from heater wire	129
Graph 4.10.2.x: Spectrum taken 0.63mm from heater wire	130
Graph 4.10.3.i: Profile of degradation around resistance heated samples (bromine peak).....	131
Graph 4.10.3.ii: Profile of degradation around isothermally heated wire (bromine peak).....	131

LIST OF MICROGRAPHS

Micrograph 4.4.2.i: Section of welded sample. (10x).....	98
Micrograph 4.4.2.ii: Stressed region around the heater wire. (10x).....	99
Micrograph 4.4.2.iii: 30 seconds heating time. (20x).....	99
Micrograph 4.4.2.iv: 50 seconds heating time. (20x).....	100
Micrograph 4.4.2.v: 70 seconds heating time. (20x).....	100
Micrograph 4.4.2.vi: 90 seconds heating time. (20x).....	101
Micrograph 4.4.2.vii: 110 seconds heating time. (20x).....	101
Micrograph 4.4.2.viii: 120 seconds heating time. (20x).....	101
Micrograph 4.4.3.i: 90 seconds heating time. (20x).....	102
Micrograph 4.4.3.ii: 110 seconds heating time. (20x).....	103
Micrograph 4.4.3.iii: 120 seconds heating time. (20x).....	103
Micrograph 4.4.3.iv: 180 seconds heating time. (20x).....	104
Micrograph 4.4.4.i: Fracture through plaque. (30x).....	104
Micrograph 4.4.4.ii: Fracture along interface (10x).....	105
Micrograph 4.4.4.iii: Yielding between wires. (100x).....	106
Micrograph 4.4.4.iv: Yielding next to wires. (40x).....	106

LIST OF SYMBOLS

Symbol	Definition	Units
A_S	Actual surface area	m^2
b	Constant	
D	Diffusion Coefficient	$Cm^2 s^{-1}$
d	Sampling depth	m
$d_{p,h}$	Dispersion, polar and H-bond components of intermolecular force	
E	Scattered ion energy	eV
E_B	Binding energy	eV
E_D	Activation energy for diffusion	$J mol^{-1}$
E_K	Kinetic energy	J
E_0	Scattering ion energy	eV
Δf	Depth of field	m
ΔG_{SL}	Reversible free energy change	$J m^{-2}$
H_γ	Incident X-ray energy	eV
m	magnification	
M_1	Scattered ion mass	g
M_2	Scattering ion mass	g
M_e	Equilibrium mass	g
n	Refractive index	
T	Temperature	$K/^\circ C$
T_m	Melting temperature	$K/^\circ C$

W_A	Thermodynamic work of adhesion	J
x	Thickness	m

Greek

γ_c	Critical surface tension of wetting	$J m^{-2}$
γ_{LV}	Surface tension or surface free energy of liquid in equilibrium with vapour	$J m^{-2}$
γ_s	Surface free energy of solid in vacuum	$J m^{-2}$
γ_{SL}	Interfacial free energy of liquid in equilibrium with solid	$J m^{-2}$
γ_{SV}	Surface free energy of solid	$J m^{-2}$
θ	Contact angle or angle of incidence	°
π_e	Spreading pressure	$N m^{-2}$
λ	Wavelength	m
ϕ	Sample work function	eV
φ	Interaction parameter	

1.0 INTRODUCTION

1.1 General Background

Plastic pipes find many uses: gas and water distribution pipes, sewage and drainage systems, ducting, under-floor heating, and many others. Perhaps the most demanding application is that of pressure pipes, including the important applications of potable water and gas distribution mains. These pipes may be in service for over 50 years and under pressure for all of this time. Recently, media pressure and mandates from watchdogs such as *Ofwat* have given the impetus to the pipe industry to provide pipe systems that are leak free. It is rare for the pipe itself to leak and although there are documented cases and probably many more undocumented, these faults can, in the majority of instances, be attributed to poor installation or factors beyond the control of the pipe manufacturer. The only real source of leaks in practice is therefore the joint connecting two sections of pipe together.

Nowadays, plastic pipes are largely produced from two materials; polyethylene (PE) and poly(vinylchloride) (PVC). While these two materials compete commercially for the same market, they each have very different characteristics. PE is a flexible material, which enables huge lengths to be coiled then unwound on installation, eliminating the need for many joints. For larger diameters that cannot be coiled, PE can be joined thermally, usually by a process known as electrofusion, producing a proven, leak-free joint.

PVC on the other hand, has superior mechanical properties to PE and when orientation is induced, these properties are further enhanced. However, at present there is no method of joining PVC pipes cohesively. The current joining method involves push fitting standard lengths of pipe together, utilising a circular rubber seal between the two pipe ends, which are shaped to fit over one another. Joints made by this method are fragile and cannot bear end loads that are often experienced in complex systems. It was not possible to join PVC pipes by standard electrofusion; PVC is thermally unstable, degrading by an autocatalytic process. There is no upper temperature control with electrofusion, rather the control is by heating time; the temperature of the heater wire increases erratically with time.

Recently, a new variation on the electrofusion theme has become available, incorporating a self-regulating wire, known as *Smarteat*. Essentially this process is capable of joining pipes *isothermally* or at a constant temperature. It is possible to control the wire temperature within a few degrees centigrade. With this precise control, the possibility of joining PVC pipe, with the same integrity as an electrofused PE pipe, is anticipated.

1.2 Objectives

The primary objective was to determine the feasibility of thermally welding two uPVC substrates. This was to be achieved using the isothermal process known as *Smarteat*, which has been used to successfully weld PE pipes. Due to the risk of overheating, it was necessary to embed the wire in a material that will conduct heat away from the wire and into the PVC. This work hoped to provide an interlayer that would do this and also aid in the welding process.

Since it was anticipated that the welding mechanism would be interdiffusion, further objectives were related to this phenomenon and the use of interlayers;

1. To devise a method by which interlayers may be used, according to a set of assessment criteria.
2. To identify the best component parts of the interlayer, from a range of resins and plasticisers.
3. To optimise the quantities of these component parts.

In order to meet these objectives it was necessary to identify or develop a range of physical and mechanical tests which rank the interlayer components in terms of their generic properties and the final strength of the welded component.

Due to the unstable nature of PVC, an important objective was to devise a test method in order to measure, at the very least in a qualitative sense, the amount of degradation produced by the welding process.

2.0 LITERATURE REVIEW

2.1 Introduction

A polymer is defined as a “compound whose molecule is formed from a number of repeated units of one or more compounds of low molecular weight¹.” This definition can be broken down further into sub-groups of thermosetting, including elastomers, and thermoplastic materials. The properties of thermoplastics are dependent on ambient temperature, and these polymers become molten at elevated temperatures. Thermosets, on the other hand, show no such changes and do not become reversibly fluid at elevated temperatures. To classify further still, those thermoplastics which contain significant crystalline structure and exhibit a defined melting point (T_m) can be termed semi-crystalline. There are those thermoplastics that soften over a temperature range, corresponding to a gradual (relative to crystalline polymers) reduction in viscosity. These thermoplastics are predominantly amorphous in structure, exhibiting no significant long-range order. As such, at room temperature, these polymers are super-cooled fluids but are treated as solids.

The properties of amorphous and semi-crystalline thermoplastics are often very different, and governed by different phenomena. For example, an understanding of how amorphous polymers inter-diffuse may not necessarily lead to a similar understanding of semi-crystalline materials. It is for this reason that only those theories and hypotheses relevant to amorphous materials are covered in this review. This is because the material used in this research programme, poly(vinyl chloride), (PVC), is generally considered an amorphous thermoplastic.

A general background and brief history of PVC technology is given. Different vinylchloride polymerisation methods are discussed as these routes can give rise to different properties in resulting products. As this thesis is concerned with the joining of PVC pipes, a description of production processes (e.g. extrusion and injection moulding) is included. Specific production methods utilised in the course of experimentation are also covered.

The process of joining PVC by an electromagnetic induction process is analogous to electrofusion as used extensively in joining semi-crystalline polyethylene (PE) pipe systems. By studying the specific stages of strength formation in welding PE

systems, it is thought that important insights may be gained. Although it is not in the remit of this thesis to propose a specific method by which PVC pipe systems may be joined by induction technology, the study of a comparable method is valuable.

It is possible to form a joint between two thermoplastic components by any one of a number of methods. A number of theories of adhesion are reviewed below, including at least one negative theory. Issues more specific to polymers are also reviewed, including important associated thermodynamic considerations.

Once compatibility of the adherends is established, the mechanisms of movement of mass across an interface formed between two surfaces must be considered. This is done in terms of diffusion by the reptation process. Reptation is the mechanism by which crack or joint healing occurs and healing is just one stage in the welding process. All stages are considered but as diffusion is the relevant mechanism of strength development, it is given a separate section, as is healing.

The plasticisation of PVC plays an important role in increasing chain mobility and is considered in the context of this work to assist the adhesion/diffusion process. A mechanism of plasticisation is presented, along with a description of the main types of plasticisers and the specific properties that may be imparted by using a particular plasticiser. Anti-plasticisation is also considered, although due to the fractal nature of a diffusion front, it was not expected to be observed in practice in this research.

PVC is a comparatively unstable material at elevated temperatures and consideration is given to the mechanisms and chemical reactions occurring during thermal degradation. Stabilisation is covered in an empirical sense, the myriad of commercial stabilisers and their complex nature mean a detailed review is of limited value within the scope of this thesis since there is no scope for alteration of additives. Thermal degradation products can be identified by spectroscopic and microscopic methods; some of these techniques are reviewed here. Not all methods have been used but are included for comparative purposes.

The resulting mechanical strength of joints (in this research in the form of plaques or coupons) is the single most important determinant of success: permanence of the bond is also important. Due to the brittle nature of unplasticised PVC (uPVC), it was decided to use the single lap shear tensile test to assess this. The relatively brittle properties of uPVC mean that peel or cleavage tests may not be used, despite their

desirable nature. When PVC is plasticised above a certain concentration, it becomes softer, with associated lowering of the glass transition temperature (T_g). Perhaps unusually for polymer characterisation, Vickers hardness was used to determine the extent of diffusion in a welded article; i.e. profiling across the weld boundary. This approach is covered in depth.

2.2 General

2.2.1 A Short History

Kaufman has presented an excellent review of early history and development of PVC^{2,3}.

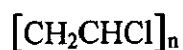
The development of what would eventually become PVC was begun in 1835 by Regnault, although it would be over a hundred years later that commercial production began in the UK⁴. In 1942 to 43, ICI successfully mass-produced PVC polymers, although some important breakthroughs in PVC technology were made before this time.

Methods of internal plasticisation were used to make the PVC resins processable below their degradation temperature, rather than to effect a change in properties. This was done in the 1930s by workers at B.F. Goodrich and this was the first genuine attempt to alter the mechanical properties of PVC. Organosols were also developed during this period.

During World War Two, an acute shortage of natural rubber led to a flurry of development on PVC as a viable substitute⁵. Equipment designed to process rubber was initially used but this was quickly modified to operate at the higher temperatures required for PVC. After the war, many companies reverted back to producing rubber once more, but enough stayed with PVC to form a burgeoning industry that is still very much active today.

2.2.2 Chemical Structure

The repeat unit of PVC is:



The units in the polymer chain are usually linked head-to-tail. The number of repeat units of a commercial resin varies from 500 to 1500, corresponding to a molecular weight of 31,000 to 94,000. Commercially, the molecular weight of the polymer is indirectly indicated by the K-value. There are different ways to calculate the K value but the method in common usage is the Fikentscher⁶ method. K-values from 50 to 80 cover the range of most commercial resins although polymers are produced outside this range for special purposes. The molecular weight distribution of commercial

resins is typically between 2 and 2.5, determined by gel permeation chromatography (GPC).

PVC polymers are essentially amorphous although about 8 to 10% crystallinity is present in the form of small crystallites⁷. The glass transition temperature of PVC lies in the range 80 to 85°C, with a T_m value near 285°C, approximately 100°C above the normal melt processing temperature.

2.2.3 Fusion of PVC Particles

The morphology of PVC depends on its method of production; suspension grades tend to be highly porous yet structured, while mass polymerised material has a more open and sponge-like structure⁶. Suspension grades are used in the production of PVC pipes. The structure of PVC suspension particles was described by Gilbert et al as showing structure at a variety of levels of scale^{7,8}, as shown in Figure 2.1. This was based on the findings of previous studies into the morphology of such materials⁹⁻¹¹.

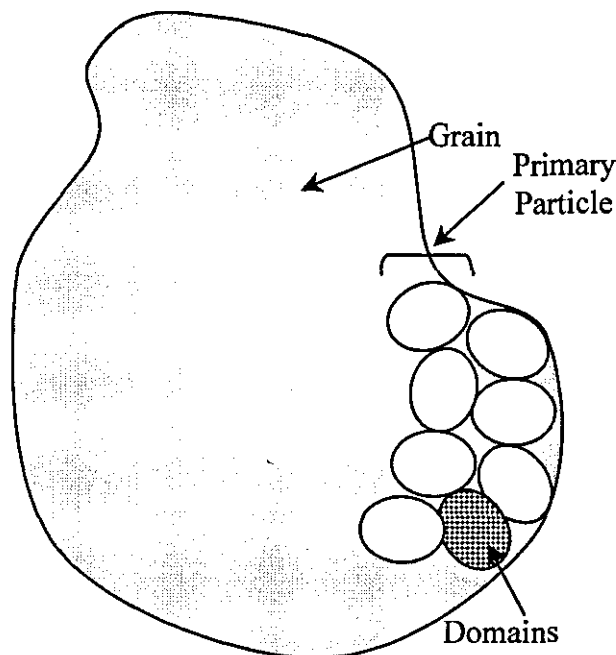


Figure 2.1: Schematic of PVC grain structure

On the largest scale exists the grain, about 100µm in diameter, visible by the naked eye and possessing a colloidal skin⁶. Each grain is made up of many primary particles approximately 1µm in diameter. It is the loose packing of these grains that leads to the porous structure. On a finer level of scale still, the primary particle is an assembly

of particles 10-30nm in size, known as domains. It is believed that the crystalline portion of PVC is located in the centre of these domains.

Fusing of PVC, or the breakdown of the initial structure and subsequent formation of a new structure, is essential in gaining optimum mechanical properties of a finished product. Allsopp conducted screw-pulling experiments in order to propose a mechanism for fusion, sometimes referred to as gelation¹². Screw-pulling describes the process of working a PVC resin in an extruder, then stopping the machine and removing the screw intact with the processed material. Due to the time taken for the material to move along the barrel, the material shows the effect of different process times. His conclusions were that fusion is dependent on four main variables; pressure, temperature, shear and residence time. He went further to propose a mechanism for fusion, and that as PVC travelled through the extruder:

The grains were compacted, reducing intergranular free volume.

Grain densification occurred and reduced the intragranular free volume.

Fusion within and between the grains occurred as a result of continued heat, shear and pressure.

The fusion of primary particles was found to be highly dependent on both shear and thermal history. It may have occurred before or after the loss of grain boundaries.

The fusion of the grains was dependent on the processing history and was believed to be influenced by the distribution of additives.

With continuing shear the fused material was elongated and eventually the grain boundaries disappeared.

Gilbert and co workers¹³ refined and extended this model where, by processing, the original particle structure is changed into a network of entanglements of primary and secondary crystallinity. The primary and secondary crystallinity comes from the melting and re-crystallisation of low and high melting temperature crystallites present in the original PVC powder. The relative levels of primary and secondary crystallinity are dependent upon the temperature to which the material was taken at extrusion. On cooling, secondary crystallinity is created. Molecules lying across old

grain boundaries intermix and become bonded by secondary crystallites, eliminating the grain boundaries and producing a fused structure.

Subsequent heating of PVC causes changes in the structure, which may be detected with a DSC test¹³, a schematic of a typical trace is shown in Figure 2.2, below.

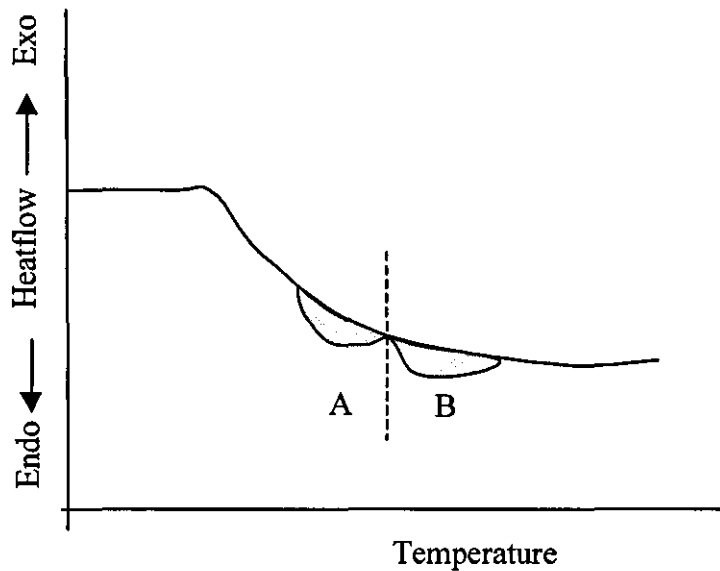


Figure 2.2: Schematic of typical DSC trace for uPVC

At temperatures above 160°C, primary crystallinity present within the domains is destroyed, followed by the development of less ordered regions (A in Figure 2.2). Higher melting point crystallinity (B) is annealed, resulting in a higher melting point. At higher processing temperatures, the B endotherm is gradually replaced by the secondary crystallinity, thus the B onset temperature correlates to the maximum temperature seen by the material.

2.2.4 Production of PVC

The polymerisation of monochloroethene (or vinylchloride) (VC)



is possible by three main methods known as suspension, mass or bulk and emulsion polymerisation. Suspension polymerisation accounts for approximately 80% of PVC production, while the remainder is split more or less equally between the other two processes.

In suspension polymerisation, a dispersion of monomer droplets in water is produced by vigorous stirring. The droplets contain a soluble initiator, which is reacted with the

monomer at 40 to 75°C in a sealed autoclave. As this reaction is exothermic, the reaction vessel should be cooled with chilled water. The polymerisation process is allowed to continue until 75 to 95% of the monomer is consumed, when it is stopped by venting off the bulk of the remaining monomer. Any residual monomer is then removed by steam assisted evaporation. The resulting polymer/water slurry is centrifuged and dried with hot air to remove the water.

Mass or bulk polymerisation uses pressure to condense and liquify the monomer, which, with the addition of an initiator and temperatures in the range of 40 to 70°C, precipitates solid PVC. To ensure uniformity of the precipitate, strong, turbine-type agitation is employed. At 10% conversion the mixture is transferred into a second reaction vessel since the level of polymer which has formed inhibits effective stirring. In the second vessel, polymerisation continues as the powder phase forms under gentle stirring. At 20% conversion, the material resembles a damp powder and at 40% a dry powder. The reaction is stopped at 80% conversion by the venting of the unreacted monomer. Steam-assisted degassing is used to remove any remaining monomer.

Emulsion polymerisation uses water borne emulsifiers and agitation to produce a fine emulsion of monomer in the water. A water-soluble initiator is normally used to produce free radicals that chemically react with monomer at its boundary with the aqueous phase. The polymer particles grow steadily in size throughout the polymerisation process, although sometimes requiring the addition of emulsifier to remain stable. As before, the reaction is stopped by venting remaining monomer at approximately 90% conversion. Removal of residual monomer is more difficult due to the physical form (irregular agglomerates) but is achieved through spray drying. Seeding an emulsion system makes it possible to control the particle size. By introducing a PVC latex into the system, it is possible to provide sites for polymerisation to initiate. The seeded particles grow and prevent the formation of entirely new (and much smaller) particles, as in unseeded emulsion polymerisation. Particle size is between 0.1 to 3µm for seeded emulsion polymerisation compared with 0.01 to 0.2µm for ordinary unseeded emulsion polymers.

Suspension resins are used to produce compounds intended for extrusion or moulding while emulsion polymers are used in pastes. Due to their purity and high clarity, mass polymerised resins are suitable for the blow moulding of bottles¹⁴.

2.2.5 Processing of PVC Compounds

Only the manufacturing processes relevant to this research project are covered here, i.e. extrusion, compression moulding, and injection moulding. An in-depth review of most methods of PVC processing is given elsewhere⁴.

i) Extrusion

Extrusion is the most important method of PVC processing, although standard extrusion technology has to be modified for PVC materials because of some specific problems in processing them¹⁵. This is due to a combination of their high melt viscosity and thermal degradation. The hydrogen chloride produced by the degradation of PVC will readily corrode and damage the metal components of an extruder.

Two-stage, single-screw, long-barrel, vented extruders dominate pipe production. As an alternative a non-vented extruder with a compression relief screw and a vacuum hopper can be used, although a vacuum hopper is only effective at very low moisture levels in the resin.

The residence time of the polymer in the extruder is also of the utmost importance. In earlier extruders, short barrel extruders were used with an increased screw speed but it was found that the PVC particles did not fuse well. To overcome this, longer barrel designs were introduced and hence the residence time was increased, leading to an increase in the thermal history of the PVC, particularly in pelletised feedstocks. However, the use of longer barrels allows complete fusion and development of mechanical properties in the material at less severe temperature and pressure profiles. The presence of double flighted screws in the first stage of a two-stage machine allows higher outputs and improved extrusion stability. The effect of the double flight is to efficiently transfer heat to the material from the barrel heaters¹⁶.

ii) Compression Moulding

Compression moulding is one of the simplest methods used to shape polymer products, one common application being the production of single and long play recording discs¹⁷ from vinyl copolymer, although the process itself is of limited commercial importance for thermoplastics. Simply, the process involves the compressing an amount of pre-compounded material to produce a finished article. Pre-compounding is conducted by means of a two-roll mill and can be performed on dry blended, pre-mixed or pellet materials. The press should be capable of maintaining a uniform temperature of at least 200°C and ideally have mould cooling facility to allow for a cooling cycle. It may be necessary to utilise a parting sheet to prevent sticking of the PVC to the mould.

iii) Injection Moulding

Injection moulding of PVC is one of the most important melt processes for PVC. Although the method of injection moulding PVC differs little to that of other thermoplastics, the polymers thermal instability and high viscosity complicate matters. These problems are not insurmountable and with proper process control, injection moulding is easily achieved; computer control has allowed further refinement of the process.

Injection moulding can be described in five stages: addition of material to the barrel; melting of the compound by mechanical and thermal effects; injection of the melt into the mould; cooling the mould and its contents and finally removing the moulded product. The melting and injection steps are critical, as it is here that the majority of thermal damage can occur in PVC materials. It was in an effort to overcome difficulties with PVC during these stages that have led to the development of injection moulding machines specific to PVC. In general the features of a PVC injection moulder are:

- Excellent internal streamlining.
- Low compression ratio.
- Short and wide flow route (gates, tapers, nozzles)
- Excellent corrosion protection or all internal metal parts.

In other respects, a PVC injection moulder is similar to other machines. Ganzeman reviews process control and gives some important considerations in injection moulding of PVC¹⁸.

2.3 The Electrofusion Process

PVC potable water pipes are currently joined by a “push-fit” method. In the examination of alternative methods used to join other pipe materials, important lessons may be learned.

The electrofusion process is used to join many of polyethylene pipe systems in use today. An excellent review of the electrofusion joining process can be found in Reference 19.

As the performance of the jointed pipe system depends on the integrity and performance of the joint, an understanding of how strength develops is essential. In electrofusion, the joint is produced by fusing the pipe to a coupler using resistance wires that are wrapped continuously around the inside diameter of the coupler, embedded in the material as shown in Figure 2.1. The wire is heated by passing an electrical current through it for a given length of time, heating the surrounding material above its melting temperature. The pool of molten material formed is constrained by “cold zones” at the middle and ends of the socket, as shown in Figure 2.2.

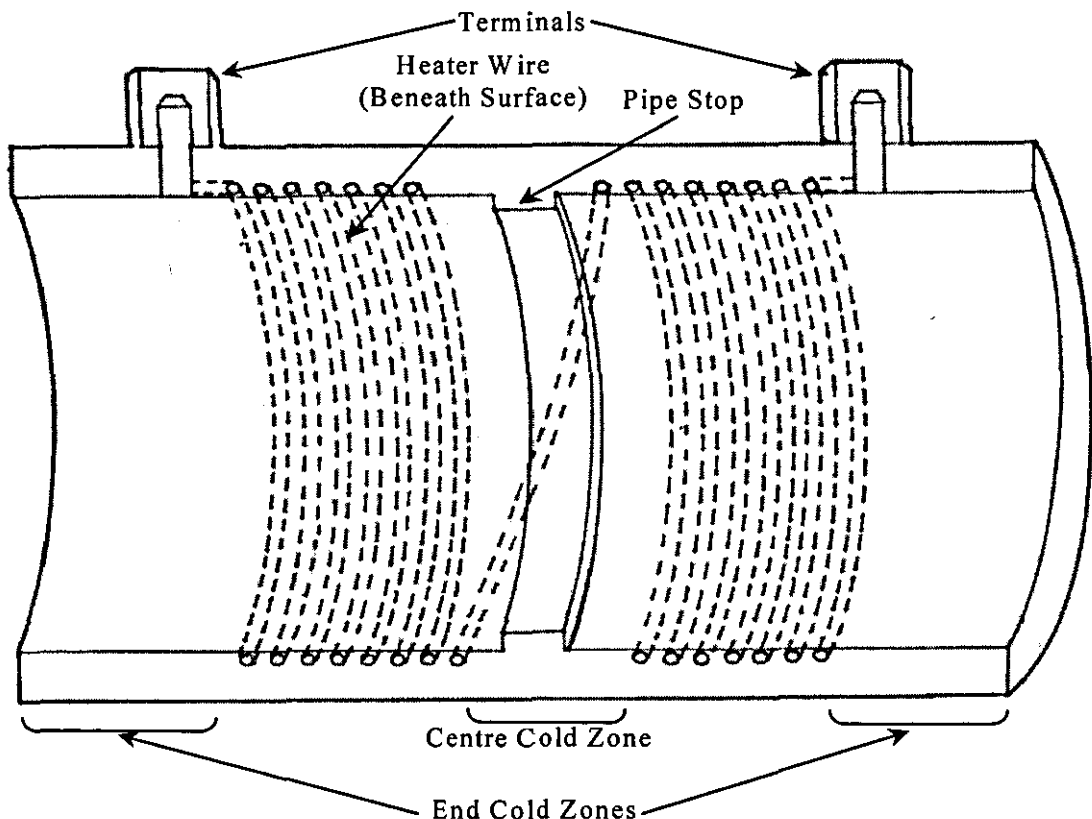


Figure 2.3: Schematic of electrofusion socket

The effect of the cold zones is to block the flow of molten material, preventing exusion of the melt pool from the coupler and allowing melt pressure to build up. These are key to obtaining a strong joint.

The resulting integrity of the joint can be assessed by a peel test. Typically, samples are cut from the joined pipe and the coupler is peeled away from the pipe on a tensometer. The ideal mode of failure is through the plane of the wires rather than the interface, with gross yielding of the surrounding material. In a poor joint, the failure will be along the pipe/coupler interface, (indicating that an interface is present).

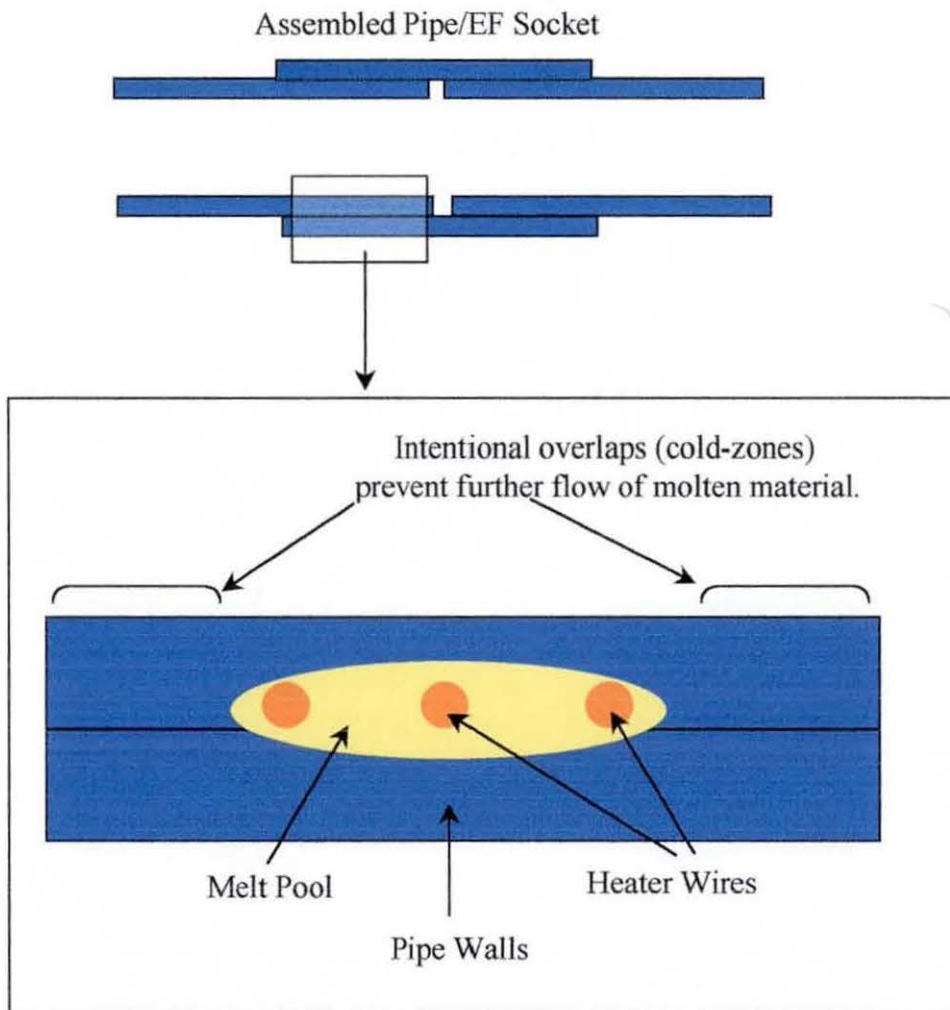


Figure 2.4: Cold zones in electrofusion

The energy to melt the polymer is supplied in the form of electrical energy, regulated in terms of current, voltage and time by a control box. Power is supplied to the control box from an external source, usually a generator. The control box is necessary

as any variation in power supplied to the fitting may result in an unsatisfactory joint. See Figure 2.3.

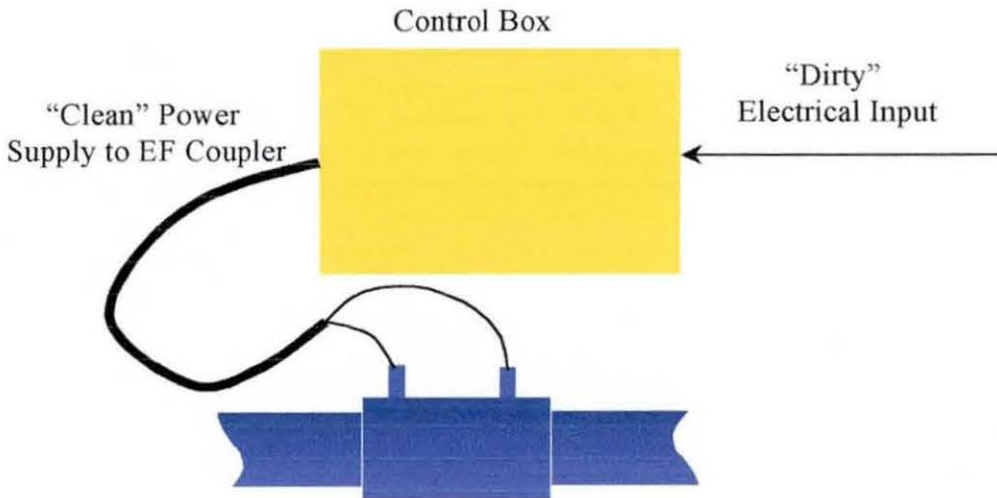


Figure 2.5: The control box

The development of strength during the electrofusion occurs in the following stages:

- incubation period
- joint formation and consolidation
- plateau region
- (degradation period)
- cooling period.

The degradation period is not part of the electrofusion process and is normally avoided, although it will occur if the fusion time exceeds an optimum.

During the incubation period, the expanding molten material in the coupler fills any gap between pipe and coupler, leading to a formation of a melt pool. The transfer of heat to the pipe causes material on the outer wall of the pipe to become molten leading to an increase in the size of the melt pool.

The joint formation and consolidation stage sees the build up of melt pressure. During this stage evidence of a joint forms and joint strength develops to an observable level. As this stage continues, melt pressure, interface temperature and joint strength increase. The cold zones prevent the flow of material that would lead to an decrease in melt pressure.

During the plateau region, it has been found that there is no increase in joint strength with increasing fusion times. The purpose of the plateau region is to allow for variables that may effect joint strength to be accommodated, for example, the pipe/coupler gap and ambient temperature. Both these factors call for different fusion times. In the plateau phase, interdiffusion of polymer molecules is responsible for the development of strength at the joint. At the end of the phase, the power is switched off allowing the joint to cool and solidify, and in the case of PE, crystallise. This is known as the cooling period. With PE, the space that was once the gap between the pipe and coupler is manifested as an increase in the inner diameter of the pipe and sometimes as voids inside the joint caused by contraction of the recrystallised polyethylene.

The temperature profiles within the coupler are influenced by a number of factors, the most noticeable being the gap between the pipe and the coupler. In practice, minimum and maximum gaps are specified in the form of pipe and coupler manufacturing tolerances, and the temperature at the pipe can be up to 70°C hotter than the coupler for a minimum gap compared to a maximum gap. The wire itself increases in temperature non-uniformly until the power is cut off. Most thermoplastics are poor thermal conductors which leads to the build up of steep thermal gradients around the wire.

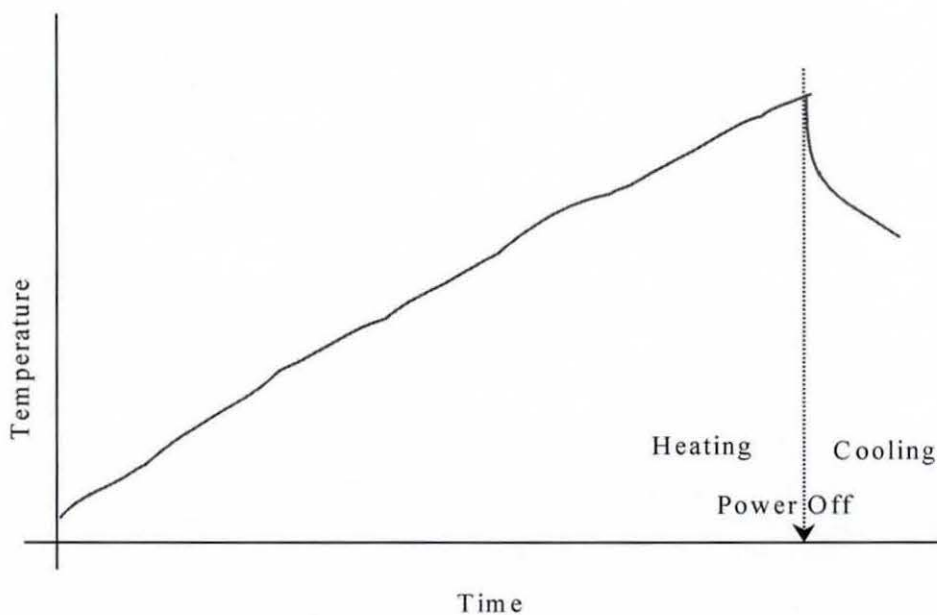


Figure 2.6: Schematic profile of resistance wire heating

For this reason, the fusion time must be carefully considered. Each coupler size and type has an optimum fusion time assigned to it determined from plots of joint strength versus fusion time. If the heating time exceeds the plateau region, the temperature of the wire continues to rise, leading to undesirable degradation, and subsequent weakening of the joint, (Figure 4). Fusion times that are too short can result in insufficient interdiffusion and hence poor joint strength.

2.3.1 *Electrofusion by Induction: The Smartheat Process*

As mentioned above, while conventional electrofusion is a very important and widely used commercial technique, it does have certain limitations. The most important of these is a limited and poor indirect control of rate and uniformity of temperature increase and hence maximum temperature. A recent innovation seeks to overcome this poor temperature control by using electromagnetic induction to heat the wire.

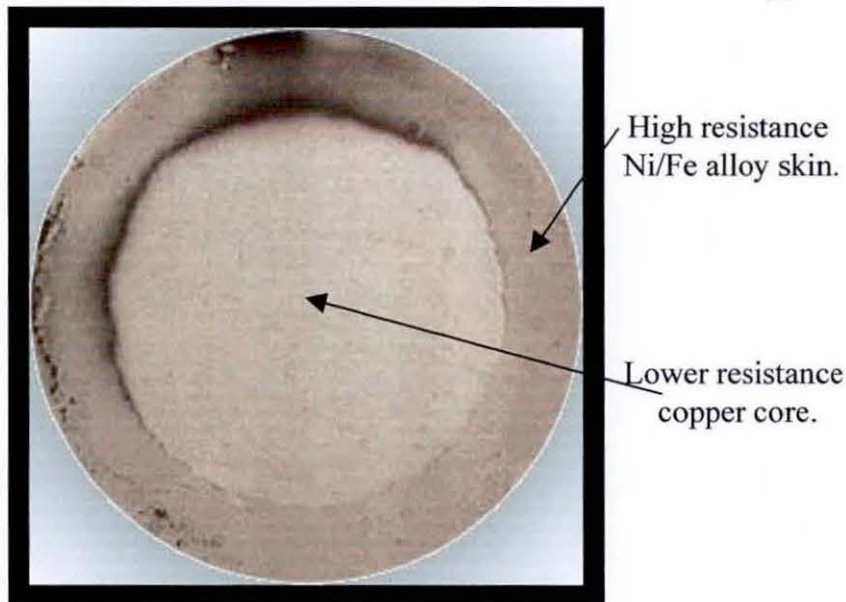


Figure 2.7: *Smartheat* wire

Originally developed as a novel, directly heated food grill²⁰, the so-called *Smartheat* process uses electromagnetic induction technology, using a novel self-regulating wire. The heater takes the form of a cage of an evenly spaced wire coil with cross-pieces in place of the continuous wire found in standard electrofusion (there is one cage for each pipe end). However, the cage does not have a physical connection to the power source; energy is supplied in the form of a continuously changing magnetic field²¹. Despite the huge commercial potential of this technique, it had not been developed

until Metcal Corporation introduced composite, temperature regulated wires and conducted field trials²².

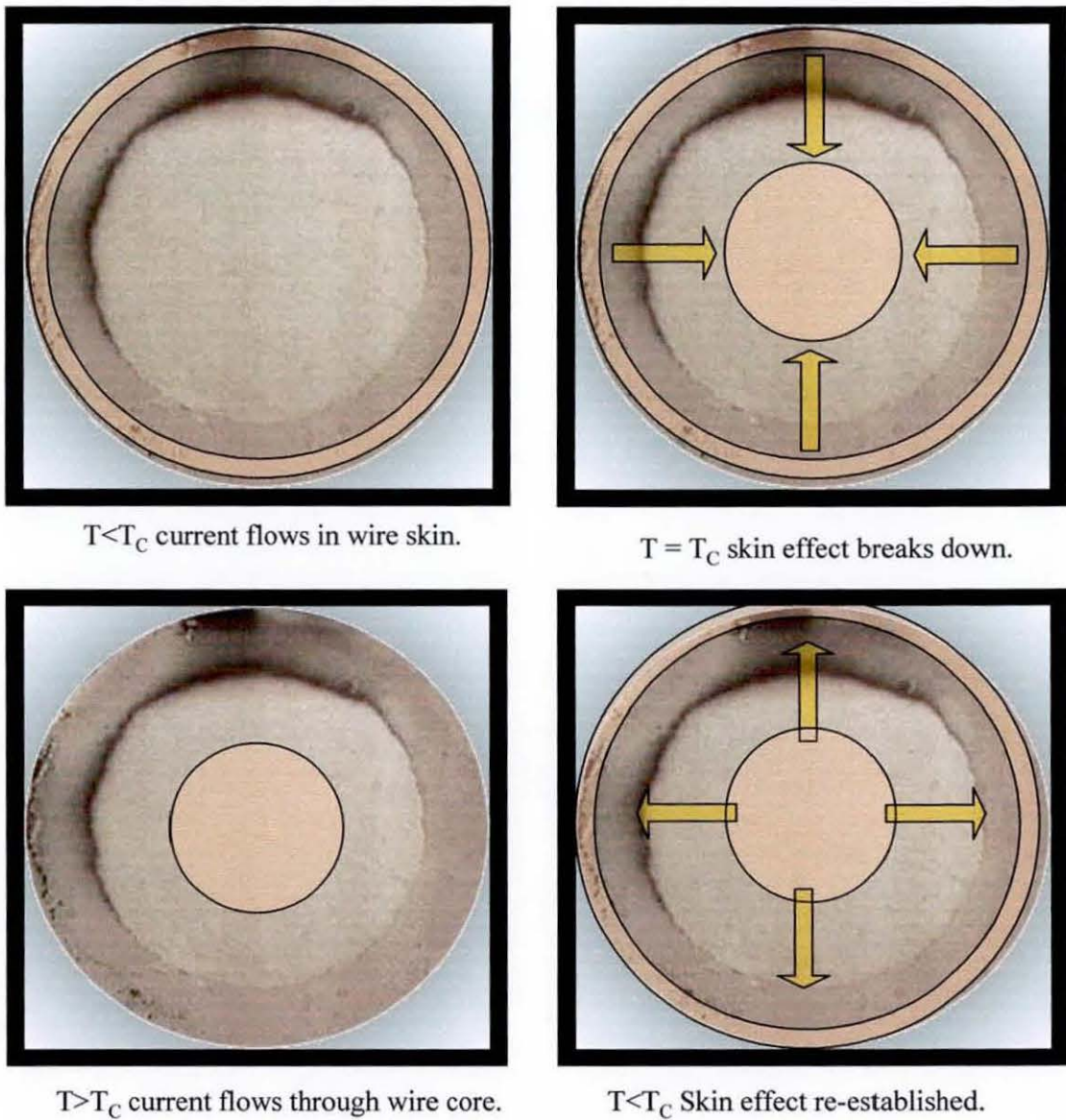


Figure 2.8: Self-regulation process in *Smartheat*

The power is transmitted in the form of a magnetic field, which, on application to the heater cage, causes a rapidly switching current to be set up. Due to electrical resistance of the metal, a temperature rise is seen. The induction wire is not a standard resistance wire; it is a composite of two very different metals. The outer skin consists of a ferrous alloy while the core is low resistance copper as shown in figure 2.5.

As the regulation process is controlled by the composition of the outer component of the wire, no thermocouples or power controls are necessary. This leads to a self-contained process with temperature control of $\pm 1^\circ\text{C}$ routinely possible²³, as shown in Figure 2.7.

On initial application, the magnetic field causes a current to flow in the cage. Due to the skin effect, current flows only in the outer layers of the wire, generating heat. The surface layers, composed of a specific ferrous alloy, exhibit a unique Curie temperature. On reaching its Curie temperature, the resistance of the outer skin increases rapidly, forcing the current to flow again through the core of the wire. In this case, the copper core has low electrical resistance and heating is effectively halted. With the heating all but stopped, the whole wire cools until it drops below its Curie temperature and current is then able to flow through the skin, causing heat to be generated. This process of heating/cooling continues until the power source is switched off. (See Figure 2.6). One of the aims of this research was to establish methods of applying this technology to PVC pipes, and to understand the effects.

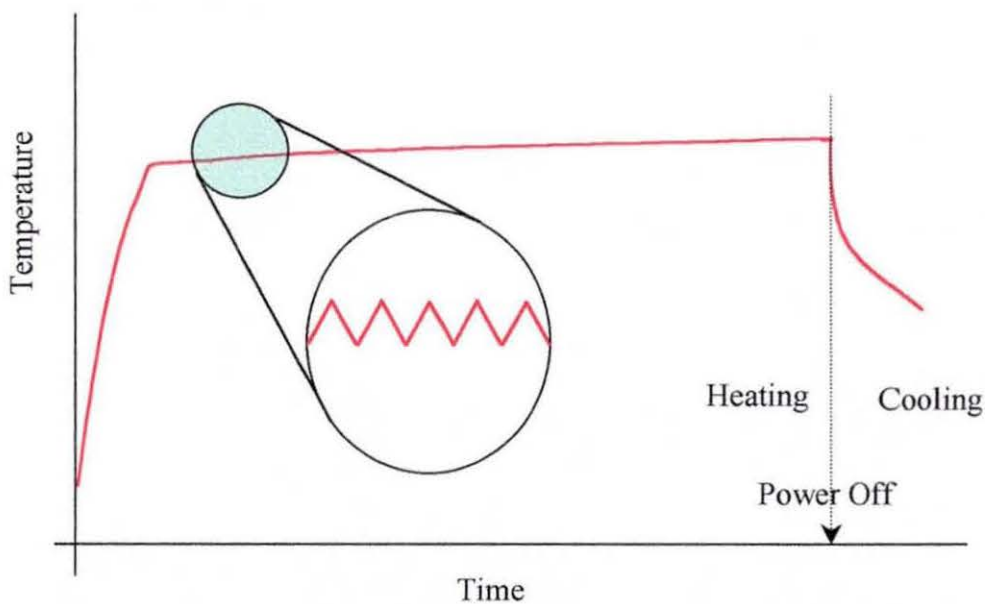


Figure 2.9: Time/temperature profile for *Smartheat* heating.

2.4 Adhesion

This research is concerned with producing a strong, permanent joint between two PVC substrates. There is more than one way in which materials join together and thus if an understanding of how a joint develops is to be gained, an understanding of all adhesion/joining processes must be sought.

2.4.1 Theories of Adhesion

Adhesive bonding has been described as the process of uniting materials, often with the aid of a third substance capable of holding those materials together by surface attachment²⁴. In the case of joining two PVC pipes together, there is no separate adhesive; rather it can be said that both surfaces are adhesive materials. As interlayers have been used in this research, it is important to have an understanding of the phenomenon of adhesion.

There are currently four theories of adhesion, these are as follows²⁵:

- mechanical
- electrical double layer
- adsorptive
- molecular diffusion

There is also one main theory of adhesion which accounts for lower than expected adhesion strength or non-adhesion when attempting to assemble a joint between an adhesive and an adherend;

- weak boundary layer

The mechanical theory proposes that one way of achieving a good bond is for the adherend to be mechanically roughened to increase the working surface area, leading to mechanical interlocking across the interface. Undercutting may also occur which means that to separate the surfaces, the adhesive or adherend must be physically fractured.

The electrical double layer theory states that attractive electrical forces occur at an interface in the form of a double layer. This can be seen in freshly cleaved mica, though this theory is not yet fully accepted or understood.

Adsorptive theory, or intimate contact, states that adhesion results from surface forces caused by molecular contact. The process of establishing continuous contact between the adhesive and the adherend (or a polymer melt) is known as wetting. Good wetting occurs when the adhesive flows into the topographic features of the adherend. After intimate contact is achieved between the adhesive and the adherend, it is believed that permanent adhesion results from the forces of molecular attraction.

Diffusion theory states that adhesion is developed through the interdiffusion of molecules in the adhesive and the adherend. This theory is primarily applicable when both adhesive and adherend are polymers with long chain molecules capable of movement and are compatible.

It is of course true that diffusion cannot occur without wetting, and it can be determined which of the mechanisms is responsible for development of a high joint strength. Korenevskaya et al²⁶ proposed a wetting theory to account for development of peel strength at short contact times. However, this theory does not readily account for the differences observed between strength arising between wetting and diffusion. Wool and O'Conner^{27,28} indicated that partial mechanical property recovery occurred after a few minutes while full recovery of properties took several weeks. The material in this case was hydroxy-terminated polybutadiene. To fully separate the two theories, incompatible amorphous polymer interfaces have been studied. These materials allow complete wetting at long contact times, but an incompatibility does not permit interdiffusion during the same period, leading to low fracture energy. Studies with polystyrene/poly(methyl methacrylate) interfaces have shown that fracture energy increases with interdiffusion at constant contact area^{29,30}.

The theory known as weak boundary layer, can account for a lower than expected bond strength. Formation of a layer between the adhesive and adherends can lower the surface free energy of the adherends, as in the case with migration of additives. A discontinuous layer may also be formed by external contaminants such as dust or fingerprints. Waxes or oils present in the polymer may also form a continuous layer, leading to poor bonding.

2.4.2 Thermodynamics of Adhesion

Bringing together two surfaces to form an interface causes two free surfaces in contact with air to be destroyed. Interactions at the resulting interface determine the

quality and strength of the bond and its likely performance in service. Interactions can only occur if the two surfaces come into contact with each other and therefore wetting is a crucial determinant of interfacial interaction. It has been discussed how wetting is achieved practically and its effect on the strength of a joint. This section examines ways of predicting whether two materials will wet and ultimately bond together, using some thermodynamic approaches. Adhesion is normally quantified in terms of surface tension of liquids and surface energy of solids, although Sutherland and Heath³¹ have theorised the use of a purely surface free energy approach for liquid and solid systems and resulting interfaces.

The surface energy of a substance can be determined by measuring the angle made by a drop of liquid on its surface, the so-called "contact angle." There are many theories that describe this and controversy continues, as the surface energy of a solid is difficult to determine directly. A thorough review of this subject has been carried out by Abrahms³² and Kinloch³³.

2.4.3 Thermodynamics of Wetting

If a liquid is in contact with a solid, a solid/liquid interface is formed to replace the original surfaces of the solid and the liquid. The reversible free energy change (ΔG_{SL}) can be given by:

$$\Delta G_{SL} = \gamma_{SL} - \gamma_S - \gamma_{LV} = -W_A \quad \text{[Equation 1.]}$$

Where γ_{SL} is the interfacial free energy of the liquid in equilibrium with the solid, γ_S is the surface free energy of the solid in a vacuum, γ_{LV} is the surface tension or surface free energy of the liquid in equilibrium with its vapour and W_A is the reversible thermodynamic work of adhesion, i.e. the work required to separate the solid and liquid.

The extent of wetting can be described in terms of a contact angle at the tri-phase line. Young³⁴ describes the relationship between contact angle and the surface free energies of the solid and liquid in Equation 2:

$$\gamma_{SV} = \gamma_{SL} + \gamma_{LV} \cos\theta \quad \text{[Equation 2.]}$$

where θ is the contact angle of the liquid drop on the surface and γ_{SV} is the surface free energy of the solid exposed to vapour, as shown in Figure 2.8, below.

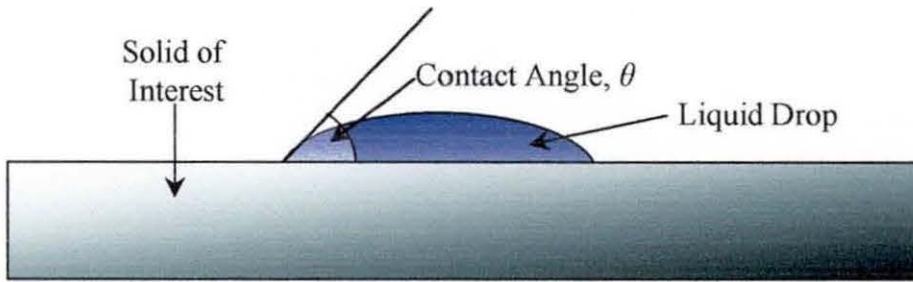


Figure 2.10: Diagram of liquid in contact with solid

A material may absorb vapour phase molecules from the liquid, which has the tendency to lower the surface energy of the solid to γ_{SV} and therefore increase the contact angle. Thus,

$$\gamma_{SV} = \gamma_S + \pi_e \quad [\text{Equation 3.}]$$

where π_e is the spreading pressure. Polymers have been found to absorb negligible amounts of liquid so the term π_e tends to zero^{35,36}.

Equation 2 states that for good adhesion the contact angle of an adhesive must be zero (i.e. $\cos\theta = 1$). If this condition were true, the number of practical adhesives would be very small indeed³⁷. In practice, real surfaces are not smooth and a liquid may not be able to penetrate into interstices (pits or scratches) on the surface of the solid. In this case, it is necessary to consider the wetting of a rough surface. Huntsberger suggested one mathematical approach to this:

$$\Delta G_{SL} = -\gamma_{LV} \left(1 + \left(\frac{\Omega_S}{A_S} \right) \cos\theta \right) \quad [\text{Equation 4.}]$$

where (Ω_S/A_S) is the ratio of actual surface area to the projected surface area. This equation suggests that free energy decreases for all cases except where $\cos\theta < 1$ and where $(\Omega_S/A_S) \cos\theta > 1$. Thus any adhesives which have a contact angle of $< 90^\circ$ are capable of complete wetting. For a rough surface, the rate of wetting may be low which leads to a poor bond, rather than the adhesive itself. Maximum rate of wetting is achieved at zero contact angle³⁸ and therefore a high rate of wetting is desirable to allow the adhesive to completely wet the surface while still in liquid form.

i) Measurement of Contact Angle

Before measurement of a contact angle, the solid surface must be absolutely clean. Unprepared polymer surfaces can be contaminated by airborne particles such as

greases and oil aerosols. The presence of silicone oil on a polymer surface is extremely detrimental to adhesion and contact angle measurement, due to the formation of a weak boundary layer. Since it has been found that a layer of only a few molecules thick will be enough to prevent adhesion, care must be taken to remove them. Rance has suggested methods by which these problems can be overcome³⁷. Another cause of poor adhesion; low molecular weight processing additives are likely to migrate to the surface and form a weak boundary layer³⁹. Polishing is one way to overcome this problem but the surface must be very flat and analysis must be conducted quickly to prevent further migration to the surface⁴⁰.

Contact angle is directly measured from the profile of a liquid drop on the solid substrate. This can be achieved using a low power optical microscope fitted with an angle-measuring reticule in the eyepiece. The contact angle may also be measured using the dimensions of the drop, providing the droplet is small enough to eliminate gravitational distortions, in which case the drop is considered a segment of a sphere. The formula for this is $\tan \theta/2 = 2 h/d$, where d is the diameter and h is the height of the drop⁴¹.

Figure 2.9 shows the various methods of measuring contact angle.

ii) Physical and Mathematical Interpretation of Contact Angle Data

The contact angle of a liquid on a solid indicates a balance of interfacial forces and extent of interaction between both phases.

Dupre⁴² has shown that the reversible work in separating unit area of solid and liquid (W_A) is given by:

$$W_A = \gamma_{LV} + \gamma_{SV} - \gamma_{SL} \quad \text{[Equation 5.]}$$

Combining equation 2 with 5 gives the Young-Dupre equation:

$$W_A = \gamma_{LV}(1 + \cos\theta) \quad \text{[Equation 6.]}$$

From this equation, it is possible to calculate W_A , the reversible work of adhesion, if a liquid of known surface tension is used. This equation is true for all low energy surfaces that give a single contact angle (assuming $\pi_c \rightarrow 0$).

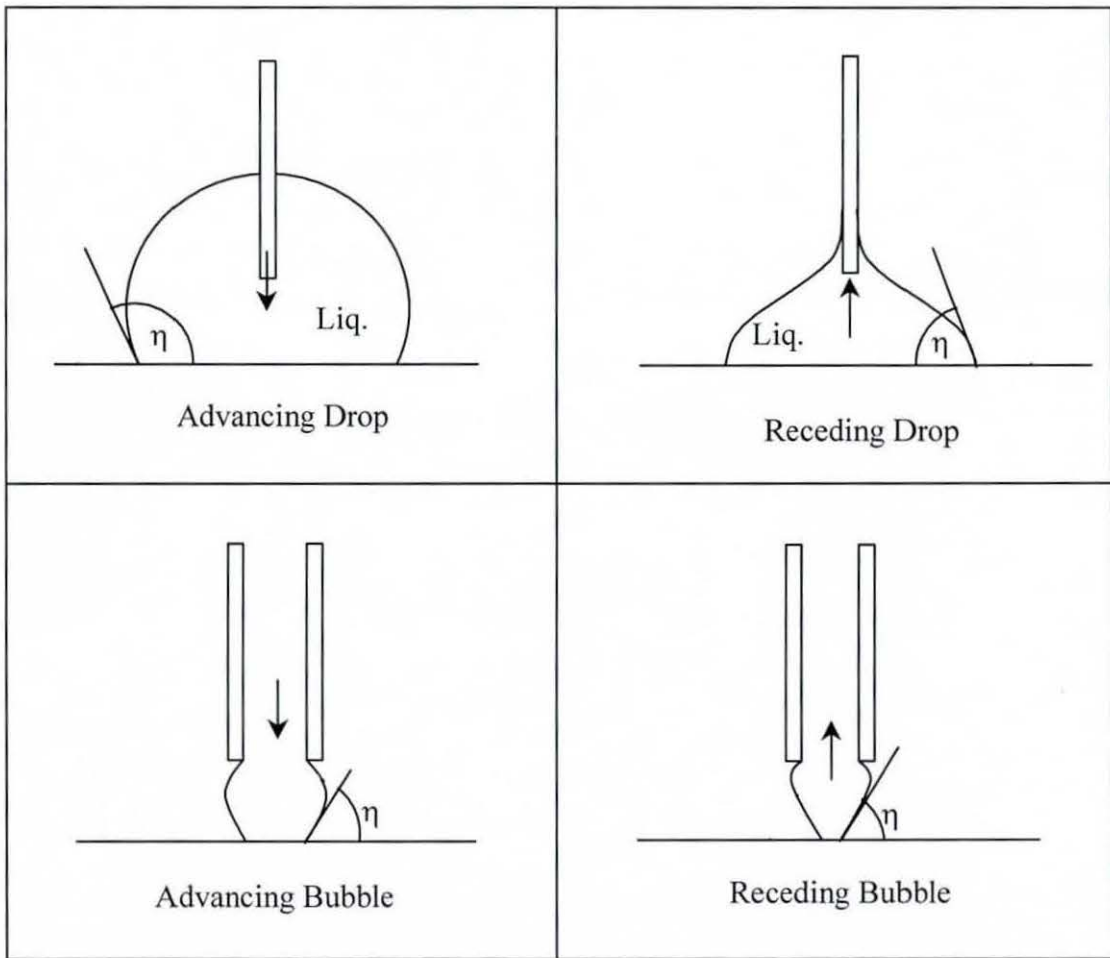


Figure 2.11: Schematic of contact angle measurement methods

Fox and Zisman⁴³ showed that plotting $\cos \theta$ against γ_{LV} for each of a series of liquids produced an estimate of the surface free energy of a solid. The relationship is as follows:

$$\cos \theta = 1 + b(\gamma_{LV} - \gamma_C) \quad [\text{Equation 7.}]$$

Where γ_C is the critical *surface tension of wetting* for the solid and b is a constant. The critical surface tension of wetting is achieved when the liquid just wets a surface with zero contact angle. However, in practice the approach is found to have some limitations and ideally a homogeneous series of liquids should be employed (e.g. hydrocarbon liquids for PTFE).

Good and Girafalco⁴⁴⁻⁴⁶ derived an equation by which the interfacial free energy of two phases may be calculated:

$$\gamma_{12} = \gamma_1 + \gamma_2 - 2\phi_{12}(\gamma_1\gamma_2)^{(\frac{1}{2})} \quad [\text{Equation 8.}]$$

Combining this with equation 2 gives:

$$\cos\theta = -1 + 2\varphi_{sl} \left(\gamma_s / \gamma_{sl} \right)^{1/2} \quad [\text{Equation 9.}]$$

Where φ is an interaction parameter derived from precise knowledge of the surface composition, (although this may be difficult in practice). A linear plot of $\cos\theta$ vs. γ_{LV} gives γ_s at the intercept when $\cos\theta = 1$. φ_{12} must be determined for $\cos\theta = 1$. This method is not often used due to the difficulty in estimating φ_{SL} ⁴⁷.

Fowkes suggested that surface free energy of a solid might be split into three different components, each one contributing to the overall energy⁴⁹:

$$\gamma = \gamma^d + \gamma^p + \gamma^h \quad [\text{Equation 10.}]$$

The letters d, p, and h denote three types of intermolecular forces, i.e. dispersion, polar and hydrogen bonds respectively. However, to reduce mathematical complexity, hydrogen bonds and polar forces are sometimes grouped together. Fowkes also suggested that where only dispersion forces operate, the thermodynamic reversible work of adhesion could be calculated by a geometric mean method:

$$W_A = 2(\gamma_s^d \gamma_L^d)^{1/2} \quad [\text{Equation 11.}]$$

Combining Equations 11 and 2 allows the calculation of the dispersion force contribution to the surface free energy of a solid:

$$\cos\theta = -1 + \frac{2(\gamma_s^d \gamma_{LV}^d)^{1/2}}{\gamma_{LV}} \quad [\text{Equation 12.}]$$

provided that values of γ_{LV} and γ_{LV}^d are known for the series of liquids used.

Owens and Wendt^{50,51} used the theory of fractional polarity and stated that polar interactions could be estimated in a similar way. This approach lead to a clearer understanding of the relationship between interfacial free energy and its constituents:

$$W_A = 2(\gamma_s^d \gamma_{LV}^d)^{1/2} + 2(\gamma_s^p \gamma_{LV}^p)^{1/2} \quad [\text{Equation 13.}]$$

Using a series of liquids with known polar and dispersive contributions of their surface free energy, it is possible to predict the polar and dispersive energies of a solid surface by combing Equation 13 with the Young-Dupre equation. This results in the following:

$$W_A = \gamma_{LV}(1 + \cos\theta) = 2(\gamma_S^d \gamma_{LV}^d)^{1/2} + 2(\gamma_S^p \gamma_{LV}^p)^{1/2} \quad \text{[Equation 14.]}$$

This method is well used but some doubt exists whether the geometric mean is as valid as other methods^{52,53}. Equation 14, often known as the Owens Wendt equation, not only gives a method of estimating the thermodynamic work of adhesion but effectively splits the types of interactions into their component parts.

2.4.4 Acid Base Interactions

In the previous section, surface free energy was defined in terms of dispersive and polar interactions. Fowkes⁵⁴ has suggested that of the polar interactions, hydrogen bonding is highly specific and should be considered separately, an approach based on the work of Drago^{55,56}. Drago suggested that hydrogen bonds are a sub-set of Lewis acid-base interactions and that the enthalpy of these acid-base interactions is the sum of acid-base and dispersive interactions. Dispersive interactions are assumed to be negligible, and so the work was conducted in neutral solvents.

There are three types of processes that lead to hydrogen bonds depending on the polymer and liquid used:

i) Electron donor/proton acceptor (Lewis base),

e.g. polycarbonate, polystyrene.

ii) Electron acceptor/proton donor (Lewis acid),

e.g. PVC, chlorinated olefins.

iii) A combination of i) and ii)

e.g. polyamides, polyimides.

By measuring the contact angle of acidic and basic liquids on acidic and basic solids, Fowkes was able to determine the differences between them by using the following equation.

$$W_A^p + W_A^{ab} - \pi_e = \gamma_{LV}(1 + \cos\theta) - 2(\gamma_S^d \gamma_{LV}^d)^{1/2} \quad \text{[Equation 15.]}$$

The term W_A^{ab} is a general term including hydrogen-bonding interactions.

Fowkes discovered that for an acidic liquid on an acidic surface, the left hand terms of Equation 15 tend to zero, the same being true for the equivalent basic system. This

means that when a surface and the liquid have the same tendency to accept/donate electrons, they will interact by dispersive forces only, despite the fact that they may be classified as polar.

It may be inferred from this concept that dipole-dipole interactions are negligible and this was indeed confirmed by Fowkes work. Equation 15, then provides a method of calculating W_A^{ab} . γ_{LV}^d can be determined from the contact angle of a liquid in contact with untreated polyethylene, since this material is known to interact in a purely dispersive way. Similarly, by using a liquid with only dispersive interactions, γ_S^d can also be determined.

In conclusion it can be said that since, with polar interactions, the dipole-dipole interaction is of negligible importance, the work of adhesion may be maximised by increasing the number of species with good electron/proton donating/accepting properties.

2.5 Joining of Amorphous Polymers

In the previous section, the theoretical basis for adhesion was discussed. This section describes how amorphous polymers specifically join. A mechanism for diffusion, known as the reptation theory, is given, describing the way in which amorphous polymer molecules diffuse into one another. This in turn describes a mechanism for crack healing; a part of the polymer welding process.

2.5.1 Reptation

In order to understand how strength is developed in a polymer/polymer joint, it is essential to understand how material is transported across the interface, eliminating the boundary. Although the large majority of papers on the subject describe this process in mathematical terms, an attempt is made here to describe the mechanisms of polymer diffusion without resorting to such methods, which are beyond the scope of this research.

In 1971, de Gennes described the movement of polymer molecules past fixed obstacles by a process known as reptation⁵⁷. This theory describes the vibrational movement of a polymer chain inside an imaginary tube, which conforms to the shape of the chain⁵⁸. External entanglements define the boundaries of the tube with neighbouring chains in the polymer and the vibrational movement of the chain is caused by thermal energy leading to the movement of defects along the polymer chain. This can be likened to a kink moving along a rope or cable when one end is jerked rapidly, with a short length of the rope “stored” in the kink. Reptation is analogous to this, with the defects storing “length” within the tube. As de Gennes argued that these “kinks” or defects are small in magnitude and occurring rapidly, the chain is observed to undergo a coherent back and forth movement in the tube while maintaining a constant arc length. The shape of the chain at any moment is the same as the shape of the tube. At some time after a nominal zero time, a portion of the chain will be outside the initial tube: Wool and co-workers⁵⁹ have described the escaped portion of the chain as “minor chains.” The length of a minor chain that is no longer in the tube increases with time and has a random Gaussian chain configuration, i.e. the minor chains retain no memory of their original conformation. New configurations are taken up by the minor chains, replacing the originals, as length (and time) increase.

In this way, polymer chains move past fixed obstacles, as they would in a heavily cross-linked material. Klein⁶⁰ has stated that if two polymers are sufficiently alike, with similar chain lengths (as in the case of polymer healing) then the reptation theory is valid. De Gennes himself has also concluded this⁶¹.

2.5.2 Healing

This thesis is concerned with the elimination of an interface between two PVC pipes by thermal welding. This process can be assumed to be partly a healing mechanism by which the movements of molecules (here polymer chains) as an interface is eliminated: i.e. the initial short distance between the surfaces (i.e. a small gap) is eliminated or healed. The molecular model of healing in polymers was first described by Voyutskii and co-workers in 1963⁵⁴. Subsequently, the aforementioned de Gennes reptation theory explains the mechanism of movement of individual polymer chains in healing.

Healing may also be defined as the process of strength development at an interface between identical amorphous polymers⁶². When the surfaces are brought into contact at a temperature above their glass transition temperatures, the interface will develop strength until it has 100% of the mechanical properties of the bulk material and is no longer distinguishable from any other part of the polymer combination. Healing occurs in three stages:

- a) Before contact, the chain ends are constrained within the polymer according to thermodynamic principles. In other words, polymer chains in one surface cannot “reach out” through free space to the other surface.
- b) The same thermodynamic principles that prevent chains extending into free space also prevent them from moving across the polymer-polymer interface immediately after contact between the two surfaces. The second stage can be said to be conformational relaxation, which enables the polymer chains to be in a position to begin moving across the interface.
- c) Finally, the continued relaxation of the chains takes some of them past the interface onto the opposing side of the component. This process occurs simultaneously between both surfaces and is evidenced by increasing mechanical strength in the resulting joint.

By analysing the healing process in individual systems, a characteristic healing time can be determined. The healing process is not the same as full diffusion, since healing involves movement of polymer chains over much shorter distances. Moreover, healing can be said to be the initial stage of interdiffusion, which, though a real and occurring process, does not contribute to further development of strength at the joint, but may be required for good masterbatch dispersion, for example.

2.5.3 Welding

Welding of polymers can be considered as exploiting the diffusion and reptation theory. Welding concerns maximising a method by which strength is developed across a polymer/polymer interface.

It is possible to characterise polymer interfaces into four groups:

- symmetric polymer – polymer, e.g. heat-sealed PVC wallets.
- asymmetric polymer – polymer, e.g. rubber toughening of PMMA.
- polymer – non-polymer, e.g. rubber to metal bonding.
- multi-component polymer, e.g. toughened ABS.

For the purposes of this review, only the symmetric polymer/polymer category which describes two identical or compatible polymers, is considered. This category describes an interface between two polymers of the same type and composition. Processes such as extrusion, injection moulding, compression moulding, powder and pellet sintering and lamination can all be considered as examples of symmetric polymer/polymer welding⁶².

As stated above, the elimination of an interface has been called crack healing. This term was first used to describe the rejoining or healing of a fractured polymer specimen but is used here to describe the joining of surfaces that have not previously been in contact⁶³. Healing is just one stage in the welding process and may be equated with the diffusion/randomisation stages. Wool and O'Conner have extensively studied the process of polymer welding in interfaces⁶³. The stages of polymer welding are as follows:

i) Surface rearrangement

This initial stage describes the effect of the roughness of the surfaces to be brought together and its properties that have an effect on welding. The distribution of chain ends near the surface can affect the welding time in that if they are far from the surface, they have further to diffuse to the opposite side of the interface. Surfaces are also prone to attack by local environments and reagents such as oxidising agents, heat, and radiation. Additives may also form a weak boundary layer which further affects welding, especially as their migration is accelerated by heating and in the melt state.

ii) Surface approach

This stage takes into account the speed with which the surfaces are brought together. For example, if they are brought together too slowly, different levels of welding will occur at different points of the substrate as various points contact each other at different times. This stage can affect the progress of the next stage (wetting), which will in turn effect the development of strength^{62,63}.

iii) Wetting

This process is time dependent in real processes but the time component can be reduced to zero for the purposes of experimentation⁶⁶. Wetting starts at random locations along the interface and spreads out radially giving a fractional wetted area. Full strength can only be achieved when the ratio of wetted to unwetted areas is unity, as diffusion will only occur at locations where wetting has occurred⁶⁷.

iv) Diffusion

In the diffusion theory, the time dependence of wetting is either ignored or reduced to zero. In real processes, diffusion will proceed to different extents at different points over the interface. It has been shown that the diffusion front around an interface is not a flat surface, and welding is a three dimensional process. Since the shape of the diffusion front has been determined as fractal in nature^{68,69}, sufficient time must be allowed for diffusion to occur over the whole interface.

v) Randomisation

This stage allows the normalisation of the molecular weight distribution and the re-randomisation of chain ends. As it is the chain ends and/or chain branches that initially diffuse across the interface, it is likely that there will be a higher concentration of them around the interfacial zone. If they are not fully randomised, failure by chain pullout may occur^{70,71}.

A mathematical review and investigation of welding of polymers can be found in Reference 64.

2.6 Plasticisation of PVC

The use of plasticised interlayers demands an understanding of how the plasticisation phenomenon occurs. Two theories of plasticisation prevail, both of which are reviewed here. At modest plasticiser concentrations it has been shown that anti-plasticisation (characterised by an increase in modulus), can occur, this is also reviewed.

2.6.1 Plasticisation Mechanism

A plasticiser can be defined as a substance or material incorporated into another material to increase its workability and its flexibility or distensability (ASTM D883)⁷¹. There are also other standards referring to plasticisers, namely ISO 472 and BS 1755, although Titow has found many of the standard definitions incomplete and has offered the following⁴:

“A plasticiser is a substance of low or negligible volatility, suitably compatible with the polymer in which it is incorporated. Whilst it improves the processability of the resulting composition, its principal role is to impart to the ultimate product – in degrees dependent upon the plasticiser’s nature and proportion – the properties of flexibility, extensibility and softness. Amongst the usual, technically significant concomitants of plasticisation are the lowering of glass transition temperature (and softening temperature generally), reduction of strength and increased impact resistance.”

Indeed, the action of a plasticiser on a polymer has a parallel effect to that observed when heating such a material. Plasticisers are usually high boiling point, chemically and thermally stable liquids, although in some cases they may be solid or semi-solids. When compared with normal polymer solvents, plasticiser effect is essentially permanent. When selecting a plasticiser, one must consider many parameters depending on final application including compatibility, flexibility, flame retardance, etc. Plasticisers can be categorised into two groups; internal and external. Internal plasticisers modify the structure of the basic polymer (e.g. by co-polymerisation), while good external plasticisers are able to interpenetrate the long chain polymer molecules breaking down intermolecular bonding to enhance chain mobility, thus

altering viscosity in the melt state. Another classification is that of primary and secondary plasticisers. Primary plasticisers are highly compatible and solubilise PVC at high concentrations. Secondary plasticisers are less compatible, but are used to produce a balance of properties when used in conjunction with primary plasticisers. Extenders, lower end compatibility secondary plasticisers, are used in place of other plasticisers often to reduce the overall cost of a material and are no more than processing aids (e.g. reduction of plastisol viscosity).

Two theories have been put forward to explain the mechanism of plasticisation. The first theory states that the plasticiser has a lubricating effect on the chains of PVC^{73,74}. The associated reduction of friction makes the material as a whole less resistant to deformation.

The second more sophisticated theory states that a plasticiser will interrupt interactions and intermolecular forces between individual chains⁷⁵. This is known as the Gel theory. Gel theory states that unplasticised PVC contains a network of fragile, pseudo “cross-links” that are in a continual state of forming/severing at “active centres” in the matrix. On addition of the plasticiser, these temporary cross-links are now between the chain and the plasticiser and are much weaker. It may be said that the plasticiser “masks” the active centres making them unavailable for polymer/polymer cross-linking, thus “loosening” the polymer structure. It has been determined that the “cross-links” are in fact small areas of order (crystallites) within the amorphous polymer⁷⁶.

Finally, it has been suggested that the plasticisation process is complex and operates on many levels, involving both bulk and atomic interactions⁷⁶.

2.6.2 Function of a Plasticiser

The basic functions of a plasticiser are its ability to impart flexibility and compatibility to the polymer matrix. However, with a deeper examination of the role of plasticisers, many other requirements will be found⁷⁷⁻⁷⁹.

i) Compatibility

Compatibility is the ability of two or more materials to mix with each other to form a homogenous or miscible composition. In the context of a plasticiser, the mix must be able to resist any conditions that may cause it to exude or spew from the resulting

material and in addition, diffuse from the PVC onto or into any contacting material. Compatibility is influenced by the type and functionality of the plasticiser molecule, the concentration in which it is used and the nature of the PVC with which it is mixed.

ii) Solvation

The solvating ability of a plasticiser is closely related to its compatibility. It follows that some highly compatible plasticisers will exhibit considerable solvent action to the point of complete solvation of the polymer. Conversely, other less compatible plasticisers will require the action of heat to achieve solvation. Depending on the application, fast solvation may or may not be desirable.

The solubility parameter provides a means of determining the solvating ability of a system. In this context, "like dissolves like" is an excellent rule of thumb: a certain polymer will be more likely to dissolve in a solvent of similar solubility parameter. As an example, PVC, which has a solubility parameter of $19.4 \text{ (MJ m}^{-3}\text{)}^{0.5}$, is likely to be soluble in acetone which has a solubility parameter of $20.4 \text{ (MJ m}^{-3}\text{)}^{0.5}$ but is unlikely to dissolve in ethanol which has a solubility parameter of $26.0 \text{ (MJ m}^{-3}\text{)}^{0.5}$. As a general rule, non-polar solvents dissolve hydrocarbon polymers and polar solvents dissolve polar polymers⁸⁰.

iii) Stability

During processing, and sometimes in service, the PVC/plasticiser system will be subjected to elevated temperatures. Under demanding conditions, the plasticiser may degrade with subsequent loss of desirable properties and eventually cause embrittlement. Incorporation of an anti-oxidant may be required. Some plasticisers are also susceptible to attack from UV radiation. Plasticisers containing unsaturated groups and phosphates are particularly prone to attack.

iv) Low Volatility

Plasticisers must have low enough volatility to resist loss by evaporation, both in processing and in service, as this leads to loss of properties and eventually embrittlement. In the context of a buried pipe, this property can be considered of low importance but it may have some bearing of shelf life in storage.

v) Mechanical Properties

Different plasticisers impart a variety of different properties to PVC. For example, esters of aliphatic dibasic acids impart low temperature flexibility and impact strength.

vi) Extraction Resistance

If the resulting plasticised system is subject to harsh environmental condition, care must be taken to ensure that the service environment will not lead to loss of the plasticiser by extraction. For example, polymeric plasticisers are resistant to extraction by solvents and oils but not to extraction by water and soapy water. Other plasticisers are quite the reverse and thus consideration must be given to select the right plasticiser for a given service environment.

vii) Migration Resistance

The migration of plasticiser from the PVC into other materials can cause problems such as swelling and crazing of other polymers in contact (both temporary and permanent) and the breakdown of an adhesive bond. Polymeric plasticisers have good resistance to migration.

2.6.3 Types of Plasticisers

From empirical data and experience, it has been possible to determine the best class of PVC/plasticiser combination. Esters are the most widely used class of plasticisers for PVC and it has been possible to make generalisations on which plasticiser structures work best^{78,81,82}:

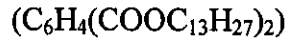
- Aromatic esters are more compatible but less efficient than aliphatics, e.g. aromatic dioctyl phthalate is more compatible but less efficient than aliphatic dioctyl sebacate.
- Normal alcohol based esters impart better low temperature properties than comparable molecular weight branched chain alcohol esters.
- There is a maximum molecular weight for plasticisers that are compatible, e.g. for the monomeric dialkyl phthalates, dodecyl phthalate is considered the maximum⁷⁹.

i) Phthalates

This class of ester materials produces a wide range of desirable properties with a bonus of being low cost. There is a wide range of useful phthalates from dibutyl phthalate (DBP)



to dinitridecyl phthalate DTDP



However, as molecular weight increases in a series of plasticisers, absolute efficiency decreases. The best known, and the material and that considered to be the industry standard is dioctyl phthalate (DOP) strictly di(2-ethylhexyl)phthalate:



This has low cost and a favourable range of properties.

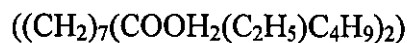
ii) Adipates and Azelates

These plasticisers are used to impart low temperature flexibility and are thus known as *low temperature plasticisers*. Although their low temperature performance is superior to that of phthalates, they do not have the compatibility of phthalates and so they are blended with phthalates in order to improve low temperature performance of PVC. The most widely used adipate is dioctyl adipate (DOA):



This material also carries FDA approval.

Another material is dioctyl azelate (DOAL):



this is significantly lower in volatility than dioctyl adipate but more expensive.

iii) Trimellitates

These are used mainly for their high permanence, trimellitates being used in the wire insulation industry where high service temperatures might be encountered. Examples are trioctyl trimellitate (TOTM):



and triisooctyl trimellitate (TIOTM):



iv) Polymeric Plasticisers (Polyesters)

These are linear polyesters with molecular weights ranging from 800 to 8000. The main advantages of these materials are their low migration and resistance to extraction by a variety of solvents including gasoline, water, soap and synthetic detergents. Although they have a slow rate of solvation compared to phthalates and are expensive, a wide range of properties can result from their use. They are characterised not only by their molecular weight, but also by the diol and acid precursors used in esterification. Due to their high resistance to extraction, polymeric plasticisers often carry approval for food contact applications.

v) Phosphates

Phosphate plasticisers have good flame resistance and stability to ultraviolet radiation. Octyl diphenyl phosphate carries FDA approval. Triaryl phosphates are used in high stressed components where flame retardence and extremely low volatility are required. Some phosphates have very low compatibility with PVC.

vi) Epoxides

Of this group of secondary plasticisers, epoxidised soybean oil carries FDA approval but has low efficiency and imparts poor low temperature properties to PVC.

vii) Benzoates

Due to their high cost, benzoate plasticisers are not widely used and have received little attention in the literature⁷⁴. However, it is possible to say they are generally fast fusing, soil resistant and non-toxic^{78,84}.

2.6.4 Anti-plasticisation

Anti-plasticisation can occur in compounds containing up to 20 pphr of plasticiser and although it is well documented, the phenomenon is not fully understood⁸⁶⁻⁹¹.

The effects of the addition of low (less than 20 pphr) of plasticisers are characterised by an *increase* in stiffness and hardness and a reduction of elongation at break of

PVC. This undesirable effect is analogous to embrittlement and should be avoided. Indeed, it is *exactly* the opposite effect sought when adding plasticisers.

Two theories have been forwarded to account for anti-plasticisation, but they are almost diametrically opposing in how they account for this phenomenon. The first was proposed independently by Jacobson⁸⁵ and Tabb⁸⁶. This theory states that anti-plasticisation is the result of structural ordering but not necessarily the formation of crystallinity.

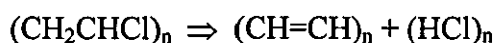
The second theory, proposed by several authors, states that molecular movement is restricted by a concentration of plasticiser which exactly occupies the free volume in a polymer and thus suppressing the effects of relaxation process occurring in the unplasticised polymer.

2.7 Degradation and Stabilisation of PVC

2.7.1 Degradation of PVC

PVC is a versatile and widely used polymer. Its properties can be tailored to yield flexible and rigid finished products and, allowing for environmentalist pressure, it is likely to remain an important material for the foreseeable future. However, PVC has several drawbacks, one of the most important being its thermal instability. The degradation of PVC has been extensively studied over the years; indeed, it may be suggested that whole forests have been set aside to provide the paper for such reports.

Model PVC compounds⁹², 2,4-dichloropentane or 2,4,6-trichloroheptane exhibit relatively high thermal stability up to 300°C, yet dehydrochlorination can occur at temperatures as low as 100°C in commercial PVC resins^{93,94}. The most common process occurring during degradation is generally accepted as being dehydrochlorination leading to polyene formation followed by cross-linking between polyenes^{86 - 89}. The dehydrochlorination/polyene process is autocatalytic, where the formation of the first double bond in the polyene sequence causes the formation of an adjacent double bond, leading to the formation of the polyene sequences. The autocatalysis by hydrogen chloride (HCl) is characterised by an induction period before the evolution of HCl is observable⁹⁰. Average lengths of polyene sequences are approximately 10 with maximum length reaching 20^{91 - 96}:



The mechanism by which polyene formation occurs is not yet resolved, with two preferred theories currently proposed⁹⁷. Potential initiation sites are also under continued investigation. Two theories presently dominate, the first stating that irregularities in the polymer are the cause, while the second presents evidence that isotacticity is of primary importance.

There are many potential irregularities in the structure of the PVC chain that could cause degradation and studies have been conducted to determine their relative

importance^{98,99}. Unfortunately, it is difficult to correlate the effect of the defects with changing degradation rates, since they are low in concentration. The method of varying the defect concentration (changing polymerisation conditions) leads to other structural changes; the very method of altering important variables may lead to degradation rate changes.

Hjertberg^{100 - 102} has determined that the tertiary chlorine defect is of greatest importance to degradation rates, while Minsker¹⁰³ and co-workers have suggested internal unsaturation is of primary importance. Martinez¹⁰⁵⁻¹⁰⁹ et al have conducted experiments to determine the effect of isotacticity in the initiation of degradation. By determining degradation rate within a range of isotacticity corresponding to usual polymerisation methods, they determined that an isotactic stereo-sequence is responsible for initiation. This result is of considerable importance since this structure was previously considered to be a normal part of the make up of a PVC chain^{104 - 108}. However, a kinetic study has yielded two possible initiation sites with distinct activation energies. These two results were ascribed to initiation at a labile isotactic triad conformation or at a random chlorine atom along the PVC chain^{109, 110}.

Although the above theories shed much light on the mechanisms of PVC degradation, the effects on the PVC product itself are visible to the naked eye. As polyene sequences form and become increasingly prevalent, discolouration of the materials occurs. This can be caused by sequences seven double bonds in length¹¹¹. The colour of natural (transparent) PVC article will change initially to light yellow through reddish brown and finally resulting in a black, charred appearance (the presence of spent stabilisers may affect the intermediate colouration). The modulus of the material increases with undesirable changes in other mechanical properties due to the cross-linking of polyene units. Chemical and electrical properties also deteriorate.

2.7.2 Stabilisation of PVC

Due to its thermal instability at normal processing temperatures, stabilisation of PVC is very important. The stabilisation additive packages included with commercial PVC formulations are complex and often closely guarded trade secrets, as in the case of the materials used in this work. As a result, there was no possibility of altering the

formulation of the PVC pipe grade used in this work, but it was important to gain an understanding of stabiliser function.

There are many types of stabiliser available, which can be classified as organic and inorganic lead containing compounds, organometallic compounds (for example Cd, Sn, Ca, Zn in type) and organic compounds. The mode of action of stabilisers can be two-fold. First, as in the case of tin-based organometallics, is to prevent the degradation occurring: this is achieved by the stabilisation of labile chlorines in the polymer chain which are replaced by a component part of the stabiliser¹¹¹. The second way in which stabilisers work is to absorb and bind HCl formed during degradation and “mop up” free radicals. Some plasticisers also react with double bonds to prevent the formation of polyene sequences¹¹².

2.8 Test Methods

Mechanical testing has been used in this research to assess the interlayer and welding performance. The essential performance measure was the strength of the joint itself, which had to be maximised. To support this data it was necessary to determine the depth of diffusion and the levels of polymer degradation. This section reviews literature on mechanical tests used and argues the best analytical methods to measure degradation in this research.

2.8.1 Mechanical Tests

i) Lap Shear Test

The lap shear test is a simple method of determining the joint strength between two rigid substrates. Details of the method may be found in ASTM D 3163. This test was previously used by Kline et al to investigate polymer welding⁵⁸. A study into the experimental parameters of the lap shear test suggested that off-axis loading was detrimental to the test and highlighted the need for careful loading of test specimens¹¹³. The results of this work concluded that off-axis loading was the most significant factor causing premature failure and recommended careful specimen loading. The lap shear test can be seen schematically in Figure 2.10.

ii) Indentation Hardness

Indentation tests have been previously used to quantify a wide range of properties in plastics. The hardness of a polymer is an indirect measure of several of its properties¹¹⁴ and it has been used to assess orientation within the polymer structure.

Hardness represents a resistance to deformation at a surface and is closely related to yield strength¹¹⁵. The indentation test is a well-understood and general method whose mechanism has been defined by Tabor¹¹⁵. When a diamond-shaped indenter is pressed into the polymer surface, under a specific load, initial elastic deformation occurs; the elastic limit is likely to be exceeded and hence the material deforms plastically, leaving an impression. The dimensions of this impression can be measured and used as a basis of the hardness of the material. Some instantaneous elastic recovery occurs in polymers but Rueda et al found this undetectable¹¹⁶.

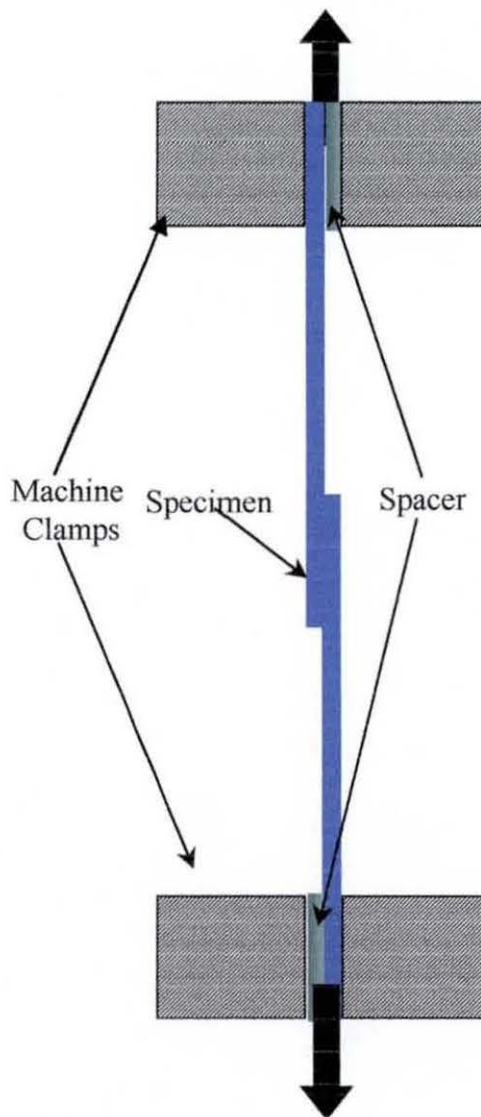


Figure 2.12: The single lap shear tensile test

iii) Factors Affecting the Test.

Long Term Recovery of Indentation.

P. Eyerer¹¹⁷ found that the length of diagonals remains unaffected for a time between 5 seconds and 24 hours. This was true for 19 different types of plastics tested, including PVC.

Humidity

Results have shown that water has no lubricating effect on the polymer and produces no significant change of hardness in a plastic. Storage of the material in distilled

water for 12 hours at room temperature did have an effect on some plastics, but PVC remained unaffected. This research did not include tests on polyamides, which are plasticised by water, and therefore the above results are not all encompassing. The work may have benefited from longer immersion times or an elevated temperature test.

Temperature

Thermoplastics are highly dependent on temperature so it is clearly vital to ensure a constant test temperature for hardness measurement. Temperature may also affect the clarity of the indentation for measuring purposes. In some plastics this can be a limiting factor as they can show low reflectivity compared to metals.

Sample Thickness

A rule of thumb states that the sample should be 10 times thicker than the indentation depth, to ensure the support platen does not contribute to the sample hardness.

Sample Orientation

When polymers contain some orientation, the impression created by a square diamond indenter is usually not symmetrical with a measurable difference in the diagonals parallel and perpendicular to the orientation direction. This variation is known as $\Delta MH = MH_{\parallel} - MH_{\perp}$, where ΔMH is the hardness anisotropy, MH_{\parallel} is the hardness parallel to the preferred orientation and MH_{\perp} is the hardness perpendicular to the preferred orientation direction. Studies on polystyrene, an amorphous polymer, have given this result¹¹⁸. Here, the orientation of injection moulded articles was tested using a micro-indentation test. The findings of this work showed that there was a decrease in the size of the indentation normal to the orientation. This diagonal also showed a larger change with changing draw ratios. The same tests conducted on (poly)4-methyl-pentene-1 (TPX) have shown similar results, i.e. that the diagonal perpendicular to the preferred orientation is the shorter and more responsive¹²⁰. However, studies on polyethylene have shown the opposite to be true, that the diagonal parallel to the preferred orientation is the shorter and more responsive¹²¹. It is clear that semi-crystalline and amorphous materials do not exhibit increased micro-

hardness in either one direction or the other, as TPX is a semi-crystalline material. In reported tests, the materials used have been drawn by ratios of 1:8 to 1:40.

2.8.2 Spectroscopic Techniques

Spectroscopic techniques are very important in characterising bulk material, surfaces and interfaces. In the context of this study, they will be primarily used for assessing degradation levels at and around the heater wire. Spectroscopic techniques differ from microscopic techniques in that they do not normally produce an image, although this distinction is becoming less clear, particularly in the case of secondary ion mass spectroscopy. All the spectroscopic techniques covered here are similar in that a sample is bombarded with radiation or ions and the interaction products or emissions determined by elemental or molecular characterisation. An ultra high vacuum is also required for most spectroscopic and electron microscopy techniques.

i) Secondary Ion Mass Spectroscopy (SIMS)

SIMS¹²² uses a beam of ions to sputter material from the surface under investigation. Although the majority of the sputtered material is uncharged, enough charged material is present to be extracted into a mass spectrometer for analysis. Two modes of SIMS are possible, known as *dynamic* and *static* SIMS^{123, 124}. In static SIMS the emphasis is on maximising molecular information while maintaining a low sputter rate. To achieve this a low energy ion beam is used so that material removal is minimal. Static SIMS produces a spectrum containing enough information to give a “fingerprint.”

Dynamic SIMS uses a high energy ion beam to produce a high sputtering rate. The detector can be tuned to a particular species of interest and its concentration profiled as a function of depth but more damage is done to the sample.

A disadvantage of SIMS is the difficulty in producing quantitative results. There are large differences in (sputtered) ion yield between different materials and as the incident ions are charged, a compensating current must be applied to avoid charging the sample.

ii) X-ray Photoelectron Spectroscopy (XPS)

Where SIMS can be operated in a surface sensitive manner, XPS is surface specific by nature¹²⁵. Soft X-rays are directed onto the sample surface causing photoelectrons to be emitted. The origin of these photoelectrons is two-fold. The strongest source originates from the atomic orbitals of the atoms present the second (much weaker) from valence band electrons. All these emissions are particularly characteristic of the atom from which they originated in terms of the binding energy of the electron. The spectra obtained from XPS take the form of binding energy versus electron intensity. The binding energy of an electron is also dependent on chemical state, meaning some chemical information can be gained from XPS.

Initially a survey scan is taken covering the whole of the binding energy range. A narrower scan (smaller binding energy range) is required to determine the chemical shifts caused by different chemical states at high binding energy resolution.

The major advantage of XPS is its ability to analyse any materials in any form and no major charging problems (any that do arise are easily dealt with by flooding the sample with low energy electrons). Despite these advantages, XPS suffers from a lack of spatial resolution, typical observation areas are in the order of several square millimetres.

iii) Laser Induced Mass Analysis

Laser induced mass analysis (LIMA)¹²⁶ is a spectroscopic technique that differs from other techniques covered here in that a high power density pulsed laser is used to ablate material from the sample surface. The resulting material is then extracted into a time-of-flight mass spectrometer (TOFMS) where it is separated according to its mass to charge ratio (m/z). The incorporation of an ion-reflecting element compensates for initial differences in the kinetic energy of ions with the same m/z ratio, thus improving mass resolution.

The advantages of LIMA over other spectroscopic techniques are as follows:

- The technique allows for full periodic table coverage, including hydrogen.
- LIMA is exceptionally fast: a complete spectrum can be recorded in about a tenth of a second¹²⁶.

- The technique allows elemental, isotopic and chemical information to be determined.
- Virtually no sample preparation is required since the material can be simply cut to the correct size for the sample holder.
- Good spatial resolution and small analysis area (as small as $0.4\mu\text{m}$ in diameter).

LIMA suffers from a major drawback in its inability to perform quantitative analysis. Indeed, a lower concentration of an element may yield a peak of greater intensity than that of another element with a greater concentration. This is the reason that LIMA has been overtaken in surface analysis by quantitative techniques (such as SIMS and XPA) and has undergone little development in recent years.

iv) Infra-red Techniques

Infrared spectroscopy uses a beam of infrared light to rotate and vibrate molecular segments and atomic groups. This differs from the other techniques described in that no electron transitions (and hence emissions) are produced. As these vibrations are highly characteristic of the molecule constitution and chemical state, so it is possible to produce a unique “fingerprint” for a material¹²⁷. There are two variations on the infrared theme, namely infrared spectroscopy and Raman spectroscopy.

Infra-red Spectroscopy

When infrared radiation passes through a material, various molecules are caused to vibrate, absorbing some of that radiation (i.e. at a specific wavelength or wavenumber). However, not all molecules vibrate and are therefore virtually undetectable in the infrared spectroscope. Since only an oscillating dipole will interact with the electromagnetic field with an associated absorption of energy, then totally symmetrical molecules will not be detected. Examples of symmetrical molecules are H_2 , N_2 , O_2 and Br_2 . Conversely, highly polar molecules (e.g. $\text{C}=\text{O}$, OH) show large changes in the dipole moment and hence have high levels of IR absorption giving an intense peak. A reference beam is compared to the sample beam to identify areas of absorption.

A polymer is invariably a complex organic molecule and shows a large number of vibrations involving the whole molecule or individual bonds of functional groups.

The localised (bond or functional) vibrations may take the form of stretching, bending, rocking, twisting or wagging¹²⁸. Vibrations resulting from the entire molecule produce a whole series of absorption bands below 1500cm^{-1} which are characteristic of that molecule, known as the *fingerprint region*. Functional groups and individual bonds can produce bands across the whole spectrum but those below 1500cm^{-1} are less useful as they are overshadowed by molecular vibrations. Those functional and bond vibrations above 1500cm^{-1} are used to supplement the data below 1500cm^{-1} .

The use of the fingerprint region to identify a compound is considerably more reliable than many other techniques, including melting point. Indeed, it is possible to distinguish between catalyst types used in the manufacture of PE, for example, by IR spectroscopy.

Fourier Transform Infra-red Spectroscopy (FTIR)

FTIR is shown schematically in Figure 2.11. With this technique, radiation covering the whole IR spectrum is split into two beams, one, or both of which pass through the sample. However, one beam is made to travel a longer path than the other, resulting in an interference pattern on recombination. By carefully changing the difference in the two paths, the interference pattern is changed, producing a detected signal that varies with optical path difference. This pattern is known as an interferogram. Fourier transform of the interferogram converts it into a plot of absorption against wavenumber, which closely resembles a normal IR spectrum. The major advantage of FTIR over traditional IR methods is speed; because it is not necessary to scan at each wavenumber, the whole spectrum can be scanned in a matter of seconds. High spatial resolution can also be obtained without sacrificing sensitivity. As the data are stored on a computer, manipulation is very easily accomplished and addition or subtraction spectra may be obtained virtually instantaneously. There are no obvious disadvantages of FTIR when compared to traditional IR.

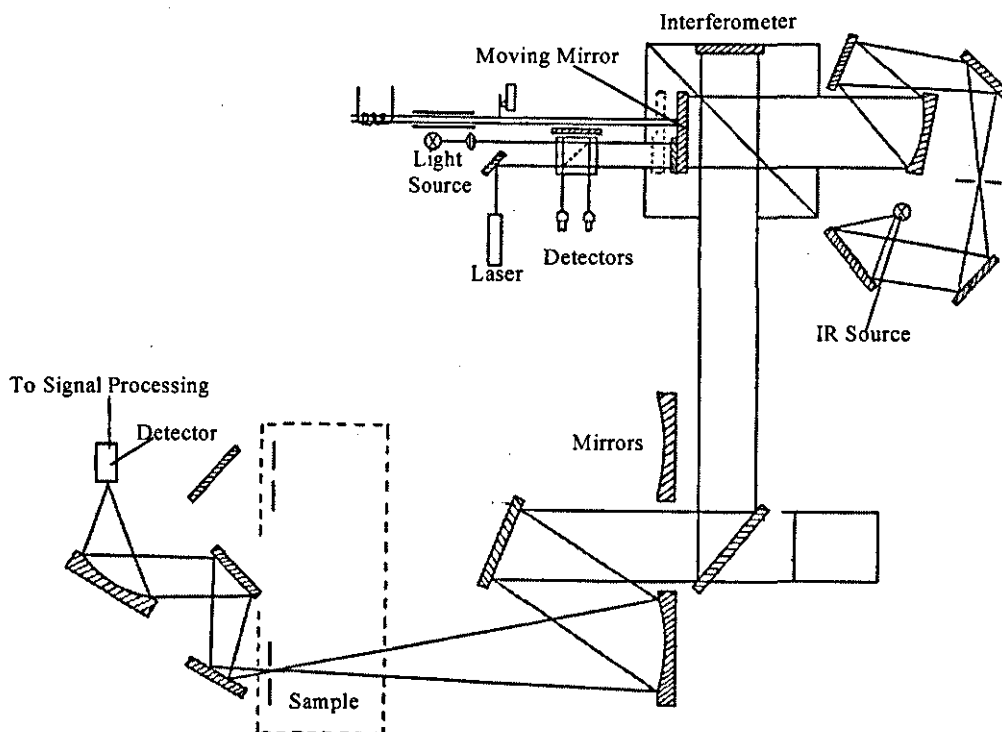


Figure 2.13: Schematic of the FTIR spectrometer

Raman Spectroscopy

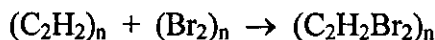
Raman spectroscopy utilises a scattering of light rather than absorption as in IR. While a vibration is induced, it is the periodic change in polarisability that produces Raman absorption rather than a change in dipole moment. In this way, molecules that are invisible in the IR or FTIR spectrometer show very strongly in the Raman spectrometer, and vice versa.

Molecular excitation is produced by a laser in the Raman spectrometer and this technique may be considered ?complimentary? rather than rival to IR or FTIR spectrometry.

Chemical Derivatisation

The structural and molecular analysis capability of IR and other spectroscopic methods can be substantially extended by chemical derivatisation techniques that result in the incorporation of unique elemental labels for reactive functional groups of

interest. An example of this is the derivatisation of surface hydroxyl groups in methyl methacrylate-hydroxypropyl methacrylate copolymers by trifluoro-acetate anhydride (TFAA)¹²⁹. In the same way, bromine may be added across a carbon-carbon double bond according to the following reaction:



This makes the normally weak absorption peak from a carbon-carbon double bond readily visible in the IR absorption spectrum. Due to the tendency of a bromine molecule to form radicals, this reaction is carried out in the absence of UV radiation. Any residual unreacted bromine is not detected by an IR device because the bromine molecule is symmetrical.

2.8.3 Microscopic Techniques

i) Optical Microscopy

An optical microscope consists of a light source and a magnification system. A condenser lens is used to produce a cone of light on or through the sample (reflection or transmission modes respectively). The magnification system consists of an objective lens and an eyepiece. While the eyepiece provides some magnification, the objective is responsible for the majority of magnification.

Reflection optical microscopy is useful for observing polymer fracture surfaces, although this is limited to relatively low magnifications. As magnification increases the depth of field Δf , is reduced;

$$\Delta f = \frac{n}{NA} \left(\frac{\lambda_n}{NA} + \frac{1}{7m} \right) \quad \text{[Equation 16.]}$$

where n is refractive index of the medium on the sample side, NA the numerical aperture, λ is the wavelength of visible light and m is the magnification.

Transmission optical microscopy is used for looking at thin films of different polymers, the lack of phase differentiation (similar refractive indices) makes this technique unsuitable for single polymer systems.

Of particular interest is fluorescence microscopy. If ultra-violet radiation is used to illuminate a sample, any carbon-carbon double bonds will fluoresce. As has been discussed above, one type of the degradation products of PVC are conjugated double

bonds. It is hoped that different amounts of unsaturation will produce different (and measurable) levels of fluorescence.

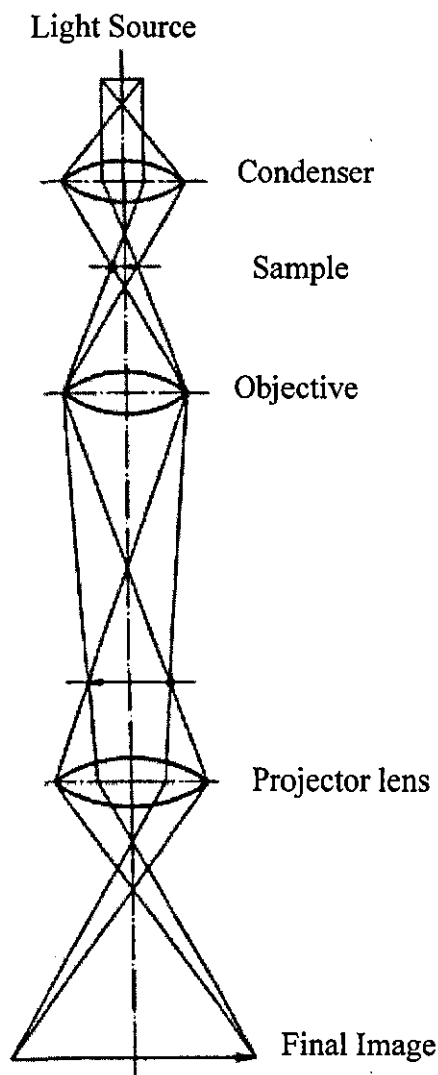


Figure 2.14: Schematic of the optical microscope

ii) Electron Microscopy

Electron microscopy is well a documented technique¹³⁰. Two main types are available; transmission electron microscopy (TEM) and scanning electron microscopy (SEM).

TEM requires extremely thin specimens (10-100nm), which are normally very difficult to prepare from polymers. Non-conducting samples require a thin metallic or carbon layer to be deposited. TEM is analogous to optical microscopy, as can be seen in Figure 2.13, below.

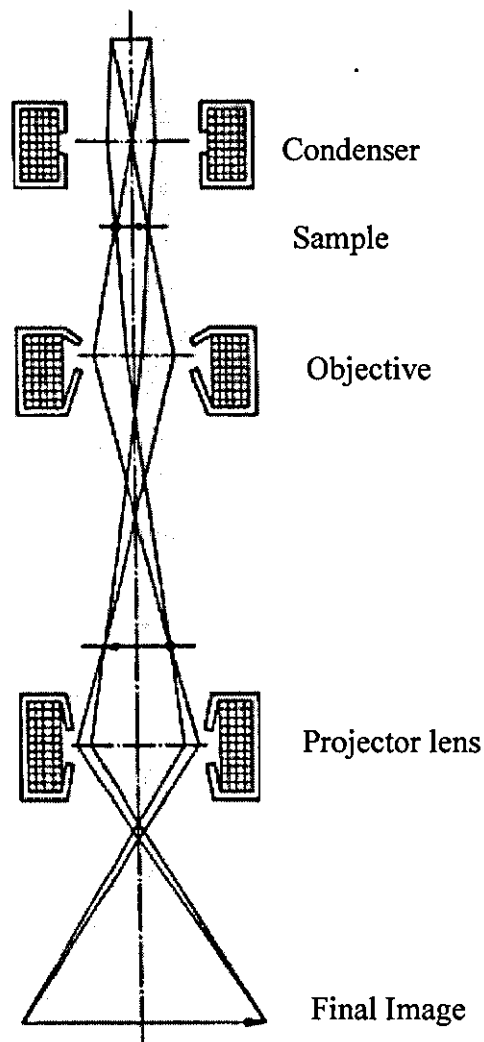


Figure 2.15: Schematic of the TEM

SEM is a much more useful technique, particularly for looking at surface topography. Compared with an optical microscope at the same resolution, the SEM has 10 to 100 times the depth of field. A particular feature of the SEM is the capability to detect backscattered electrons and hence perform elemental analysis. This technique is known as energy dispersive X-ray analysis, (EDX). The operator can simply select the area of interest and perform EDX to generate a composition “map” of that area. SEM can be used for a wide range of materials and again the only problem is that of

charging non-conductive samples. This is overcome by depositing a thin metallic layer over the specimen. A schematic of the SEM process is shown in Figure 2.14.

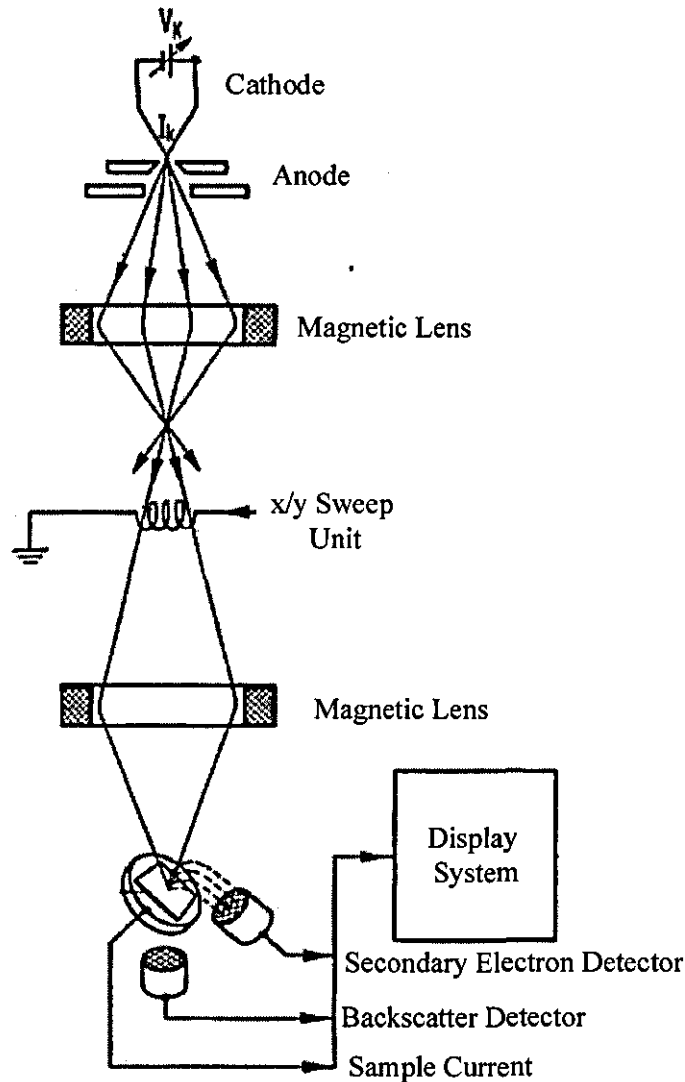


Figure 2.16: Schematic of the SEM

iii) Scanning Probe Microscopy

Traditional microscopes use a lens to focus a beam of radiation (i.e. visible light, UV radiation or an electron beam) onto the surface of a specimen. The resolution of these types of microscopes is limited by the wavelength of the radiation or Abbe's criterion¹³¹. This criterion defines the resolution of a microscope that uses lenses to focus a beam of radiation as $\lambda/2$, where λ is the wavelength of the radiation. These microscopes are known as "far field" microscopes.

If an aperture is used to provide a beam instead of a lens, Abbe's criterion is no longer valid. Resolutions of $\lambda/200$ have been reported for this type of microscope, known as "near field" microscopes¹³². Using a tiny aperture in an opaque film and microwave radiation of wavelength of 3m, it has been possible to achieve the resolution of 150 μ m. Such a large wavelength was used because the technology to position and scan with nanometre precision was not available. Today, it is possible to achieve this precision using piezo-ceramics with feedback loops.

The search for smaller and smaller apertures led to the development of the Scanning Tunnelling Microscope (STM), which allows atomic resolution. The resolution of such a microscope is directly proportional to the size of the aperture. In a STM, the aperture is a single atom of tungsten, which acts as an aperture by permitting electrons to tunnel through it onto the surface of the specimen. The size of the aperture is therefore about 0.2nm. The wavelength of the electron beam is 2nm and the tip scans across the specimen, measuring topography by monitoring the intensity of the field generated by the probe. In this way, a constant tip/specimen is maintained. This technique is only suitable for highly conductive samples.

Atomic Force Microscopy

The Atomic Force Microscope (AFM) measures the topography of a specimen by monitoring the repulsive forces acting on a small diamond tip. This is due to the overlap of the electron cloud of the last atom on the very end of the tip with that of atoms on the specimen surface¹³³. The diamond tip is attached to gold foil whose deflection is monitored by a STM. This device operates in a repulsive mode and is in contact with the specimen. Forces of the order of 10^{-9} N are detectable¹³⁴.

For non-contact measurement a very fine tungsten wire attached to a fine cantilever spring, is used to measure repulsive forces as small as 10^{-11} N in magnitude¹³⁵. A laser deflection sensor has to be used to track the movement of the tip that is attached to a long thin cantilever. The principle of operation of an AFM is shown in Figure 2.15.

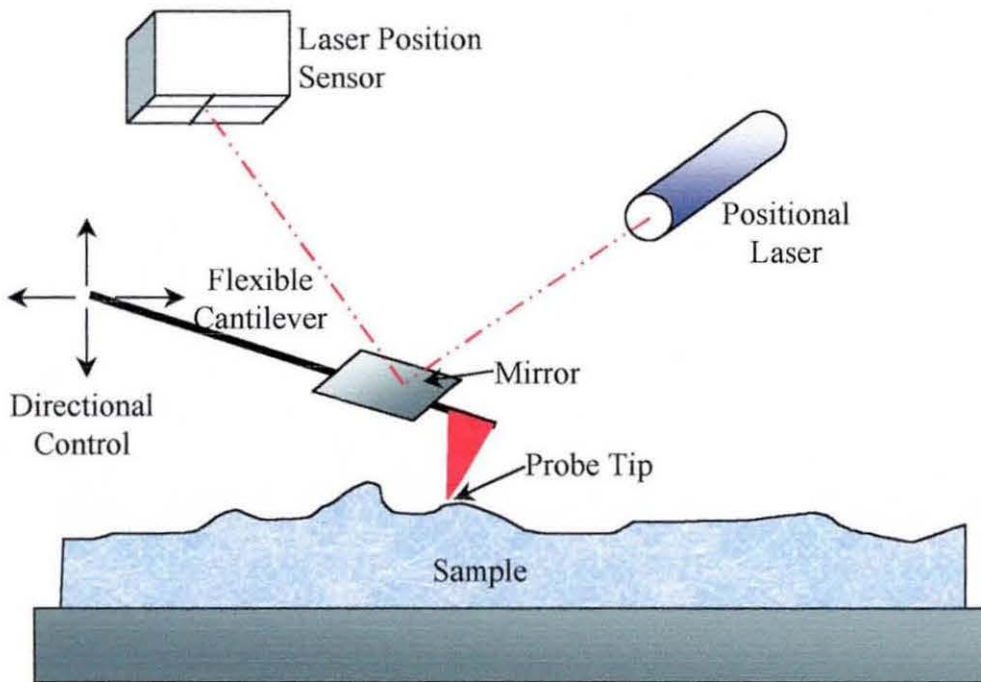


Figure 2.17: Diagram of AFM operating principles

Many recent developments have been made to AFM to enhance and refine the technique¹³⁶. A large range of probe tips is now available to measure many different aspects of a material:

- Lateral Force Microscopy (LFM).
Measures frictional forces between the tip and the specimen.
- Magnetic Force Microscopy (MFM).
Measures magnetic force gradients and distribution above the surface.
- Electric Field Microscopy (EFM).
Measures the electric field gradients and distribution above the surface.
- Electrochemical Scanning Probe Microscopy (ECSPM).
Measures topographic change in-situ due to electrochemical reactions.
- Tapping Mode.
Measures topography in air or under a fluid by tapping the surface with an oscillating probe tip.

- Scanning Thermal Microscopy (SThM).

Measures a variety of thermal properties.

SThM was used in this research programme.

In SThM, the probe tip consists of an ultra-fine wire connected to a Wheatstone bridge enabling both electrical current measurement and modulation. The wire is kept at constant temperature while it is rastered over the surface and records both topography and thermal properties. By varying the frequency of the applied voltage, it is possible to alter the depth to which the scan is sensitive. In this way, sub-surface features can be analysed which would not be possible using a conventional microscope. With the "Micro Thermal Analysis"¹³⁷ package it is possible to perform a topographic and thermal conductivity/diffusivity scan simultaneously. Once the image from this scan is viewed, points of interest can be selected and thermal analysis can be carried out on specific parts of the surface, which can be as small as a few cubic microns. As the microscope can measure both thermal change and vertical (z) displacement of the probe, it is possible to conduct many types of thermal analysis from DSC to DTMA. This can provide valuable information about microscopic features in the specimen that would have been impossible to obtain using conventional, comparatively large scale thermal techniques.

3.0 EXPERIMENTAL

3.1 Introduction

The application of any findings of this research will be in the joining of PVC pipes. In order to model the pipe/coupler/heater system, described in the Chapter One, a heater element was placed between compression moulded plaques. It was decided to mould these plaques from extruded pipe sections manufactured by Uponor Limited, rather than PVC pellets or powder as the use of this type of material gave the exact additive package used in the manufacture of PVC pipes. In order to aid diffusion between the plaques, a plasticised vinyl interlayer was sandwiched between them with an embedded heater wire. The incorporation of an interlayer provided a means by which heat could be transferred from the wire to the plaques; without this, the wire rapidly overheated, scorching and severely degrading the material. The heater was manufactured from Nichrome wire and shaped to the required size and heated by an electrical current. The use of resistance heating allowed a large number of potential interlayers to be assessed without requiring the use of *Smartheat* equipment, the use of which was subject to limitations. *Smartheat* was used to determine the effect of time, the main variable in the isothermal process, once interlayers were investigated. The degradation effect of *Smartheat* was studied and compared with resistance heating.

Welded components were sectioned to provide single lap shear tensile specimens. The lap shear strength of the specimens was measured and used as the primary performance measure of successful welding. Fracture surfaces were examined by optical microscopy, as was the development of the interface with increasing welding time. Depth of interlayer diffusion into the plaques was measured by Vickers hardness testing, the diamond indenter of the Vickers equipment allowed any orientation to be assessed by the difference in the perpendicular dimensions of the hardness impression, (it should be noted that this technique is not normally used in the analysis of polymers). The hardness of the heavily plasticised interlayers was determined by Shore A testing.

The rate and activation energy of diffusion of the plasticisers into PVC was determined by "wipe and weigh" or immersion diffusion testing. This was an important property of the plasticisers that merited exact measurement.

When the plaques were welded together, a temperature gradient was produced around the heater wire and as PVC is thermally unstable, it was necessary to identify any degradation caused in the welding process. Several methods were evaluated but with only limited success.

(a) Micro-thermal atomic force microscopy (μ TA) measured the change in softening point of the PVC around the heater wire caused by different levels of degradation at various distances from the wire. Despite early success resulting in publication, this technique did not have sufficient sensitivity to analyse anything but charred PVC. The lack of compositional information inherent in this technique was compensated for by laser induced mass analysis (LIMA) due, in part, to its ability to analyse a small area of material. However, LIMA is purely qualitative and cannot measure a degradation profile, the objective of the study, merely the presence of conjugated carbon to carbon double bonds.

(b) The tendency of carbon-carbon double bonds to fluoresce under ultraviolet (UV) radiation was exploited by using a microscope with an UV illumination source and light meter. The difference in fluorescence intensity was proportional to the concentration of carbon-carbon double bonds and hence degradation.

(c) By diverting the infrared beam from a standard FTIR spectrometer, it was possible to produce an "infrared microscope." This equipment, which had switchable visible and infrared illumination, allowed a small area to be "spotted" with the visible light, in exactly the same way as a standard optical microscope. By switching to infrared illumination, it was then possible to record a FTIR spectrum. The resolution of this equipment was improved by means of an adjustable aperture placed in the infrared beam path and was found sufficient to provide a profile of degradation away from the heater wire. Weak absorption of infrared radiation by carbon-carbon double bonds was overcome by derivatisation with bromine using a novel vacuum technique.

3.2 Materials

The substrate material was extruded and sectioned *Mondial* molecular oriented PVC pipe, manufactured by Uponor Limited for potable water transport. This material was chosen as it had the exact additive package that would be present in the intended application. The use of a “virgin” PVC resin, free of additives, would mean that any finding of this research would not necessarily be true for the type of PVC used by Uponor Limited. The additive package was a proprietary secret and was not revealed by Uponor Limited to the author during the course of this work.

Interlayer resins were made in this research of two types, vinyl chloride/vinyl acetate copolymers, and PVC homopolymers, as described in table 3.1.

Table 3.1: Interlayer formulations

Notation	Trade Name	K-value	% Acetate Content	Manufacturer
6	GA6015	45	14	Elf Atochem
7	GA7701H	57	9	Elf Atochem
9	GA9028	59	10	Elf Atochem
57	N/A	57	0	EVC
60	N/A	60	0	EVC
68	N/A	68	0	EVC
74	N/A	74	0	EVC
80	N/A	80	0	EVC

Plasticisers were chosen to give a reasonable range of diffusion rates. Di(2-ethylhexyl) phthalate or di-octyl phthalate (DOP) was chosen as it was a commonly used benchmark plasticiser, i.e. it had a desirable combination of properties and was well used and understood. DOP was known as plasticiser D.

Benzoflex 2088 (manufactured by Velsicol Chemical Corporation) was chosen as it was a fast fusing benzoate-based plasticiser. This was known as plasticiser B.

Benzoflex 2088 had the following composition:

Diethylene glycol dibenzoate	45.00 wt.%.
Dipropylene glycol dibenzoate	23.10 wt.%.
Triethylene glycol dibenzoate	24.20 wt.%.
Diethylene glycol monobenzoate	2.93 wt.%.

Dipropylene glycol monobenzoate 1.25 wt.%.

Admex 523 (also manufactured by Velsicol Chemical Corporation), was chosen as it was a slow fusing polymeric plasticiser ($M_w \sim 9000$) with high permanence. Admex 523 was known as plasticiser A. Admex 523 was a dibasic acid glycol polyester.

Both Benzoflex 2088 and Admex 523 carry FDA certification for food contact applications, an important issue in potable water transport.

The stabiliser used was a generic tin-based stabiliser.

3.3 Sample Preparation

3.3.1 Compression Moulding

The base material used in compression moulding was sectioned *Mondial* feedstock, the trade name of Uponor Limited's MoPVC (oriented PVC pipe). The feedstock was removed before the orientation process, see Figure 3.1, below.



Figure 3.1: Compression moulding feedstock

The reason for using this material was that it ensured the correct additive formulation and meant that compression moulding was essentially a re-shaping rather than a fusion process, (as would be the case if pellets were used), and allowed a much shorter compression moulding cycle time. The early attempts made in this programme to produce test plaques from PVC pellets resulted in incomplete fusion at acceptable moulding times and temperatures, i.e. the thermal history of the plaque was such that a further thermal process (welding) was possible without causing excessive degradation.

Backing plates were specially made for this programme from polished steel to the same dimension as the press platens, 180 x 180mm. The reason for this was that an oversize mould was found to give the best surface finish, with no trapped air, which had been observed when using moulds of the exact plaque size. 4mm spacers were used to give the required plaque thickness and sheets of Melinex were used to prevent PVC sticking to the backing plates, protect the moulds from degradation products and give a high quality surface finish.

During compression moulding, three separate presses and two sets of backing plates were used. One press was used for heating the pipe sections and compression moulding, one for pre-heating the backing plates and the third for cooling. The heating/moulding press was kept at 200°C and used for pressing the material from a half cylinder to a rough plaque as shown in Figure 3.2.



Figure 3.2: Plaque after compression moulding

The second press was operated at 200°C and was used for pre-heating one set of moulds while the other set was in use. Without the pre-heating press, the compression moulding process took considerably more time to complete. The third press was used as a cooling press and was constantly cooled by a flow of water at ambient temperature. The presses were hydraulic, hand operated, electrically heated and water-cooled. The heating and cooling presses were capable of achieving and maintaining a piston pressure of 7 MPa.

The moulding cycle was as follows:

1. Bottom backing plate, Melinex and spacer placed in heated mould at 200°C, then pipe section placed on top.
2. Second backing plate positioned on top of the pipe section, no pressure.
3. Pipe heated for 60 seconds.
4. Press slowly closed until a pressure of 1.6 MPa was reached.

5. Material allowed to flow for 60 seconds.
6. Pressure raised to 4.9 MPa in 1.6 MPa increments, allowing a few seconds for flow at each increment.
7. Pressure maintained at 4.9 MPa for a further 60 seconds.
8. Mould transferred to cooling press and pressure steadily raised to 4.9 MPa.

(Note: Machine scale was imperial tons on a 4" piston)

The heating and shaping process took 4 minutes to complete, whilst the cooling stage took a further 90 seconds to reach approximately 15 to 25°C, depending on cooling water temperature. The pressure cycle used is illustrated below in Figure 3.3.

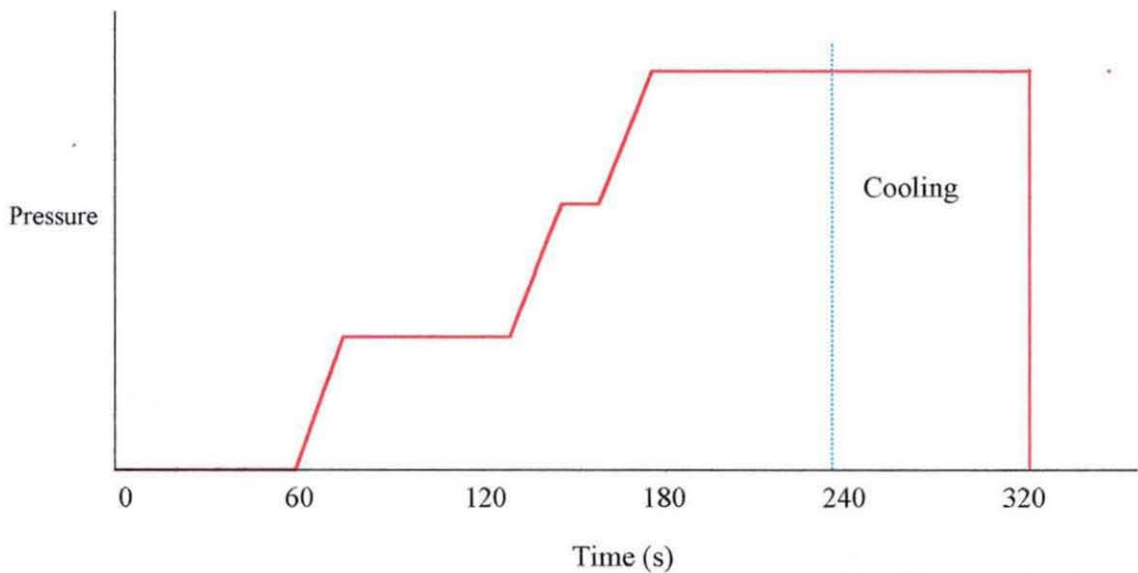


Figure 3.3: Schematic of compression moulding pressure cycle

Following compression moulding, the plaques were cut to size using a high-speed saw with a diamond blade. This type of saw allowed plaques to be cut accurately with smooth edges, free from cracks and other defects, which required no further finishing.

Figure 3.4 shows the finished plaque.



Figure 3.4: Completed plaque

3.3.2 Interlayer Preparation

The purpose of using an interlayer was to provide an effective means of conducting heat from the wires to the substrates. It was also apparent that the highest strength joint would be one where interdiffusion across the interface had occurred, causing interlocking of the polymer chains from either side of the interface. With this in mind, and an awareness of the low thermal stability of PVC, it was decided to use an interlayer as a heat transfer agent capable of promoting and accelerating the interdiffusion process.

Other requirements of an interlayer material were as follows:

- Correct quantities of plasticiser and resin.
- Thermally stabilised.
- Highly compatibility with the PVC substrates.
- Ease of handling.

A solvent-casting method was selected to produce interlayers, as this method fulfilled all the above requirements and importantly, this process did not cause premature thermal ageing of the interlayer. The solvent originally selected was acetone, as this was a good solvent and readily dissolved all components. However, this was changed to tetrahydrofuran (THF) soon afterwards, with improved solvent properties for the interlayer raw materials.

The method of interlayer preparation was as follows:

THF (250ml) was poured into a beaker with the required volume of plasticiser. The resin was accurately weighed with an additional 5% weight employed to allow for material which became adhered to the weighing beaker. The resin was added very slowly to the THF/plasticiser under moderate (~100rpm) stirring. Finally, the stabiliser was added, stirring continuing for a minimum of five minutes using an electrical stirrer with a short rotor designed for high viscosity liquids. Agglomerates were found to form very easily if the resin was added too quickly and longer stirring times encouraged any agglomerates to dissolve.

The resulting solution was then poured into a stoppered flask and stored at -30°C for at least five hours. The purpose of cold storage was to prevent solvent and other volatiles evaporating. As a bonus, it was found that interlayers that were cast from pre-chilled solution exhibited no gas entrapment whatsoever with any formulations, while non-pre-chilled interlayers were generally unusable due to the extent of gas entrapment.

The moulds for casting interlayer sheets was made from a poly(tetrafluoroethylene) (PTFE) backing plate surrounded by a compression moulding spacer and the gap between the two was sealed using cellulose tape. Casting was carried out in a fume cupboard and took approximately 8 hours to produce a solid, coherent sheet of interlayer, depending on ambient temperature. When the solvent had fully evaporated, the interlayers were peeled from the PTFE sheets and stored between Melinex sheets or used immediately.

The following system was used to identify interlayers throughout the project.

Example 1: 57/40B.

57 denotes the resin used (see Table 3.1).

40B denotes the concentration and type of plasticiser used, in this case 40 wt.% Benzoflex.

Example 2: 9/20A

GA9028 with 20 wt.% Admex.

Tables showing all interlayer formulations are described fully in Appendix 1.

3.4 Welding of Plaques

Heater elements were prepared by shaping Nichrome or *Smartheat* wire around a jig, as shown in Figure 3.5.

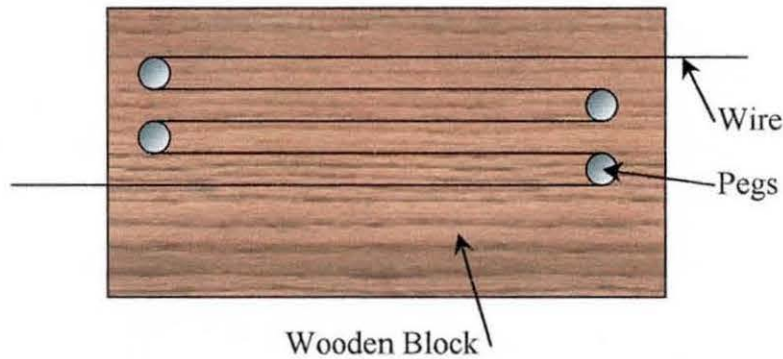


Figure 3.5: Schematic of heater jig

The heater wire came supplied on small rolls and had a tendency to remain coiled even when cut from the roll. To prevent curling of the heater element, it was necessary to straighten the coiled wire before it was shaped. This was done by cutting the required length of 700mm, followed by the application of a tensile force along the whole length of the wire. To ensure an even spacing of the wires the ends were taped with high melting point, solvent resistant tape.

The interlayer was cut to half the size of a plaque and placed on top, with the heater element above it. The second PVC plaque was placed over the heater element and the element pressed into the interlayer using a mass of 11kg, as illustrated in Figure 3.6.

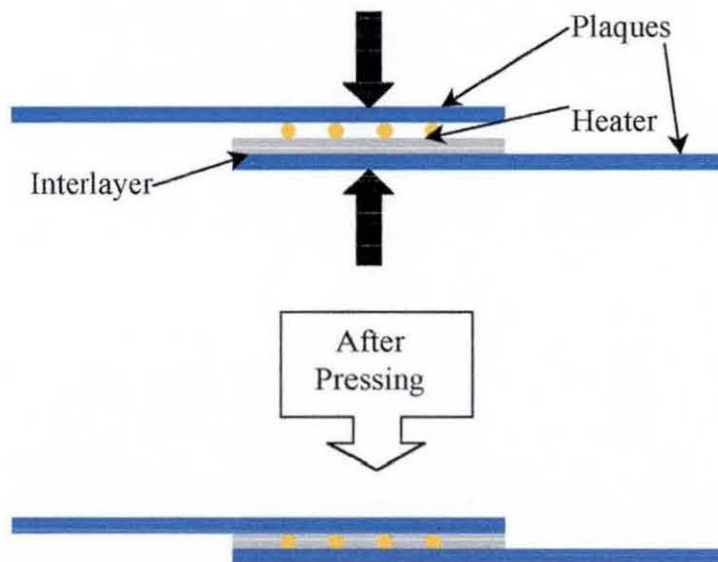


Figure 3.6: Assembly of component before welding

Once the component was assembled, the heater element was connected to the power supply, the timer set for 120 seconds and the welding operation was begun. The power supply consisted of an electrofusion control box, supplied by Uponor Limited that had been modified to both measure and adjust its power output. The power output was set to give 22.5 ± 0.5 volts and 3.5 ± 0.2 amps. These settings were kept constant in the production of welded samples throughout the project. The assembly was held together by a mass of 11kg that was not varied during the course of the research, as this parameter was not under investigation. The control box was switched on and automatically stopped after the required welding time.

Once cooled, each welded assembly was sectioned to give a sample width of 22mm, allowing three samples per assembly after removal of the end sections of the element. By removing the edges of the plaque, (containing the 180° bends of the heater wire and the securing tape) it was possible to reduce errors. Before this practice was adopted, experimental scatter was obscuring any trends in the data; this deleterious scatter was significantly reduced by adopting the sectioning technique described. The samples were then ready for testing.

3.5 Lap Shear Testing

Lap shear testing was conducted using a *Lloyd* universal tester in the single lap tensile mode, with the samples off-set in the jaws of the tensile tester, using custom made aluminium spacers. The purpose of offsetting the sample is to prevent deleterious off-axis loads during testing¹³⁹. The machine settings were as follows: 5kN load, 20mm extension and 25 mm min⁻¹ crosshead speed.

The mode of failure was recorded for each specimen, along with the number of pieces resulting from fracture created during failure (if necessary), and the load and extension at failure. An x/y plotter was used to record the test data. Due to the problem of jaw slippage, heavy duty, hand-tightening grips had to be used.

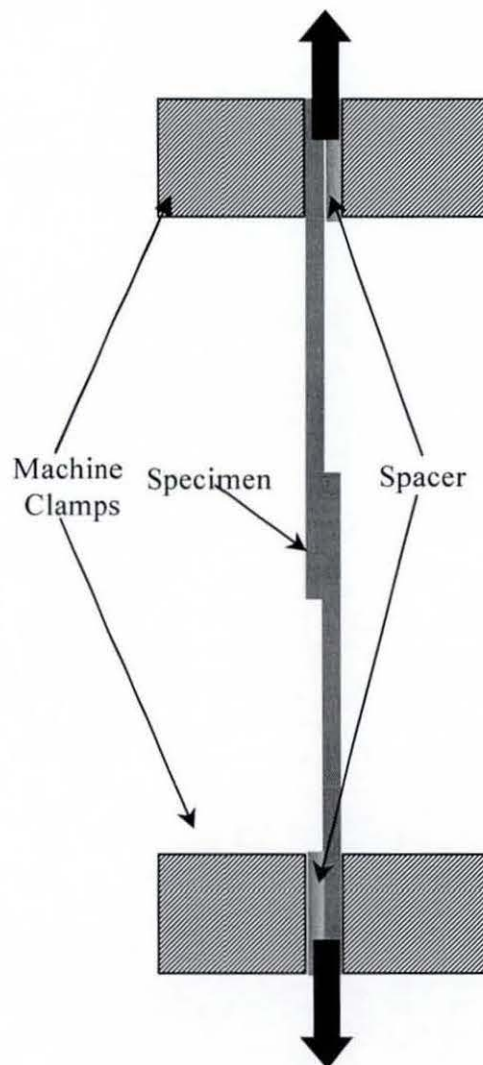


Figure 3.7: Lap shear testing schematic showing spacers

3.6 Optical Microscopy

Low power optical microscopy was used to examine fracture surfaces for signs of yielding and hence interdiffusion. This was conducted on a *Ziess* stereo zoom microscope. To produce micrographs a CCTV camera attached to a *Sony Mavigraph* colour video printer, connected via a monitor, was used.

Fracture surface analysis required no additional sample preparation. However, interface analysis required polishing with wet and dry emery cloth followed by polishing on a 6 μ m nylon polishing wheel. Due to the low magnification used, it was found that polishing was not necessary. The use of a 6 μ m diamond polishing paste and a lubricating/cooling liquid greatly facilitated polishing. Samples were cleaned in an ultrasonic bath using liquid soap, since using solvents for cleaning was not possible due to the risk of solvent extraction of the interlayer.

3.7 Hardness Testing

3.7.1 Vickers Hardness

Vickers hardness was conducted in order to determine the depth of diffusion in samples. This was achieved by taking measurements across the interface and into the bulk of the material.

Although Vickers hardness testing is not normally used for polymer testing, a review of literature has shown that this technique is also able to measure orientation in a material¹¹⁴⁻¹²¹. The plaques themselves contained no orientation but it was important to test for any orientation in the interfacial zone that may have resulted from flow of material during the welding process. This property manifests itself as a difference in the perpendicular dimensions of the hardness indentation. If the material possessed no orientation, the perpendicular dimensions were the same.

3.7.1.1 Depth of Diffusion

Samples were prepared by polishing to $6\mu\text{m}$ using wet and dry emery cloth followed by a polishing wheel, using the same method as described for microscopy samples (it was necessary to polish samples to provide sufficient reflectivity of the specimen to view the indentation). A standard Vickers hardness tester with a 1kg mass and diamond indenter was used, with specimens being clamped in a drill vice, as shown in Figure 3.8.

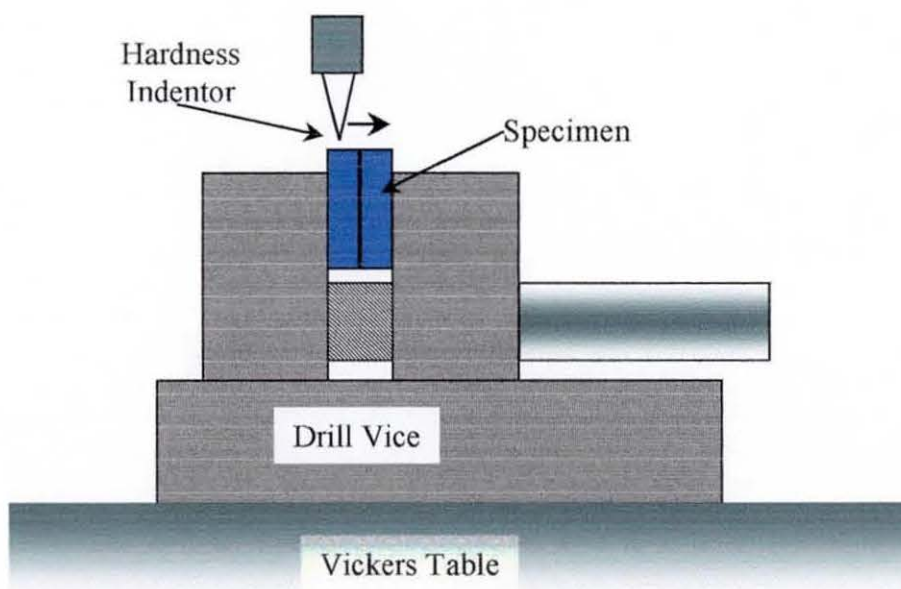


Figure 3.8: Diagram of Vickers hardness testing

By using the built-in magnification system on the Vickers equipment, it was possible to position and reposition the specimen to give a separation between hardness indentations of 0.5mm. This subsequent separation was measured using a travelling microscope and plotted against hardness number to produce a graph showing hardness at different points across the interface of a specimen. This technique has not been widely used for measuring the hardness of plastics but by accurately reproducing the test each time, it gave acceptable results. The tracking of hardness indentations produced can be clearly seen in Figure 3.9.

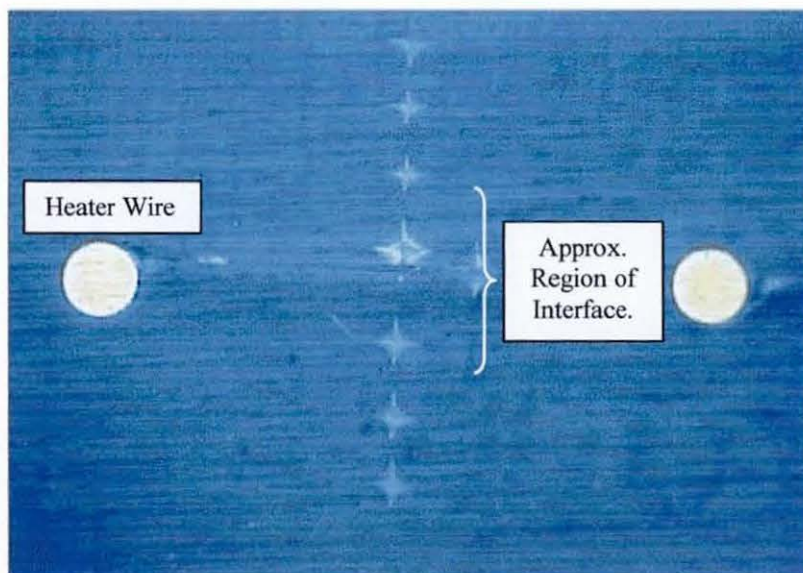


Figure 3.9: Vickers hardness indentation track

3.7.1.2 Evaluation of Orientation

Samples were taken from three sources: unoriented feedstock (as used in compression moulding), fully oriented MoPVC (*Mondial*) pipe and MoPVC pipes that had undergone a recovery process. The recovery was achieved by heating in an air oven at 90°C until no further dimensional change was observed. These materials were chosen as they were identical in every way to any welded specimens that could be tested except for the extent of orientation present.

Coupons were cut from the samples to a size of approximately 400mm² and polished in the manner described for diffusion testing, taking extreme care that opposite faces of the sample were parallel. The perpendicular dimensions of the indentation were influenced by how parallel the specimens were and this was checked by making an

indentation and then examining its dimensions. Any non-parallel samples could be identified by a distorted indentation, as indicated in Figure 3.9.

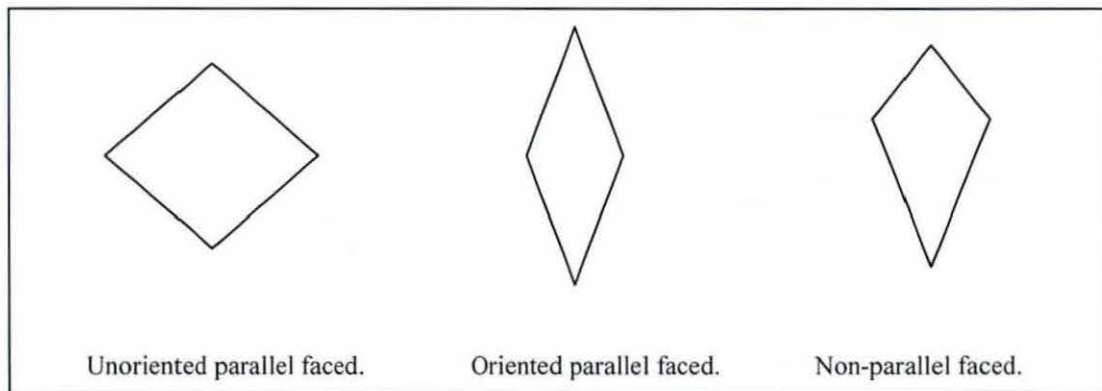


Figure 3.9: The three types of indentation observed

If a non-parallel indentation was observed, the sample was re-polished and re-tested. Since even a small deviation from parallel would affect the results, the samples were rotated by 90° and re-tested; differences in the two sets of results indicated a misalignment of the Vickers equipment itself. Five suitable indentations were taken from three different positions on the MoPVC samples at the inside and outside diameters and at the edge. The recovered material was tested in the bulk and the feedstock on the inner diameter and the edge. The MoPVC was most thoroughly tested because it had been intentionally oriented whereas the other samples contained only small amounts of residual orientation.

3.7.2 Shore A Hardness

In order to provide comparative data to supplement the Vickers micro-hardness, Shore A testing was conducted. This was done in a completely standard fashion, according to BS EN ISO 868:1998, using thick interlayer samples. These were prepared in a standard manner but were cast into small PTFE dishes to produce a sample with a thickness of 5mm. The equipment was checked against calibrated rubber standards of known hardness and 10 tests conducted on each sample.

3.8 Immersion Diffusion Testing

In order to determine the rate of diffusion of plasticisers into the PVC substrates, it was necessary to make several measurements of mass uptake. These readings were obtained at 50, 60, 70 and 80°C by immersion diffusion testing.

The immersion diffusion test (shown schematically in figure 3.10) consisted of suspending a test specimen (30x30x3mm) in a plasticiser contained in a beaker, the container being heated in an even temperature oven to the desired temperature. To prevent possible evaporation of the plasticiser, the top of the beaker was covered with aluminium foil. At appropriate time intervals, the samples were removed from the liquid, wiped to remove the plasticiser from the surface and weighed; for this reason the test is also known as “wipe and weigh” diffusion testing. The mass increase may be plotted against the square root of immersion time and the testing is continued until an accurate weight measurement can no longer be obtained due to sample disintegration.

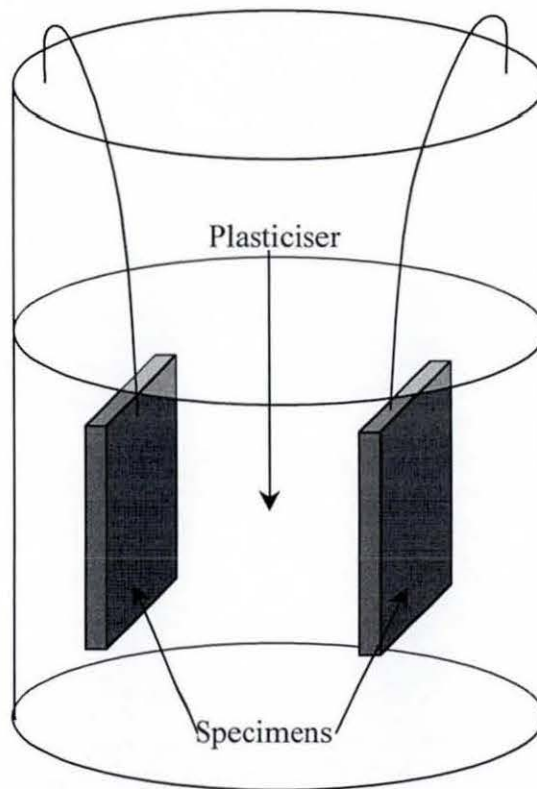


Figure 3.10: Schematic of immersion diffusion test

3.8 Immersion Diffusion Testing

In order to determine the rate of diffusion of plasticisers into the PVC substrates, it was necessary to make several measurements of mass uptake. These readings were obtained at 50, 60, 70 and 80°C by immersion diffusion testing.

The immersion diffusion test (shown schematically in figure 3.10) consisted of suspending a test specimen (30x30x3mm) in a plasticiser contained in a beaker, the container being heated in an even temperature oven to the desired temperature. To prevent possible evaporation of the plasticiser, the top of the beaker was covered with aluminium foil. At appropriate time intervals, the samples were removed from the liquid, wiped to remove the plasticiser from the surface and weighed; for this reason the test is also known as “wipe and weigh” diffusion testing. The mass increase may be plotted against the square root of immersion time and the testing is continued until an accurate weight measurement can no longer be obtained due to sample disintegration.

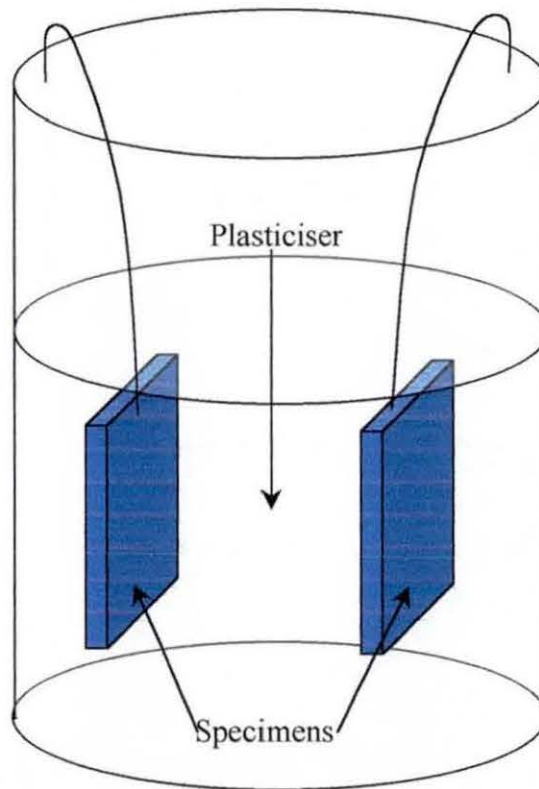


Figure 3.10: Schematic of immersion diffusion test

3.9 Atomic Force Microscopy

With the aim of assessing degradation of PVC in terms of changing softening point, micro-thermal (μ TA) atomic force microscopy (AFM) was carried out on a sample supplied by Uponor Limited. The sample was a PVC pipe and coupler welded using the *Smarteat* process. It was composed of a pipe and coupler of different colour which aided analysis, the coupler was brown and the pipe was blue. The sample had been fused using a high temperature wire; Uponor Limited reported that the pipe and coupler assembly began to emit smoke and therefore had to be stopped at 30 seconds due to charring of the sample.

The AFM has a maximum vertical (z) displacement of $100\mu\text{m}$ so it was important that the sample did not contain any irregularities of greater height. To prepare the sample for the AFM, it was first sectioned to a suitable size and then hand polished using the method previously described; the specimen required no further preparation for analysis in the AFM. The sample was sectioned in such a way as to slice through the wire in both the hoop and longitudinal directions to enable the effect of heating on more than one plane to be evaluated. Along the wire in the longitudinal direction, the PVC was found to be heavily degraded and voids had formed around the wires. These voids showed up as areas of high contrast on the AFM and so it was essential to avoid them. As a result, it was necessary to choose a wire that was in contact with the PVC and not one surrounded by voids, in order that the wire/PVC interface could be scanned.

By choosing a wire that still had material in contact with it, the wire could also be scanned so that the wire/PVC interface could be analysed. AFM can collect data in a variety of modes over a $100\mu\text{m}$ square area and both topography and thermal conductivity features were measured. One scan in the thermal diffusivity mode was completed but this showed little useful information. Both sets of data are collected simultaneously and provide complimentary information. In this case, particles of the metal wire dislodged during sample preparation showed a large contrast on the thermal conductivity scale, due to their large heat capacity in comparison to the PVC. By comparing both thermal and topographical data, it was possible to see the position of the particle and whether it was continuous with the PVC. Pits and troughs also showed as areas of contrast and the topographic information helped differentiate these features from areas of different thermal conductance.

The first scan was close to a wire but did not go over the wire itself. On completion of the thermal conductivity and topography scan, three points were selected on the topography "map" and micro thermal analysis was performed at these points. The mode of thermal analysis in this case enabled the softening point of the material to be determined. The tip of the probe was heated to 400°C at 10° per second and its vertical displacement recorded, enabling features identified in the scans to be further investigated. After the μ TA was completed, another scan was performed to survey the extent of the damage done by the probe.

The second scan was positioned to overlap the first but was placed further away from the wire to enable the effect of the temperature profile caused by the heating of the embedded wire to be investigated. Successive scans were positioned in this way, moving away from the wire until the weld line was reached. As the microscope had no way of measuring the distance from one scan to the next, the damage produced by micro-thermal analysis was used as a marker. It was necessary at one point to clean the probe of PVC degradation products, which was done by raising the probe clear of the sample surface and rapidly heating it.

The video camera attached to the microscope was black and white meaning that the two sides of the assembly did not show any contrast. However, in the topography image a weld line was visible as a thin line running along the sample. Both the thermal conductivity and the topography clearly showed the weld line and enabled μ TA to be performed on top of the weld line and also on either side. On reaching the weld line the probe was moved parallel along it to permit another scan to be made. As before, μ TA was performed on either side and over the weld line itself. The resulting maps were assembled to produce a L-shaped composite image, reaching from the heater wire to the interface itself.

As the sample described above had been exposed to a large amount of heat, individual coupons of PVC were prepared in an oven at 220°C at times from 1 to 5 minutes in order to determine the sensitivity of the AFM technique. Samples were prepared and tested in exactly the same way as the first experiment, topography images were produced, softening points taken and results compared to the control sample.

3.10 Laser Induced Mass Analysis

Laser induced mass analysis (LIMA) enables elemental analysis to be performed over a small area and it was this ability that led to the selection of this technique over other spectroscopic techniques available.

The device used in this analysis was a LIMA 2A manufactured by Cambridge Mass Spectrometry. The objective of the experiment was to determine the composition of the unidentified material found along the weld line during the first AFM analysis. The sample analysed by LIMA was the same degraded sample supplied by Uponor Limited that was analysed by AFM, as described in Section 3.8. The sample was cut to the correct size for the LIMA sample holder and was not altered in any other way. During cutting, two halves of the sample became separated and care was taken to ensure that the original interface could be located and remained undamaged.

Like most other spectroscopic techniques, LIMA requires a vacuum in the sample chamber. Once the vacuum was reached, both positive and negative spectra for the sample were taken; these are used together to determine the species present. Several background spectra were obtained for comparison purposes.

The spectra labelled “background” were taken from the bulk of the coupler (brown).

The spectra labelled “edge” were located on the edge of the coupler where the unidentified material was located.

The spectra labelled “blue particulate” were taken from the accidentally exposed interface on the pipe (blue) side of the sample.

The spectra labelled “blue bulk” and “brown bulk” were taken away from the interface in the bulk of the material.

3.11 Ultra-violet Fluorescence Microscopy

When PVC degrades, carbon-carbon double bonds are formed. UV fluorescence microscopy exploited the tendency of these bonds to fluoresce in the visible region of the electromagnetic spectrum when exposed to UV light. A mercury vapour bulb was used as the source of UV and was attached to a universal microscope. By measuring the intensity of fluorescence at various distances from the heater wire it was hoped that a profile of degradation could be obtained; this phenomenon is shown in Figure 3.11.

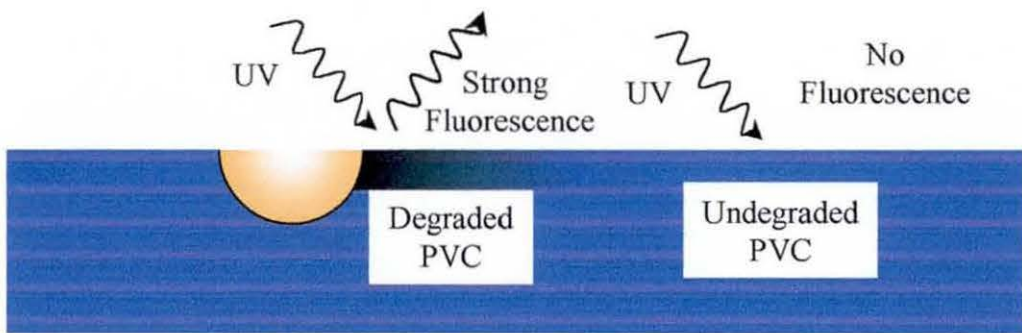


Figure 3.11: Schematic of degradation profiling using UV fluorescence

3.12 Infrared Spectroscopy

Infrared spectroscopy consisted of three stages. The first stage consisted of preparing samples for the second, derivatisation stage while the third stage was the analysis itself.

Infrared spectroscopy was conducted using a standard *Nicolet* Fourier transform infrared spectrometer (FTIR). By diverting the beam from the main body of the FTIR it was possible to attach accessories. The accessory used in this study was a *Spectra Plan* infrared microscope having selectable infrared and visible light illumination. The desired area is located by using the microscope in the same way as a conventional optical microscope, followed by switching to infrared to allow the diverted IR beam to pass through the sample and back into the detector of the FTIR to produce the usual spectrum. By blocking part of the infrared beam with an adjustable aperture, the area analysed could be reduced. In this study, the area was made as small as possible while retaining sufficient infrared signal throughput. It was essential to ensure that the infrared beam was precisely aligned along the signal path and focussed in the same plane as the visible light. If this was not achieved, the signal throughput was insufficient for the FTIR detector to function.

3.12.1 Sample Preparation

Welded samples were prepared and sectioned in the same way as for lap shear samples but with a 10mm sample width. After removal of the wire sections using a punch and hammer followed by preliminary polishing, specimens were microtomed from the surface perpendicular to the plane of the wire. A glass knife was used at room temperature and gave excellent results, but due to the fragility of the knife it had to be changed frequently. The thickness of the microtomed samples was 10 μ m.

3.12.2 Derivatisation

A carbon-carbon double bond exhibits a weak IR absorption peak¹⁴⁵ between 1700 and 1600 cm^{-1} , depending on its chemical state. An isolated double bond has a peak between 1680 and 1600 cm^{-1} , which is usually very weak, while dienes ($\text{C}=\text{C}=\text{C}$) and trienes ($\text{C}=\text{C}=\text{C}=\text{C}$) have stronger peaks at 1650 and 1600 cm^{-1} respectively. A carbon-bromine bond has a strong peak at 750 to 550 cm^{-1} . Since a polymer that contains a distribution of conjugated alkene groups will give a series of peaks, some

of them weak or overlapping, it was advantageous to replace them with a single strong peak.

Bromine may be added across a carbon-carbon double bond at room temperature in a normal atmosphere. Early attempts to derivatise the double bonds under a normal atmosphere and room temperature were unsuccessful, and thus it was decided to utilise more stringent reaction conditions.

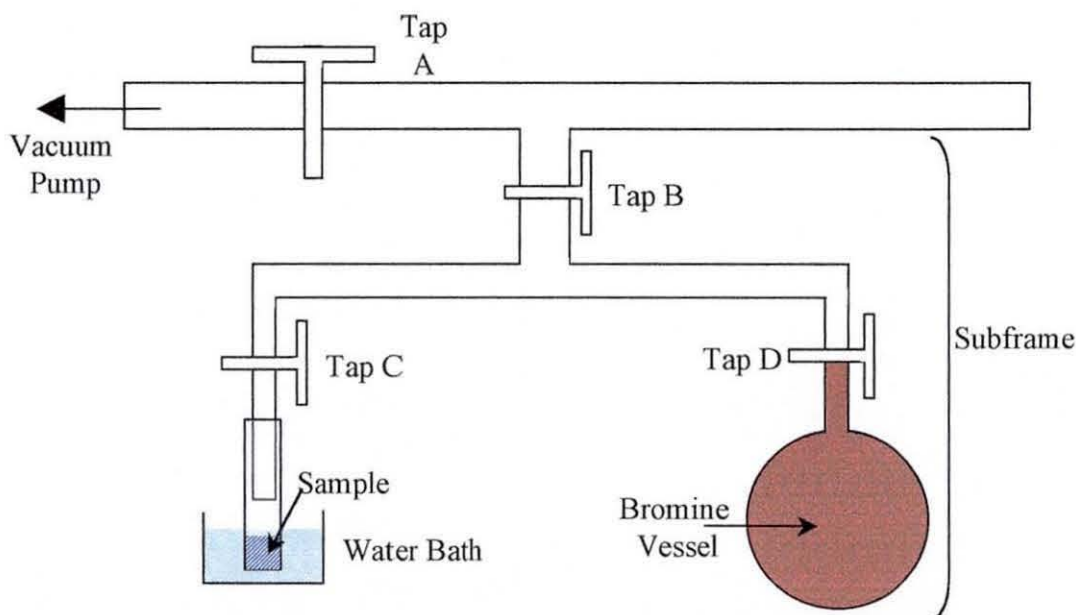


Figure 3.12: Schematic of bromination sub-frame

Figure 3.12 shows the configuration of the equipment used that consisted of a sub-frame attached to the main tube of a custom made vacuum frame.

During this experiment, any contaminants and diluting gases (air) were removed by holding the sample in a vacuum frame. The bromine was held in a separate vessel connected to the other half of the sub-frame. The samples were heated to their softening point (80°C) and contained in a vacuum test tube suspended in a water bath as it was anticipated that the increased molecular mobility at this temperature would significantly enhance the diffusion of bromine into the sample.

The bromine was freeze/thaw purified with liquid nitrogen several times to remove air and contaminants from the system and was introduced to the samples by opening Tap D, while isolating the sub-frame from the main vacuum frame by closing Tap B. Due to the vacuum above the samples, the bromine gas surrounded them instantly and rapidly reached its saturated vapour pressure. After one hour the unreacted bromine

was drawn back into its vessel by freezing with liquid nitrogen. Tap D was then closed to contain the bromine and Taps A, B and C opened to allow removal of excess bromine by the vacuum pump, with a cold trap being used to prevent reactants from contaminating the pump and vice versa. Using this method, several samples could be brominated at once by placing them in the same sample vessel.

3.12.3 IR Analysis

The set-up procedure for the IR microscope consisted of aligning the IR beam and focussing it on the same plane as the visible light beam and optimising the aperture size with respect to the signal throughput of the IR beam. Specimens were mounted onto a metal microscope slide across a 10mm circular hole and held in place with double-sided tape. The slide was placed onto the microscope table and the specimen examined until a suitable place for analysis was found. The microscope was then focussed using the visible light beam, following which the beam selector was switched to IR and the analysis begun. In order to compensate for the poor signal to noise ratio inherent in this type of IR analysis, 600 scans at 4 cm^{-1} were taken. Using the aperture as a positional guide, the field of view was moved radially away from the wire and another spectrum recorded. The aperture was regularly calibrated using a $1\text{ mm} \times 0.01\text{ mm}$ graticule. The spectra obtained were compared with a control spectrum taken from the bulk of a non-brominated sample. A nitrogen purge through the microscope was used to reduce noise due to water vapour and carbon dioxide in the immediate atmosphere.

Several different samples were analysed in the same way to ensure reproducibility and reliability of the data. Both resistance and isothermally heated samples were analysed at welding times of 90, 110, 120 seconds and in the case of the isothermally welded samples, 180 seconds. In total, five separate degradation profiles were obtained.

4.0 RESULTS AND DISCUSSION

4.1 Introduction

The objective of this work was to determine if a commercial grade PVC can be thermally welded. A simplification of the intended application, a pipe/coupler arrangement, consisting of a heater wire embedded in an interlayer between two flat plaques, allowed a number of different systems to be analysed. The main performance indicator for these interlayer systems was the tensile single lap shear test. Data from this test has allowed the identification of the mechanisms responsible for the development of strength in the system and additional tests have been conducted to support these results.

Lap shear data for all copolymer resins in combination with all plasticisers are given and homopolymer resins are shown with Benzoflex 2088 only. Benzoflex 2088 was identified as the best plasticiser when testing copolymers and it was decided to use this plasticiser alone with homopolymers since producing inferior interlayers was deemed unnecessary.

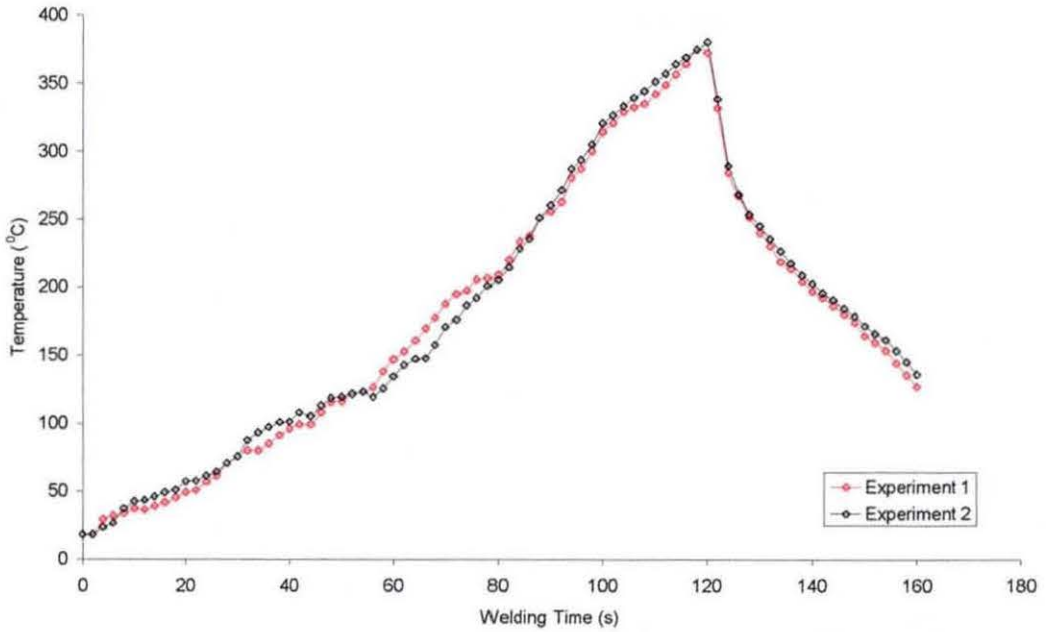
Optical microscopy shows how the interface developed as welding time was increased, giving rise to gradual elimination of the interface, Micrographs for both resistance and isothermal heating are also presented. Vickers hardness was used to determine the depth of diffusion by producing a track of indentations across the interfacial zone. The initial hardness of interlayers was measured by Shore A hardness testing and this was related to eventual lap shear strength. Immersion diffusion testing was used to determine the diffusion coefficients at different temperatures and hence the activation energy of diffusion for each plasticiser. It was found that the activation energy of diffusion, and hence diffusion rate, had a strong influence on lap shear strength. Atomic force microscopy was used in an attempt to analyse degradation around a heater wire by monitoring changing softening temperature but the technique lacked sufficient sensitivity and was not continued. Ultra-violet fluorescence was used for the same reason but lacked satisfaction due to a very large background fluorescence, most likely due to the pigment itself.

Microscopic infrared spectroscopy allowed a semi-quantitative measure of degradation. This was achieved by derivatising specimens removed from the

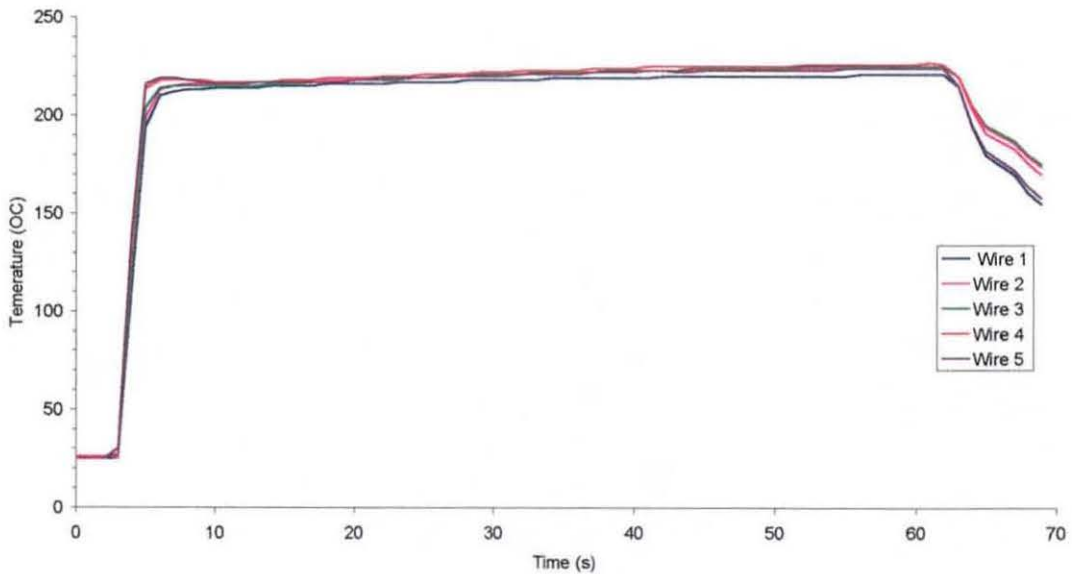
interfacial zone of the samples with bromine. Bromination was conducted at 80°C in saturated bromine and was entirely successful. The use of a small aperture allowed the plotting of a degradation profile around the wire. It was found that the profile of degradation products in isothermally welded samples had a plateau region immediately adjacent to the wire and decreased exponentially after this. The resistance welded sample showed no such plateau and degradation products decreased exponentially with increasing distance from the wire.

4.2 Welding

The following graphs present data obtained during the welding process. They provide a useful comparison of the two processes used in the course of this research.



Graph 4.2.i: Resistance welding temperature profile

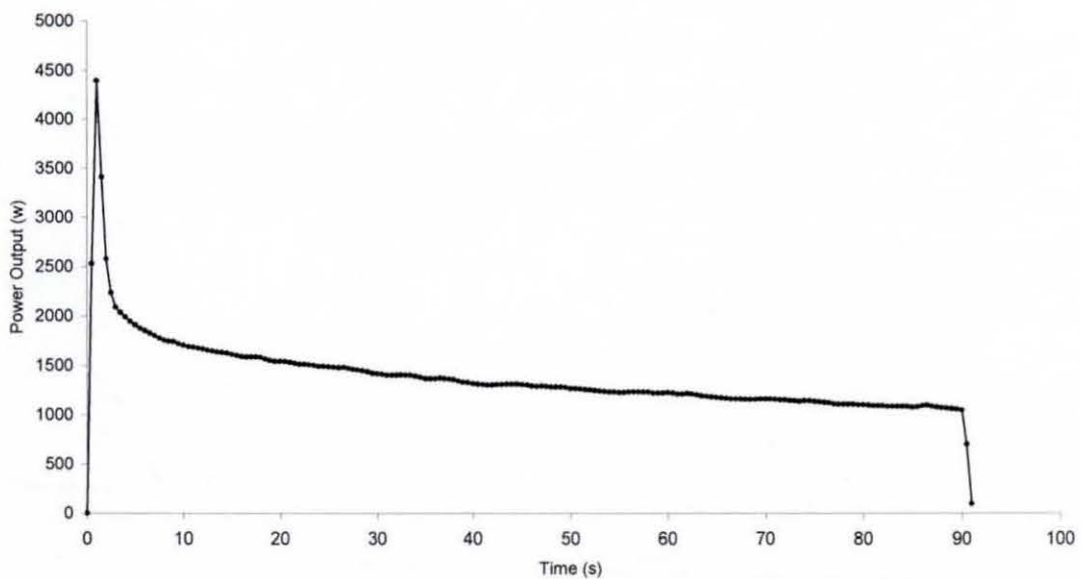


Graph 4.2.ii: Smartheat welding temperature profile

A multi-channel, data-logging thermocouple was used to collect data during *Smartheat* welding, which took several readings every second. As this was unavailable to take measurements during resistance welding, a single channel digital thermocouple was used, with one reading every two seconds. Other differences in the methods used to collect data were as follows: five E-type thermocouples were welded to *Smartheat* wires, whereas a single K-type thermocouple was placed as close to the resistance wire as possible.

Despite these differences, the isothermal advantage of *Smartheat* over resistance heating is clear to see. This advantage stems from the fact that PVC degrades in an autocatalytic way, leading to an exponential increase in degradation with increasing temperature. For example, to reduce the risk of degradation it was advantageous to hold the welding temperature at 220°C for 120 seconds, rather than reaching this temperature at 60 seconds and letting it increase to 440°C. For the same welding time and *energy* input, a wire with gradually increasing temperature will reach double the temperature of a isothermal process.

The power consumption of the *Smartheat* process provided a way to monitor progress during welding and this was achieved through built in meters, which did not interfere with the process in any way.



Graph 4.2.iii: *Smartheat* welding power consumption

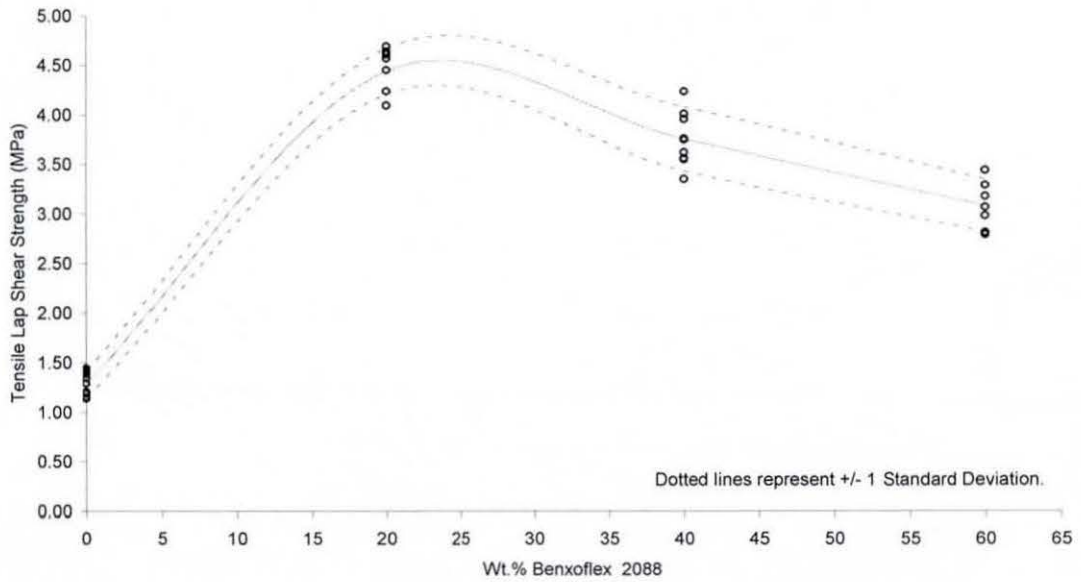
Graph 4.2.iii shows the power output of the *Smartheat* control box; the initial spike indicates the amount of power that was required to heat the wire to 220°C; the time taken to peak power shows the time the wire took to reach its autotherm temperature.

It was possible for the wires to move during the welding process. This would show up as an irregularity on the power curve as an unexpected minima or maxima.

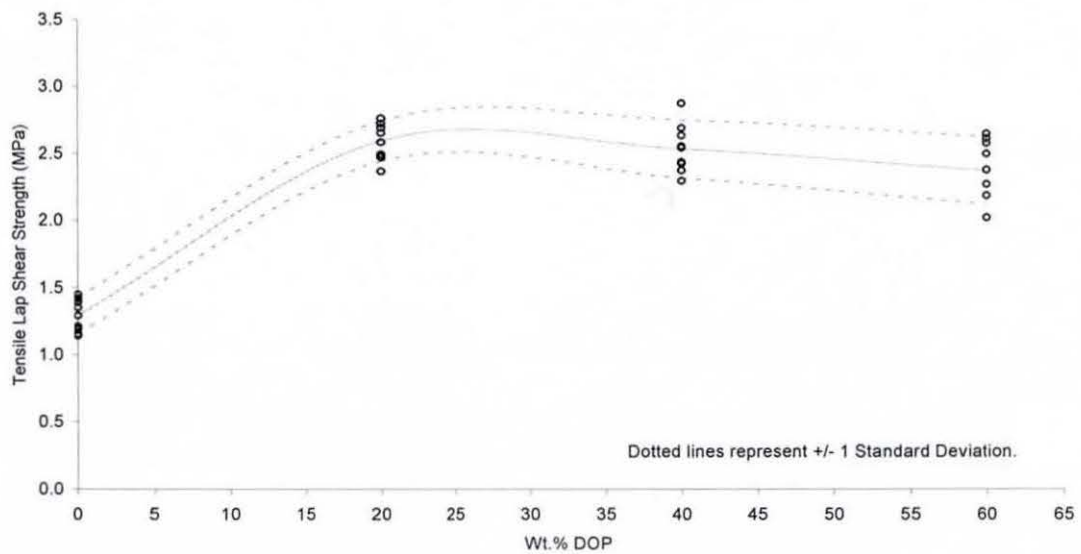
4.3 Tensile Lap Shear Testing

Lap shear tests were carried out on samples cut from welded plaques. The peak load during the test was noted, as was the mode of failure. The data are presented in groups corresponding to the resin type.

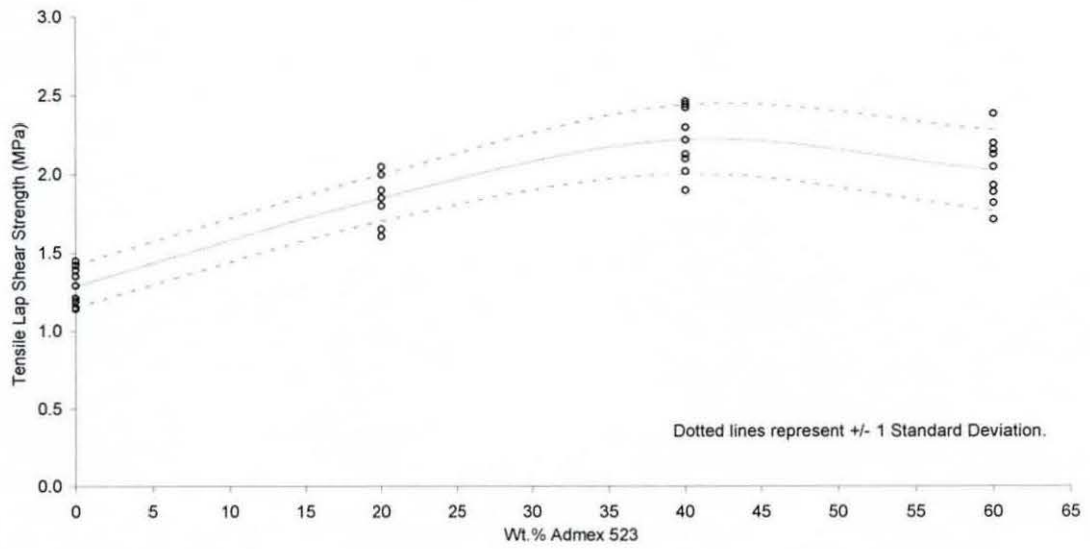
4.3.1 GA6015



Graph 4.3.1.i: GA6015H with Benzoflex 2088

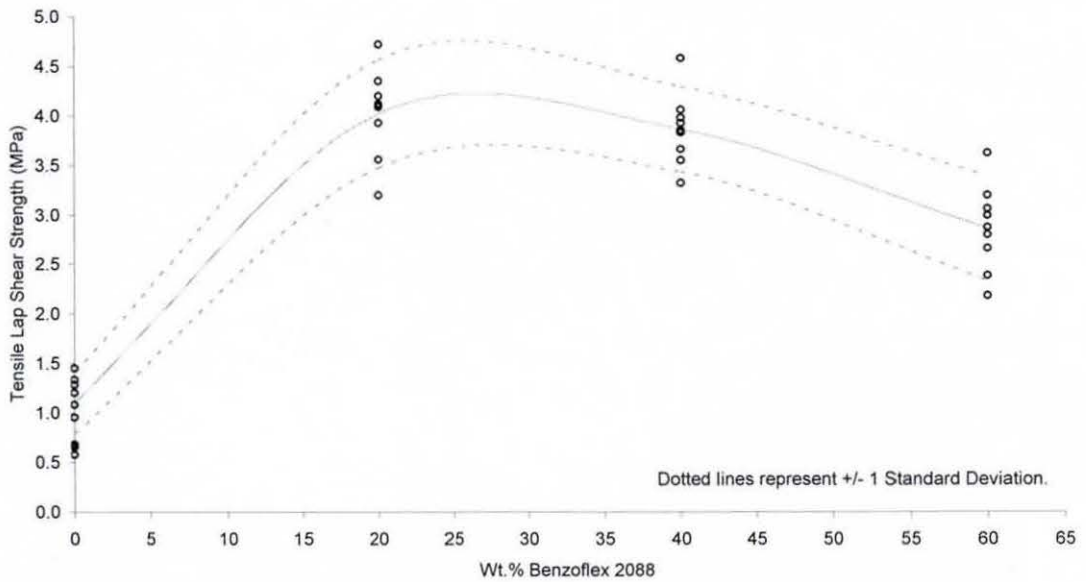


Graph 4.3.1.ii: GA6015H with DOP

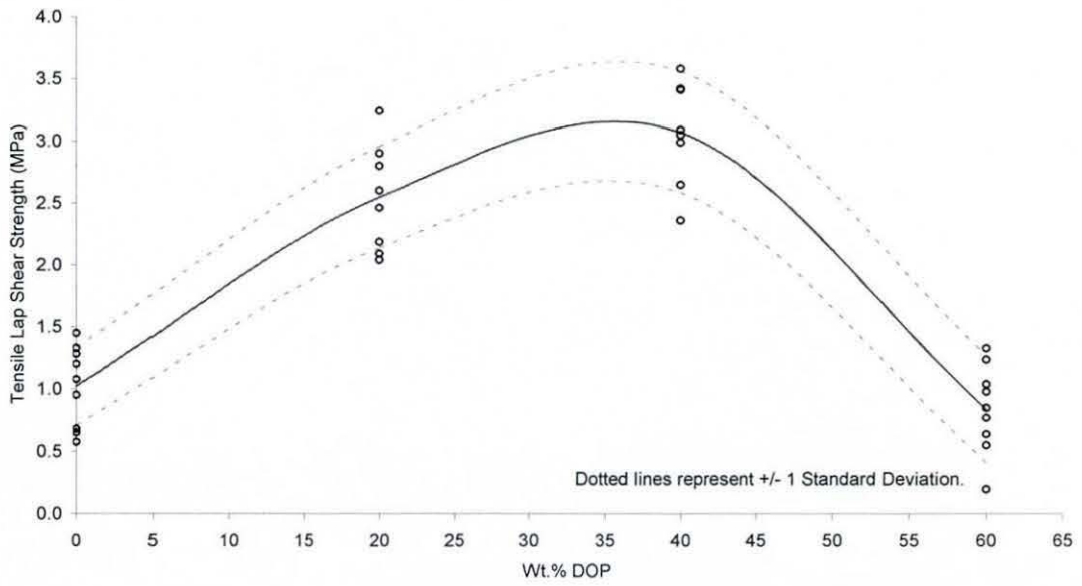


Graph 4.3.1.iii: GA6015H with Admex 523

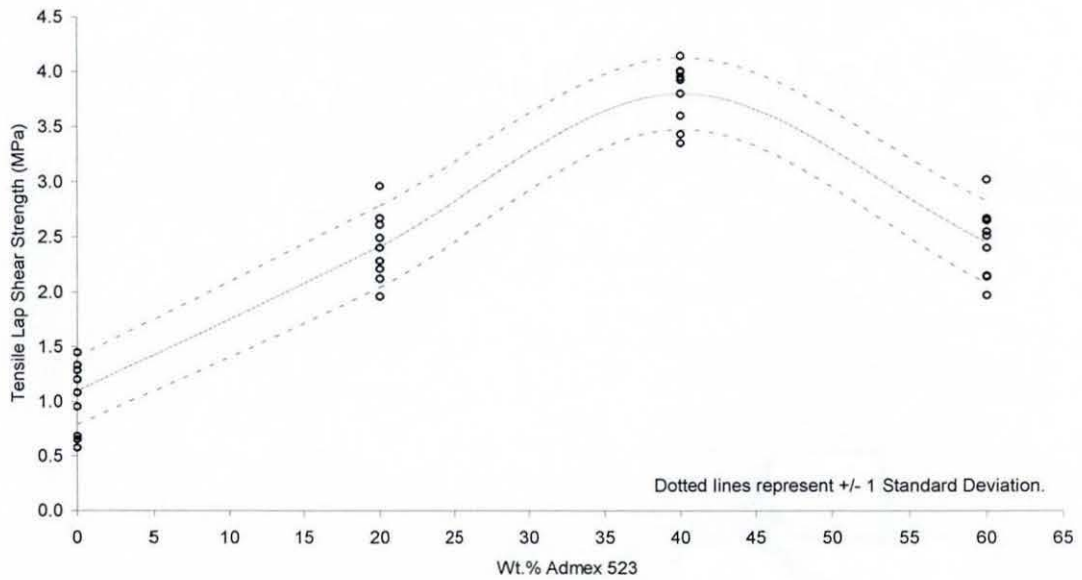
4.3.2 GA7701H



Graph 4.3.2.i: GA7701H with Benzoflex 2088

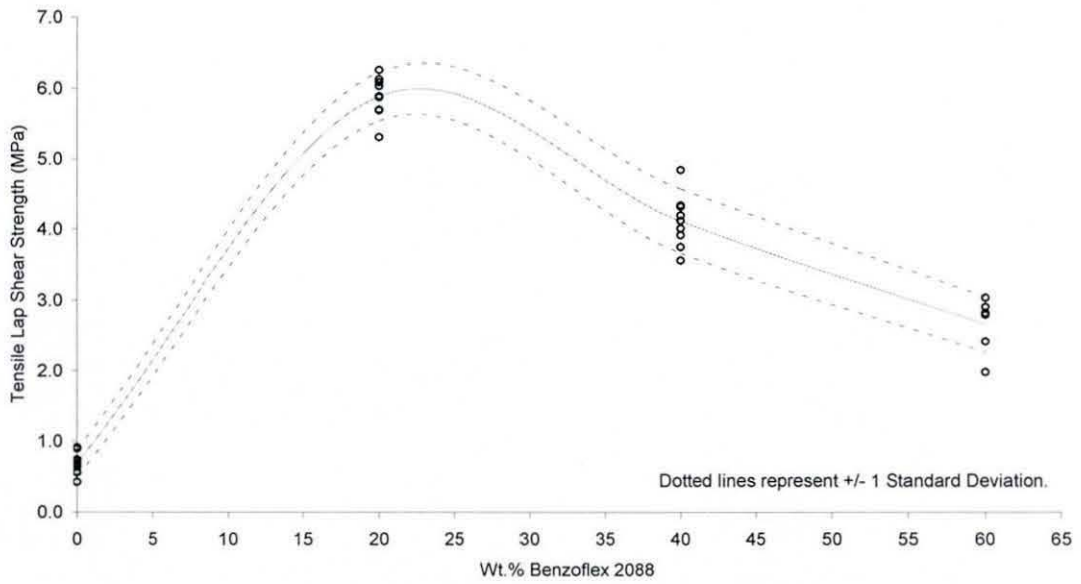


Graph 4.3.2.ii: GA7701H with DOP

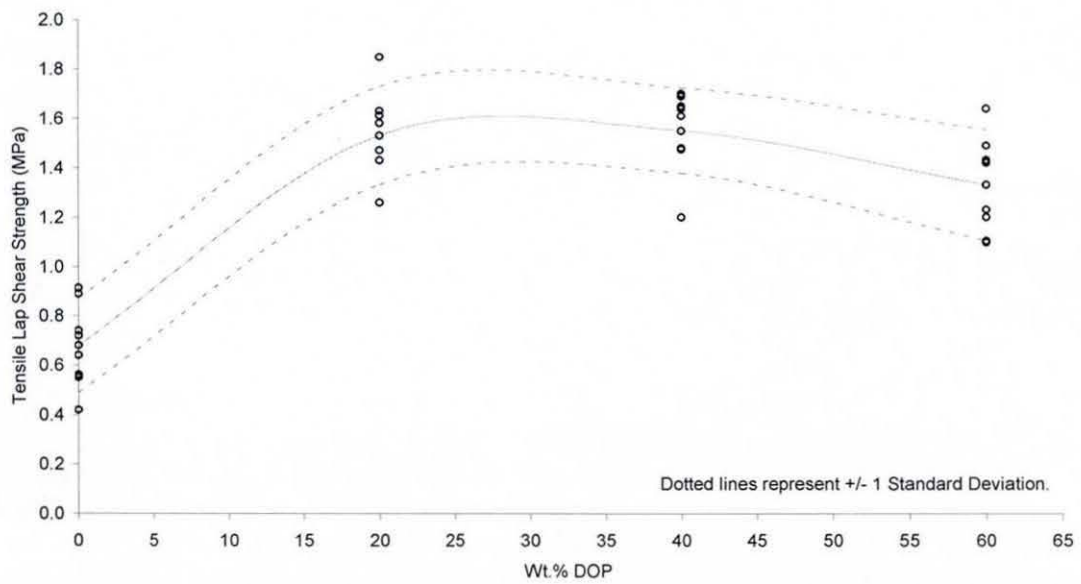


Graph 4.3.2.iii: GA7701H with Admex 523

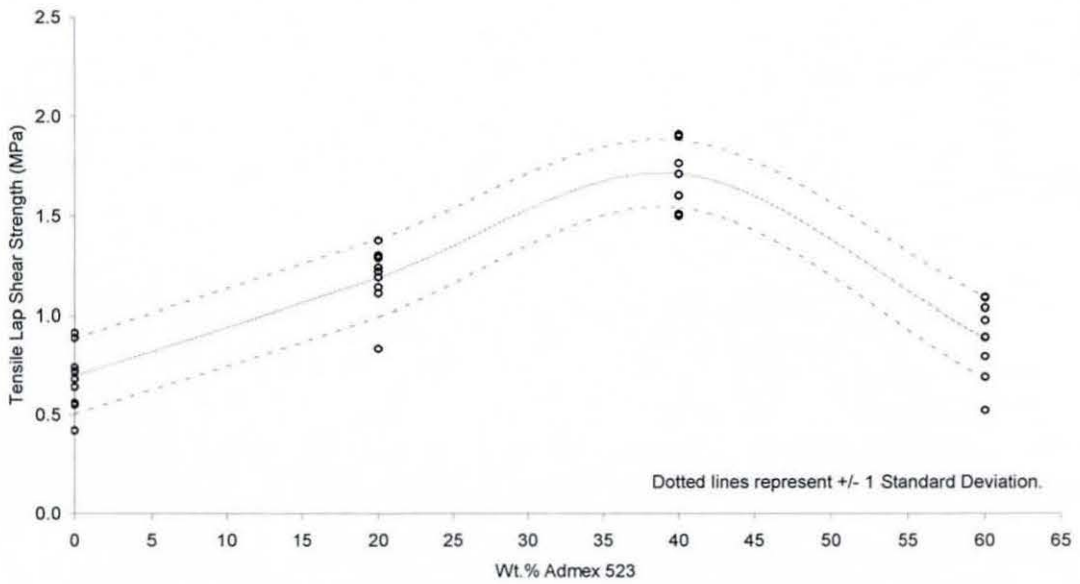
4.3.3 GA9028



Graph 4.3.3.i: GA9028 with Benzoflex 2088



Graph 4.3.3.ii: GA9028 with DOP



Graph 4.3.3.iii: GA9028 with Admex 523

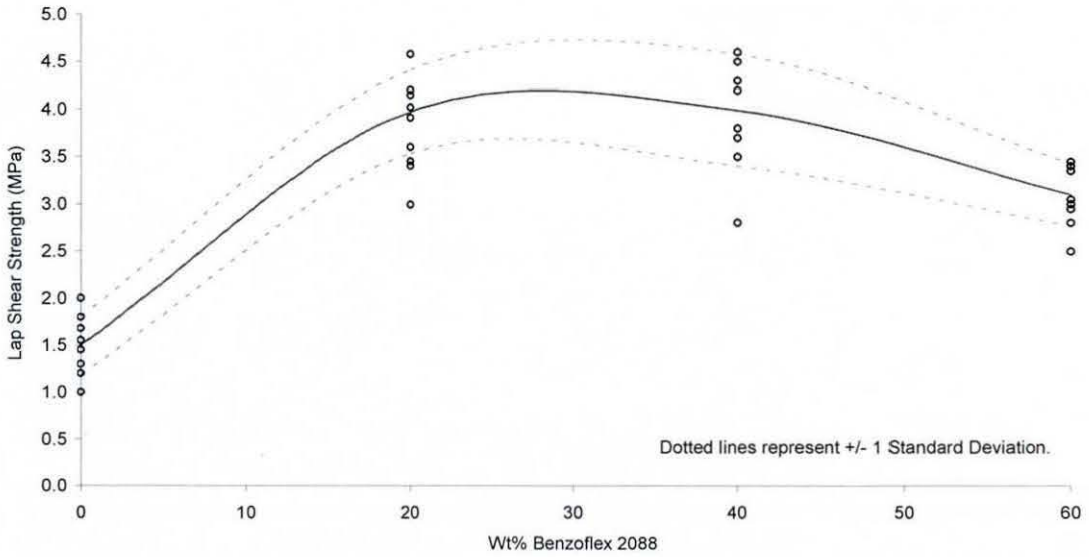
This set of data shows that Benzoflex 2088 produced the highest lap shear strength compared with DOP and Admex 523. All the graphs show a peak lap shear strength which varies for each plasticiser: Benzoflex 2088 had a peak at approximately 20 to 25 wt.%; DOP was at 30 to 40 wt.%; Admex 523 was at 35 to 45 wt.%. These values represent the relative diffusion efficiency of the plasticisers, the slower fusing Admex 523 required a larger concentration to adequately plasticise the substrates while the faster fusing Benzoflex required a lower concentration. Using a fast fusing plasticiser allowed more diffusion to occur in the welding time.

At concentrations below the peak value, fracture surface microscopy revealed no yielding but there was a measurable lap shear strength that was thought to be due to intimate contact. Above the peak value it was thought that too large a concentration was leading to an overly plasticised interlayer which lacked in strength and behaved as a very thick weak boundary layer.

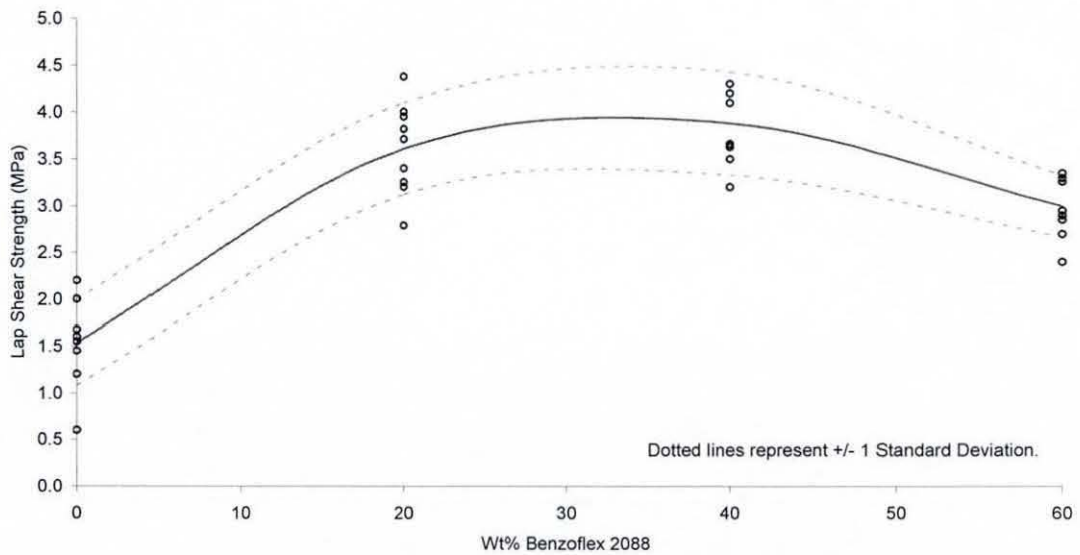
Results show that acetate content in the interlayer between 9 and 14 wt.% had no measurable effect. Indeed, any attempt to represent these results was meaningless. The effect of acetate in an interlayer was determined by comparison with data obtained from PVC homopolymers that contained no acetate.

4.3.4 Homopolymers

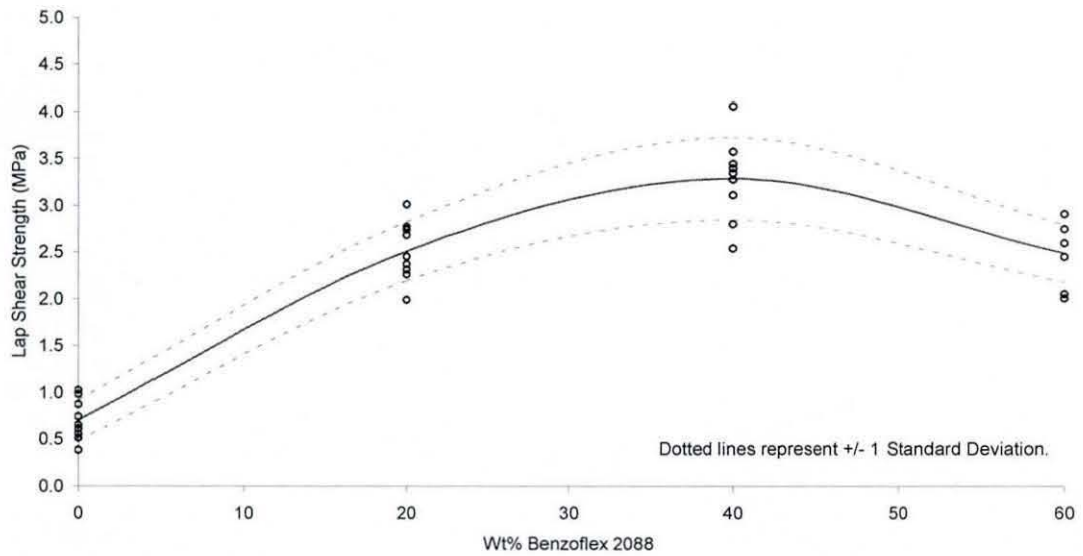
These results show the lap shear strength of welded samples made with homopolymer resins.



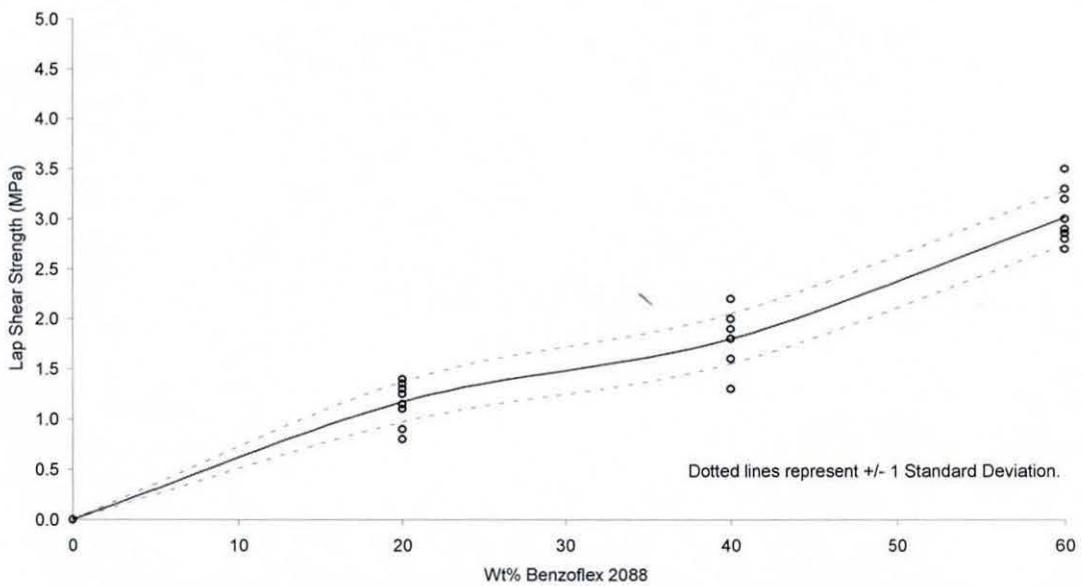
Graph 4.3.4 i: A K57 Resin with Benzoflex 2088



Graph 4.3.4 ii: A K60 Resin with Benzoflex2088



Graph 4.3.4 iii: A K74 Resin with Benzoflex 2088



Graph 4.3.4.iv: A K80 Resin with Benzoflex 2088

An increase in K-value of PVC is related to the molecular weight of the polymer, and hence the extent of chain entanglement present. The above results show that for increasing molecular weight and hence decreasing molecular mobility, more plasticiser is required to produce a peak lap shear strength. Indeed, even 60 wt.%

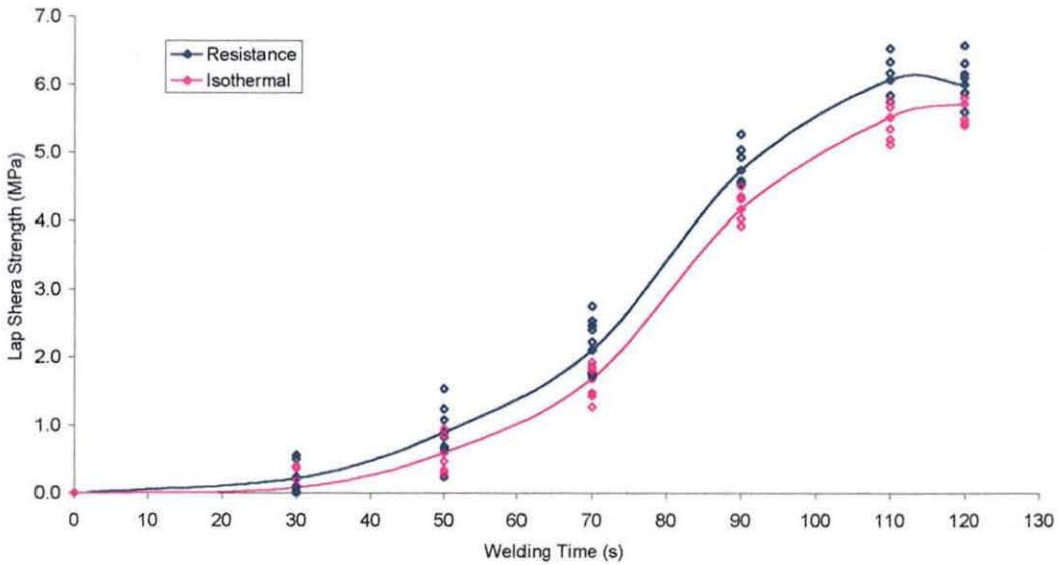
concentration of a fast fusing plasticiser is insufficient to cause a peak in the lap shear strength of a K80 homopolymer. The greatest lap shear strengths were observed when using a resin of similar K-value to the substrates. Unfortunately, the precise K-value of the PVC used in plaque production was not revealed during the course of this work, but it was estimated to be in the region of 55 to 60.

Within the range of copolymers tested, the amount of acetate had no measurable effect on the lap shear strength. However, when comparing homopolymers with copolymers it became apparent that K-value was the most important factor. The highest lap shear strength was observed with copolymer GA9028 that had a K-value of 59 and an acetate content of 10 wt.%. The presence of the acetate in the copolymer was designed to provide internal plasticisation and hence aid flow of the material. The combination of a compatible K-value and ideal plasticisation was believed to be the crucial factor. The effect of the acetate was to provide additional plasticisation (when compared with a homopolymer of similar K-value), without compromising the strength of the interlayer.

The failure mode of samples also changed with changing lap shear strength. At low plasticiser concentrations and low lap shear strengths the failure mode was interfacial, as seen in Micrograph 4.4.4.ii, changing to partly cohesive as the strength and plasticiser concentration increased, as shown by Micrographs 4.4.4.i, iii & iv. At above optimum plasticiser concentrations and low lap shear strengths, the failure was again interfacial.

4.3.5 Lap Shear Strength of Isothermally Welded Specimens

Due to restrictions on the use of isothermal welding equipment it was not possible to fully characterise the effect of isothermal welding on all samples joined by resistance welding. However, it was possible to determine the effect of varying the welding time on the lap shear strength of isothermally welded samples. Resistance welding was used to identify the best interlayer, which was subsequently used to produce isothermally welded samples. Note that the maximum welding time permitted by the health and safety practices of Uponor Limited was 120 seconds due to the possible production of toxic fumes (HCl) and on only one occasion was this time increased to 180 seconds for the purposes of infrared degradation analysis.



Graph 4.3.5.i: Effect of welding time on lap shear strength

The development of strength with both processes followed a very similar pattern. The time at which real strength began to develop (i.e. the point where interdiffusion overtook intimate contact as the joining mechanism) was the same for both heating methods. It follows, therefore, that there may be a minimum energy input required for diffusion to occur. This criterion was investigated in Section 4.6.

The only difference between resistance and isothermal heating was the point at which maximum strength was developed: At 120 seconds, resistance heating had reached a maximum value whereas isothermal heating had not. As previously stated, it was not possible to lengthen the welding time beyond 120 seconds due to health and safety considerations but it is anticipated that the lap shear strength of isothermally welded specimens would be stronger for the same amount of degradation. This is discussed further in section 4.10.

4.4 Microscopy

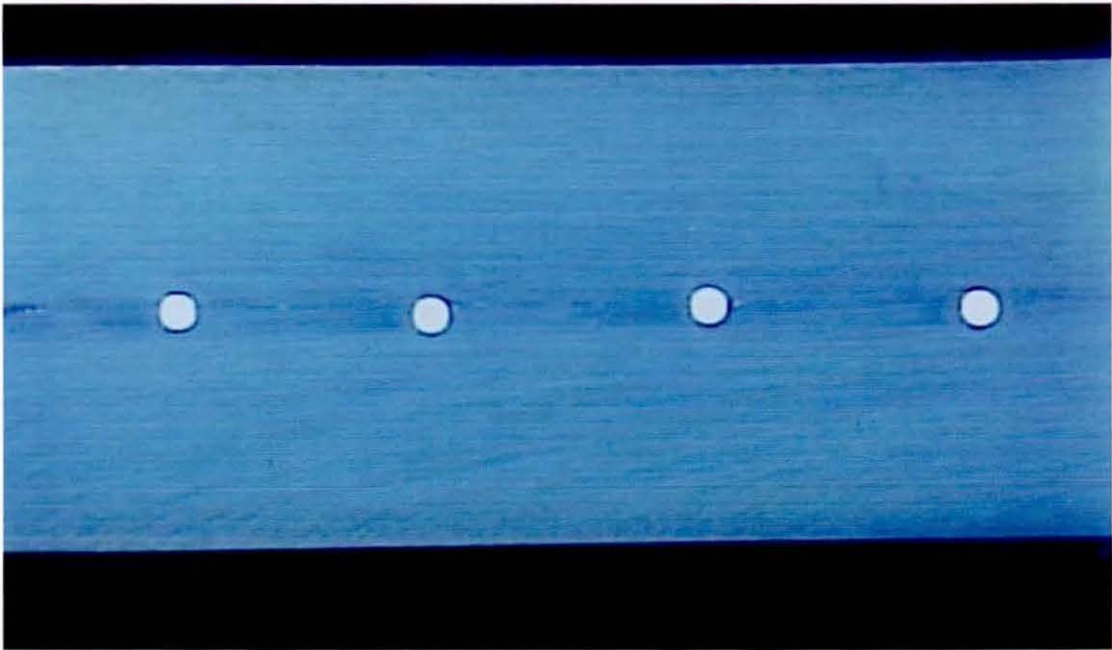
4.4.1 Introduction

The configuration of the welded specimens in this work made low magnification light microscopy an ideal technique for examining interfaces and fracture surfaces. Since the interlayer gave a relatively high degree of contrast, it was possible to produce an image of the development of the interface during the welding process. The tendency of PVC to whiten during yielding made it possible to identify conditions and interlayers where interdiffusion had occurred.

4.4.2 Resistance Heating

The following micrographs show how the interface developed during 30 to 120 seconds heating time. Additional micrographs are presented to aid the understanding of sample configuration and fracture surfaces.

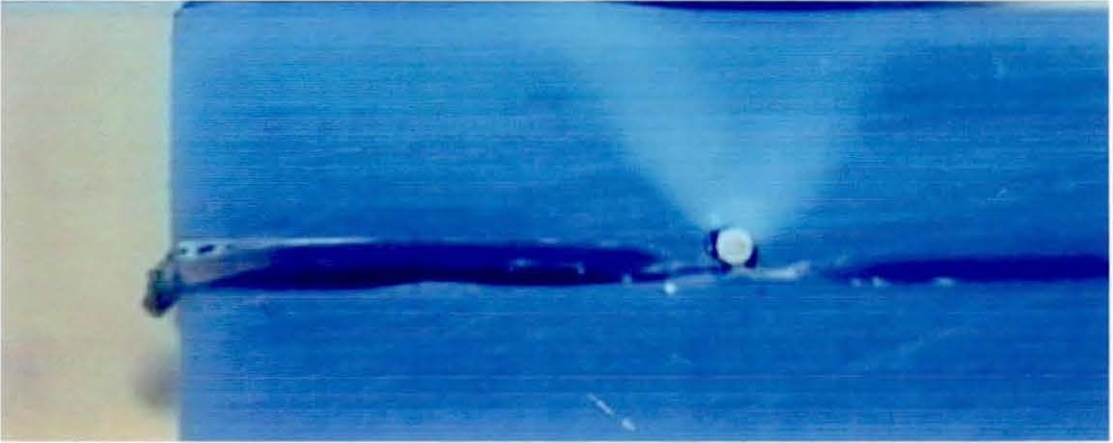
Micrograph 4.4.2.i: Section of welded sample. (10x)



This micrograph of a welded sample before lap shear testing shows the eliminated interface. Note that the wires have retained their position along the old interface; this could not be avoided or influenced in any simple way, and was unfortunate as they provided a straight-line path for a failure. This had occurred because the wires were joined to the PVC by intimate contact and mechanical interlocking and as this was a relatively weak bond, the wires act as stress raisers. During lap shear testing the wires

were readily dislodged as shown in micrograph 4.4.2.ii, where regions of high stress show up as whitened areas in a specimen tested below the fracture strength.

Micrograph 4.4.2.ii: Stressed region around the heater wire. (10x)



This micrograph illustrates the stress distribution around the wire during the lap shear test. The direction of the stress was advantageous as it was directed into the bulk of the material and away from the softer interfacial zone, (the region where the interlayer had diffused into the plaques). This is illustrated well in Micrograph 4.4.4.i, which shows a failure into the plaques.

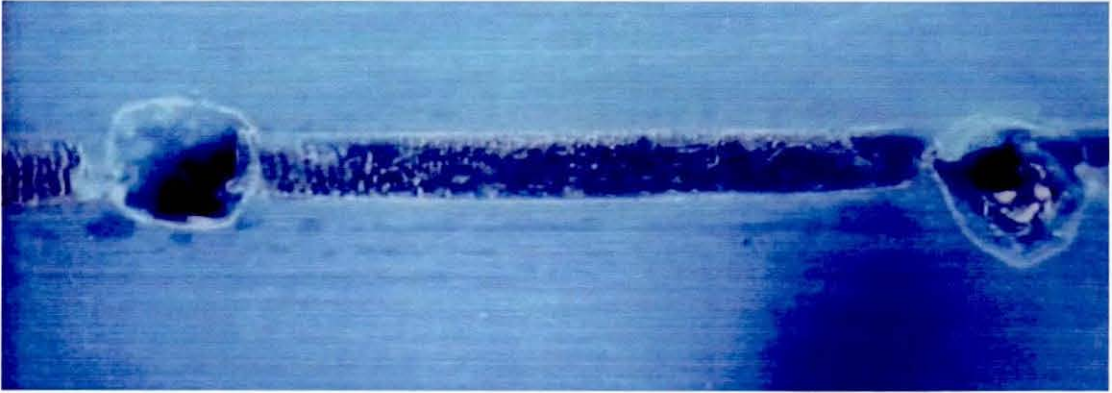
Micrograph 4.4.2.iii: 30 seconds heating time. (20x)

Note: 9/40B formulation used in all Micrographs.



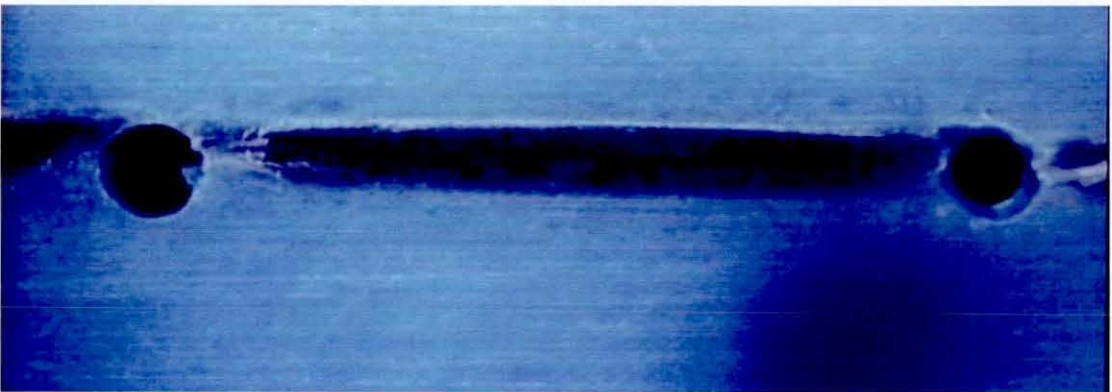
In this micrograph, it can be clearly seen that there was no discernible effect of this low heating time, as shown by the lower plaque, which remained detached from the interlayer. There may be evidence of some degree of melting and movement of the PVC, particularly around the right hand wire.

Micrograph 4.4.2.iv: 50 seconds heating time. (20x)



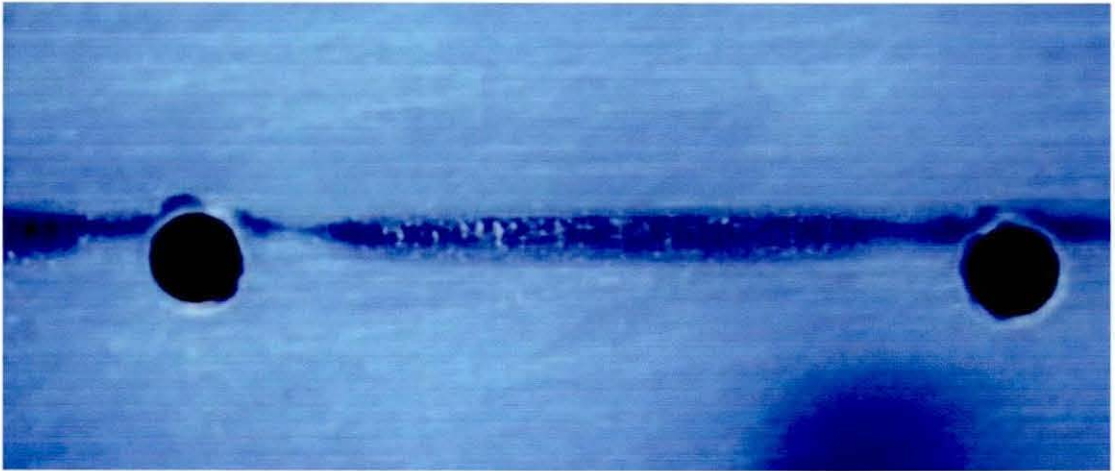
In this instance, the micrograph shows that the interlayer had made contact with both plaques, although there was still little evidence of large scale heating/melting. The holes left by the wires were enlarged during their removal.

Micrograph 4.4.2.v: 70 seconds heating time. (20x)



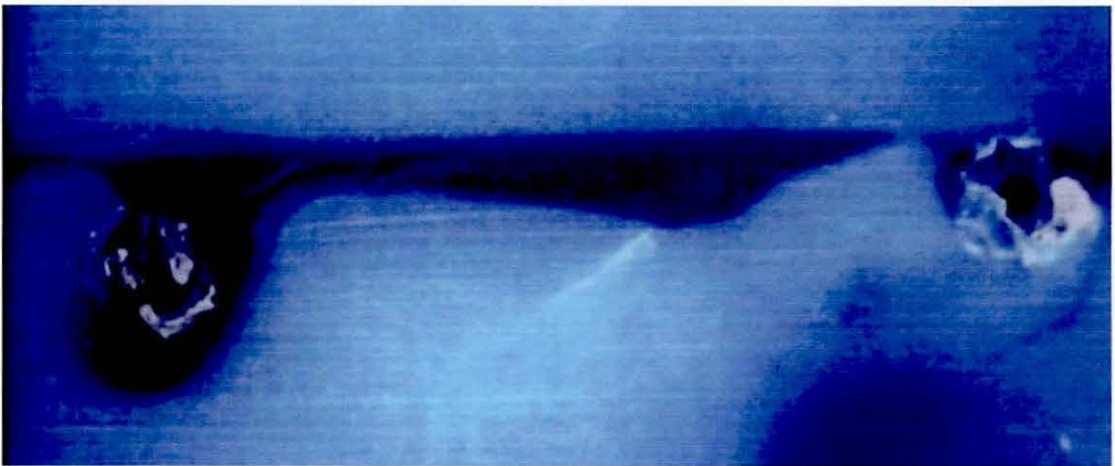
This micrograph shows that as heating time was increased to 70s, there was growing evidence of heating/melting, particularly around the left hand wire and it was at this time that a measurable lap shear strength began to develop. In addition, the boundary between interlayer and plaque had begun to delineate, particularly on the lower edge of the interlayer.

Micrograph 4.4.2.vi: 90 seconds heating time. (20x)



At this level of heating the interlayer had begun to diffuse into the plaques, to a noticeable degree, although it still formed a boundary between the two plaques.

Micrograph 4.4.2.vii: 110 seconds heating time. (20x)



The effect of heating/melting was now clearly visible; the wires had started to move into the lower plaque; in isolated places, the original boundary had been eliminated.

Micrograph 4.4.2.ix: 120 seconds heating time. (20x)

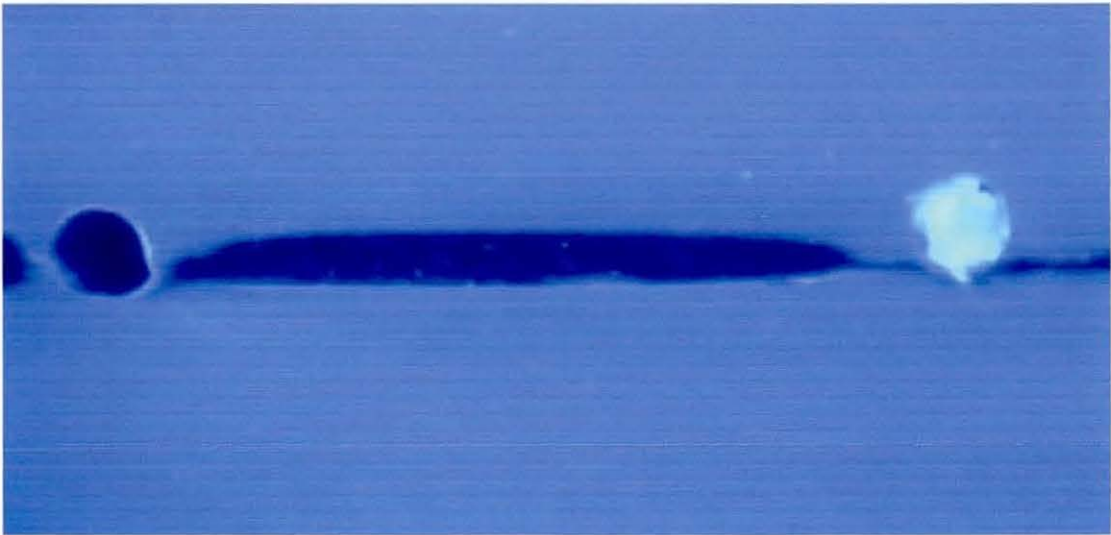


Micrograph 4.4.2.vi shows that the interlayer had diffused into the plaques and the interface between them is discontinuous. There are no visible signs of charring, although some smoke was produced during the welding process caused by overheated wires where they entered the component. It was anticipated that any further welding would cause visible signs of degradation. Lap shear results have shown that increasing the welding time beyond 120 seconds did not lead to improvements in the strength of welded components.

4.4.3. Induction Heating

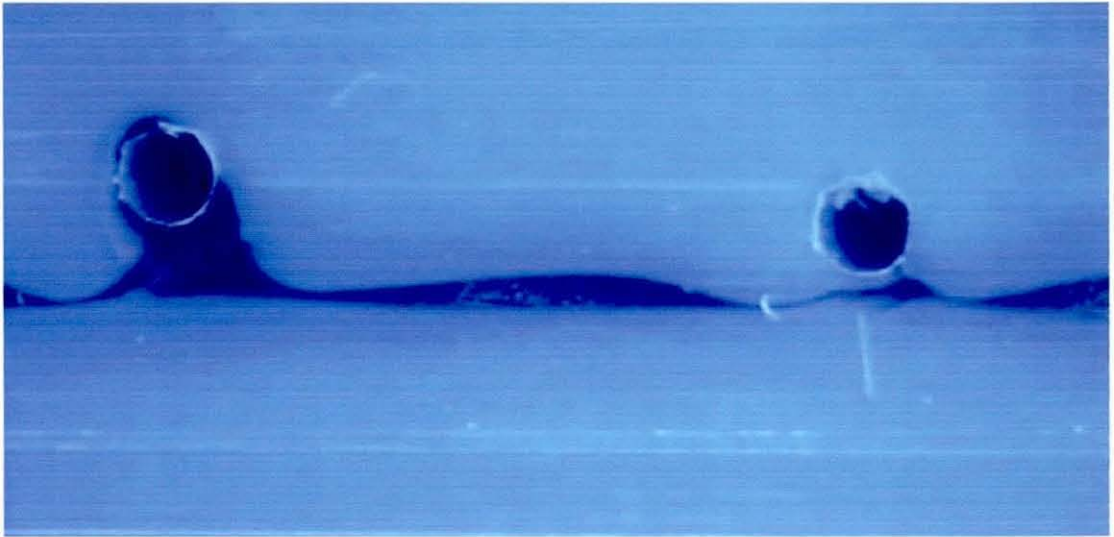
This series of micrographs shows how the interface developed during *Smarteat* welding. Samples welded below 90 seconds did not show significant interfacial diffusion.

Micrograph 4.4.3.i: 90 seconds heating time. (20x)



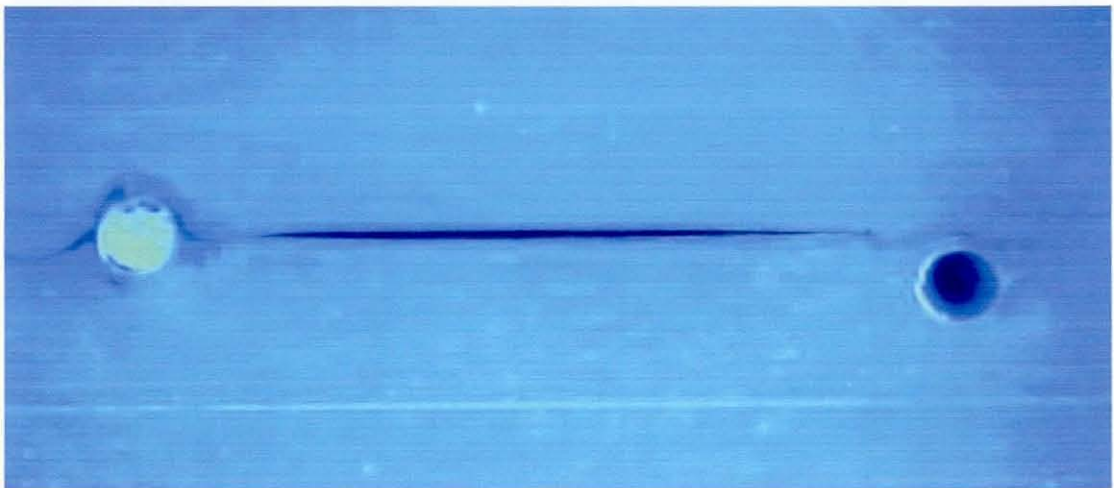
At 90 seconds of isothermal welding, material around the wire began to move. The thickness of the interlayer close to the wire was reduced and continued to diminish as welding time increased.

Micrograph 4.4.3.ii: 110 seconds heating time. (20x)



At 110 seconds heating time, the interlayer had diffused into the substrates along a considerable length of the interlayer. This process continued as long as there was material to diffuse into the substrates.

Micrograph 4.4.3.iii: 120 seconds heating time. (20x)



After 120 seconds, the thickness of the interlayer was much reduced as shown in Micrograph 4.4.3.iii.

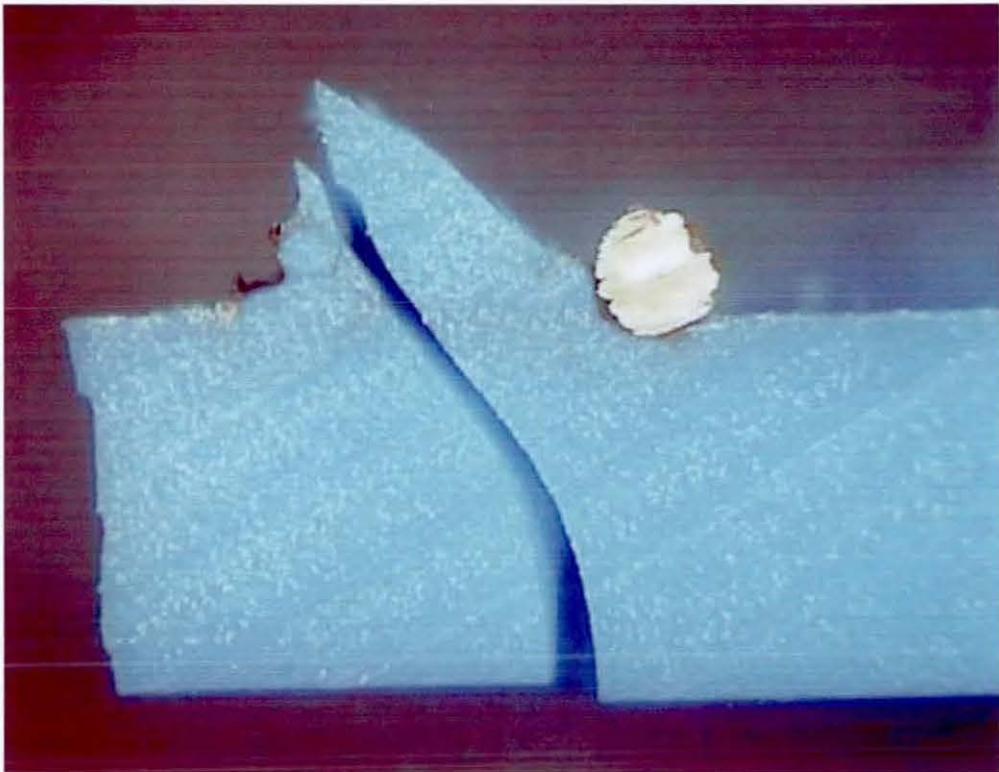
Micrograph 4.4.3.iv: 180 seconds heating time. (20x)



After 180 seconds of isothermal welding, the interlayer had been eliminated. The onset of degradation can be seen as a delineation of the wire cavity as voiding began to form around it.

4.4.4. Fracture Surfaces

Micrograph 4.4.4.i: Fracture through plaque. (30x)



Partial cohesive failure is evident in micrograph 4.4.4.i. The interface is no longer visible, indicating that interdiffusion had occurred.

Micrograph 4.4.4.ii: Fracture along interface (10x)

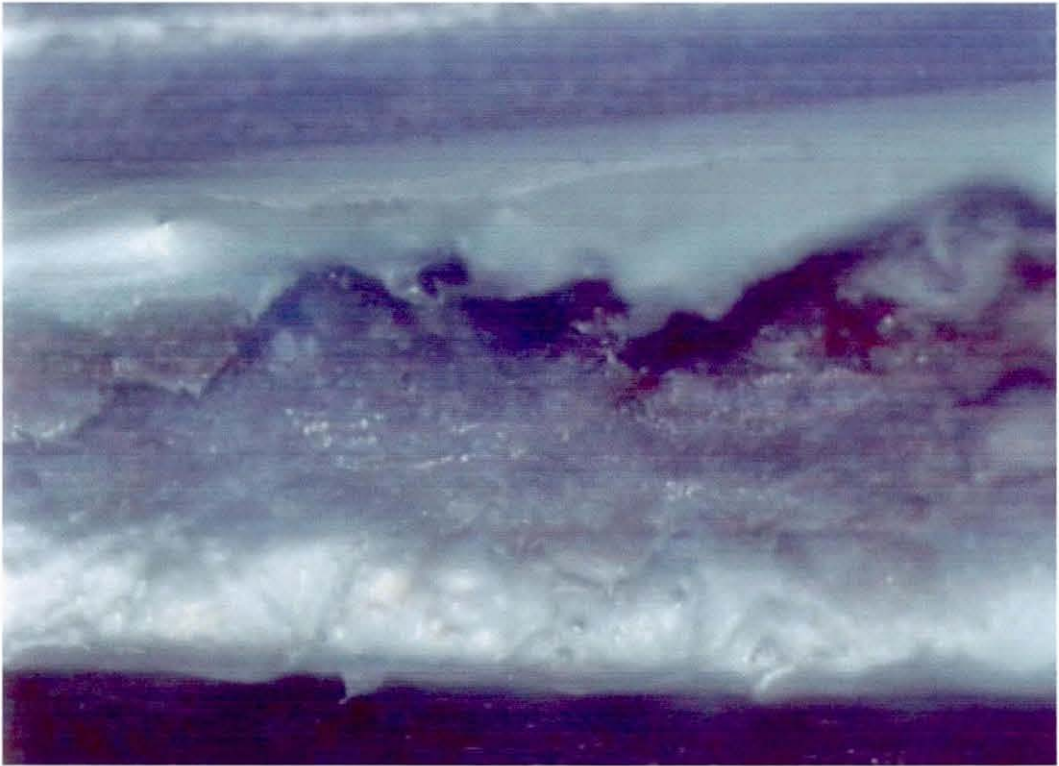


This micrograph shows a fracture caused by interfacial failure. Here the crack has propagated straight through the interface and there is little evidence of interdiffusion. This type of failure was observed with low lap shear strengths, whereas cohesive or part cohesive failure was observed with higher strength specimens.

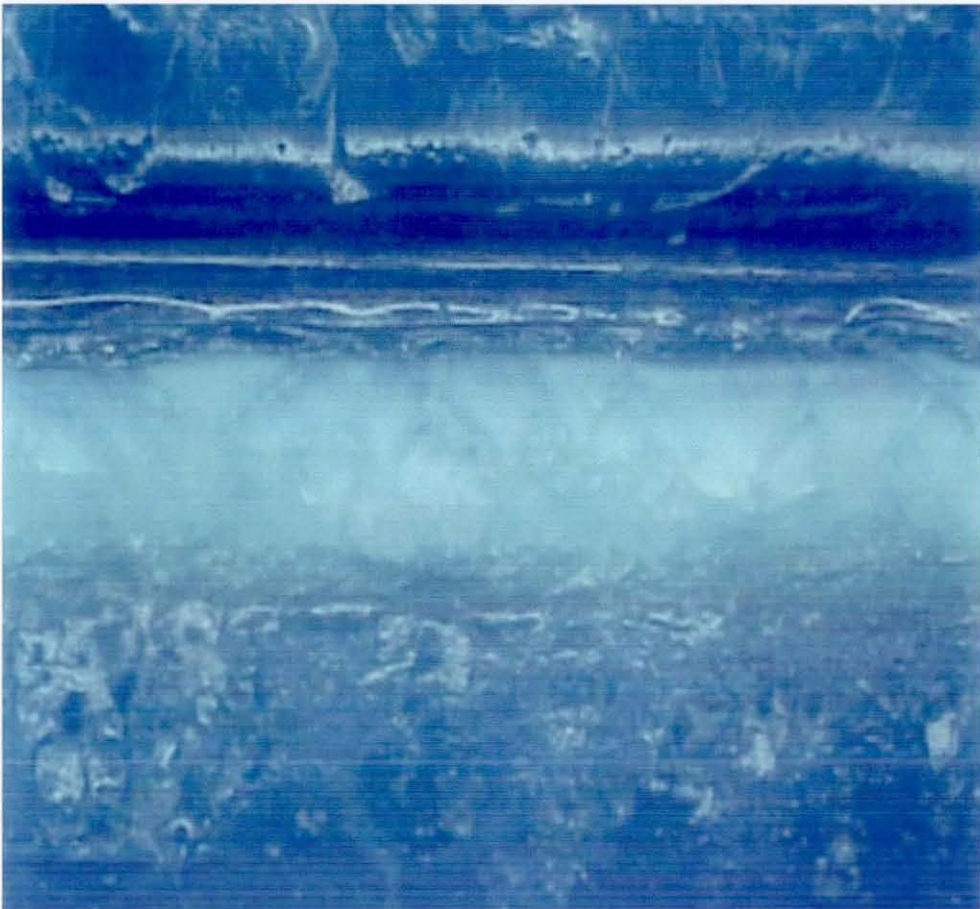
Micrograph 4.4.4.iii shows a typical result of yielding in PVC. Whitening and elastic deformation are clearly visible as is a small amount of drawing. Although PVC does not normally draw to any great extent, samples tested here contained plasticiser. This result provides firm evidence of interdiffusion as this type of fracture surface does not occur with any other form of bonding.

Micrograph 4.4.4.iv, below, shows further whitening around a heater wire. The wire ran along the top edge of the picture and its impression can be clearly seen. The amount of whitening and plastic deformation was greatest next to the wire and reduced with distance from it.

Micrograph 4.4.4.iii: Yielding between wires. (100x)



Micrograph 4.4.4.iv: Yielding next to wires. (40x)



4.5 Hardness Testing

4.5.1 Introduction

As hardness is affected by plasticiser content, it was possible to monitor the movement of such material by a change of hardness. The hardness of welded samples was measured by Vickers hardness testing, a technique primarily used for metallic samples. However, the repeatability and acceptable resolution of the Vickers test made it applicable for this research study. The ability of the Vickers hardness test to measure orientation was exploited in an attempt to determine any orientation caused by the welding process. The amount of plasticiser and the type of resin used to prepare interlayers had a strong influence on their hardness and was measured using Shore A apparatus.

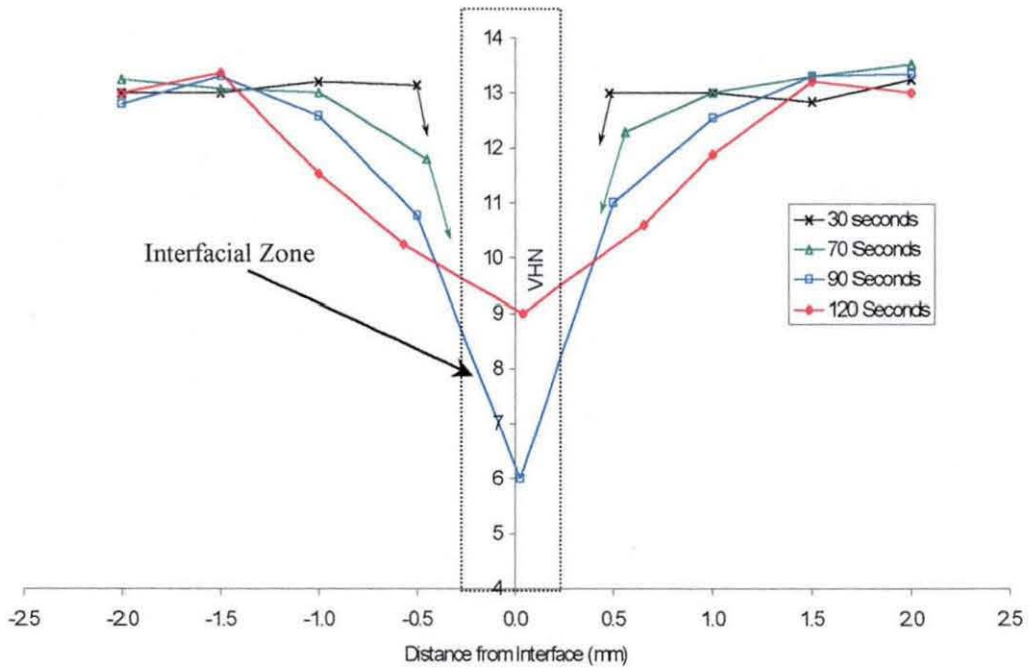
4.5.2 Vickers Hardness

Vickers hardness was used to determine the extent of diffusion of the plasticiser into the plaques after welding and was evaluated in terms of detecting orientation in welded samples. The evaluation process measured the perpendicular dimensions of an indentation in PVC samples varying in orientation only. Welded samples were tested for orientation at the same time as depth of diffusion.

4.5.2.1 Diffusion Depth

The following graph, 4.5.2.i, shows how the hardness varied across the bulk PVC, through the interfacial zone and back into bulk PVC. The interlayer used was K57 resin with 40 wt.% Benzoflex 2088.

After 30 seconds welding time, all the plasticiser remained in the interlayer resulting in a very soft region beyond the lower limit of the apparatus. The reading at 0.5mm from the interface showed no change in the hardness compared with that of the bulk at 30 seconds heating time. At 70 seconds, the plasticiser had begun to move into the plaque, and showed a small decrease in hardness at 0.5mm depth. At 90 seconds, the plasticiser had softened the PVC to a depth of between 1.0 and 1.5mm and it was at this time that interdiffusion of the PVC began to occur and yielding type failures occurred.



Graph 4.5.2.i: Hardness variation across interface at various welding times (sample 9/40B)

The movement of plasticiser away from the interlayer led to a measurable increase in the hardness of the interfacial zone. At 120 seconds, more of the plasticiser had moved away from the interface leading to further hardening with associated softening of the surrounding material as the plasticiser concentration profile widened and flattened.

The resolution of this technique was not sufficient to identify anti-plasticisation and although it was anticipated that a failure due to this phenomenon would produce a brittle type fracture surface, but away from the interlayer. However, no such failure was observed at any time.

4.5.2.2 Orientation

The following tables show Vickers hardness data for different states of orientation. The term *parallel* denotes the indentation dimension running parallel to the hoop direction and *perpendicular* denotes the indentation dimension at right angles to this.

Table 4.1: Vickers hardness data for MoPVC feedstock (un-oriented)

MoPVC Feedstock (Inner Diameter)						
Measurement	1	2	3	4	5	Mean
Parallel	556	561	562	571	571	
Perpendicular	574	560	562	563	572	
Difference	-18	1	0	8	-1	-2
VHN	14.2	14.8	14.2	14.4	14.1	14.3
MoPVC feedstock (edge)						
Measurement	1	2	3	4	5	Mean
Parallel	550	576	577	570	560	
Perpendicular	554	576	578	577	567	
Difference	-4	0	-1	-7	-7	-4
VHN	15.2	13.9	13.9	14.0	14.6	14.3

Table 4.2: Vickers hardness data for MoPVC pipe (oriented)

MoPVC (Outside Diameter)						
Measurement	1	2	3	4	5	Mean
Parallel	556	549	564	567	560	
Perpendicular	547	536	548	532	550	
Difference	9	13	16	35	10	17
VHN	15.2	16.0	15.0	15.4	15.1	15.3

MoPVC (Inside Diameter)						
Measurement	1	2	3	4	5	Mean
Parallel	549	556	558	565	569	
Perpendicular	534	546	540	545	540	
Difference	15	10	18	20	29	18
VHN	15.8	15.3	15.4	15.1	15.1	15.3
MoPVC (Edge)						
Measurement	1	2	3	4	5	Mean
Parallel	569	583	578	576	579	
Perpendicular	556	564	557	569	555	
Difference	13	19	21	7	24	17
VHN	14.9	14.0	13.9	14.1	14.6	14.3
MoPVC (Outside Diameter) *						
Measurement	1	2	3	4	5	Mean
Parallel	549	554	557	554	553	
Perpendicular	552	551	555	549	555	
Difference	-3	3	2	5	-2	1
VHN	15.1	15.2	14.8	15.3	15.1	15.1
MoPVC (Inside Diameter) *						
Measurement	1	2	3	4	5	Mean
Parallel	557	553	552	550	563	
Perpendicular	548	554	553	550	550	
Difference	9	-1	-1	0	13	4.4
VHN	15.2	15.3	15.2	15.0	14.8	15.1

MoPVC (Edge) *						
Measurement	1	2	3	4	5	Mean
Parallel	581	573	567	567	553	
Perpendicular	570	559	568	562	536	
Difference	11	14	-1	5	17	9
VHN	13.9	14.6	14.4	14.5	15.6	14.6

* denotes specimens rotated by 90° to check equipment alignment.

Table 4.3: Micro-hardness data for recovered MoPVC pipe

Recovered MoPVC						
Measurement	1	2	3	4	5	Mean
Parallel	554	550	563	566	563	
Perpendicular	566	558	558	558	559	
Difference	-12	-8	5	8	4	-1
VHN	14.8	15.1	14.7	14.2	14.7	14.7
Recovered MoPVC*						
Measurement	1	2	3	4	5	Mean
Parallel	562	554	558	562	553	
Perpendicular	562	554	558	561	552	
Difference	0	0	0	1	1	0
VHN	14.7	15.1	14.9	15.0	15.0	14.9

* denotes specimens rotated by 90° to check equipment alignment.

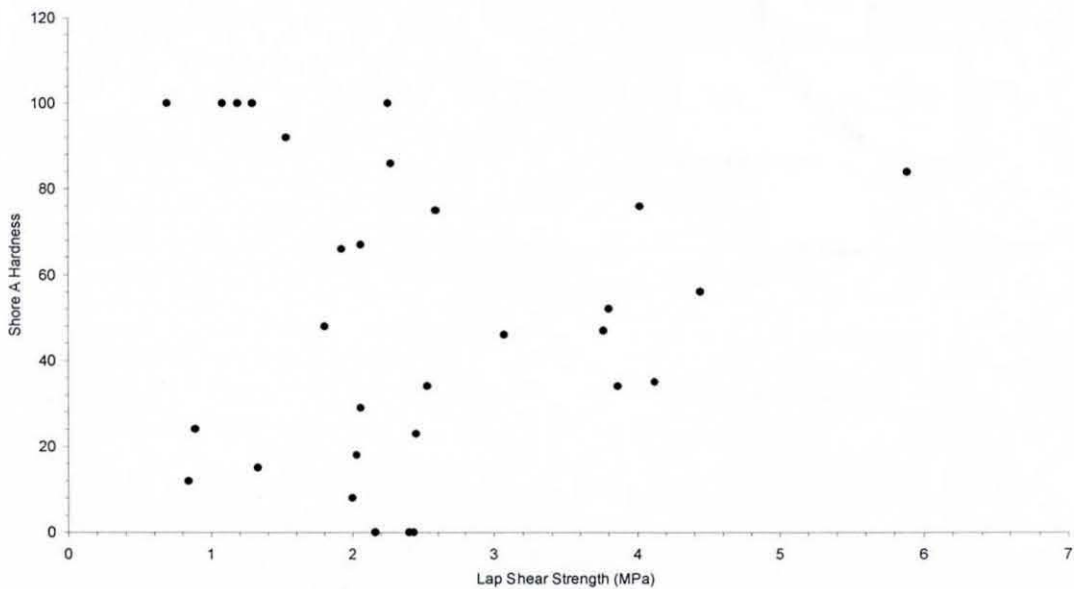
The above results show that the orientation was measurable in the purposefully oriented MoPVC but was not consistent when the sample was rotated, a factor attributable to misalignment of the equipment. The difference in perpendicular

dimensions was measured at a maximum of 18, which is very small compared to the acceptable difference, recommended by the testing procedure, of 15 units.

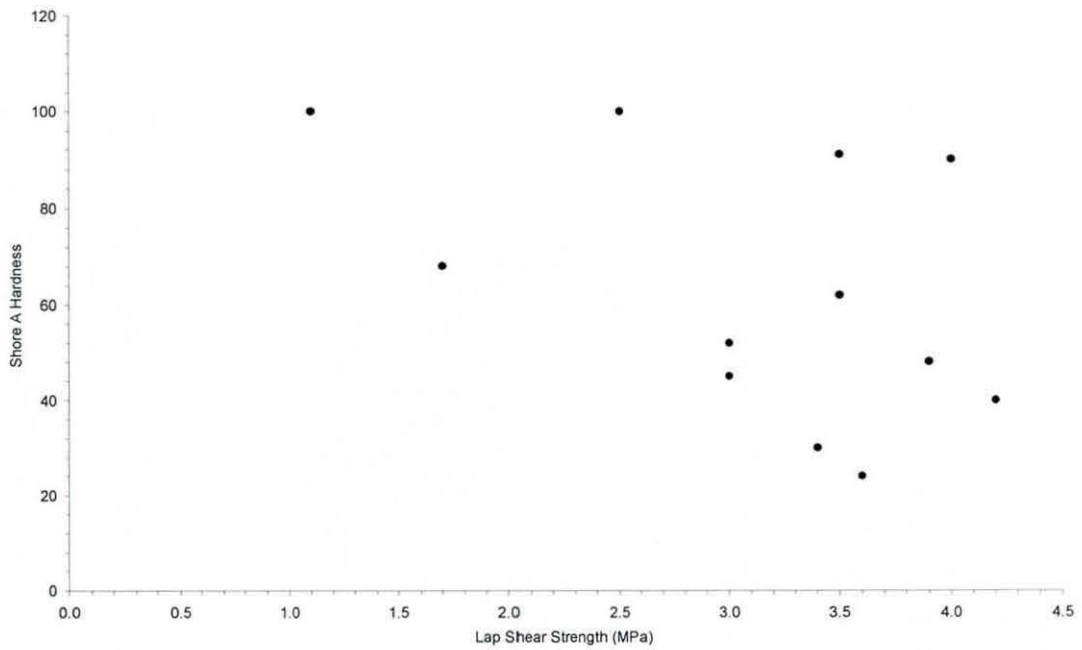
The failure of this test to detect orientation in these samples in the face of strong evidence from the literature can be accounted for by examining the draw ratios of materials tested in the different experiments. In this experiment, the draw ratio of the MoPVC pipe was measured to be 1:1.6 compared to ratios of up to 1:40 reported in the literature. The draw ratio for MoPVC pipe was measured by the dimensional change after recovery and was confirmed by Uponor Limited.

4.5.3 Interlayer Hardness

Original interlayer hardness was too low to be measured using Vickers hardness. For the reason that the samples were highly elastic and as such, interlayer hardness was measured using the Shore A technique. The resulting interlayer hardness values may be given credence by presenting them in conjunction with lap shear results. In this way, interlayers that impart the greatest lap shear strength may be identified in terms of their original hardness.



Graph 4.5.3.i: Shore A hardness of interlayers prepared with copolymer resins compared with average lap shear strength values



Graph 4.5.3.ii: Shore A hardness of interlayers prepared with homopolymer resins compared with average lap shear strength values

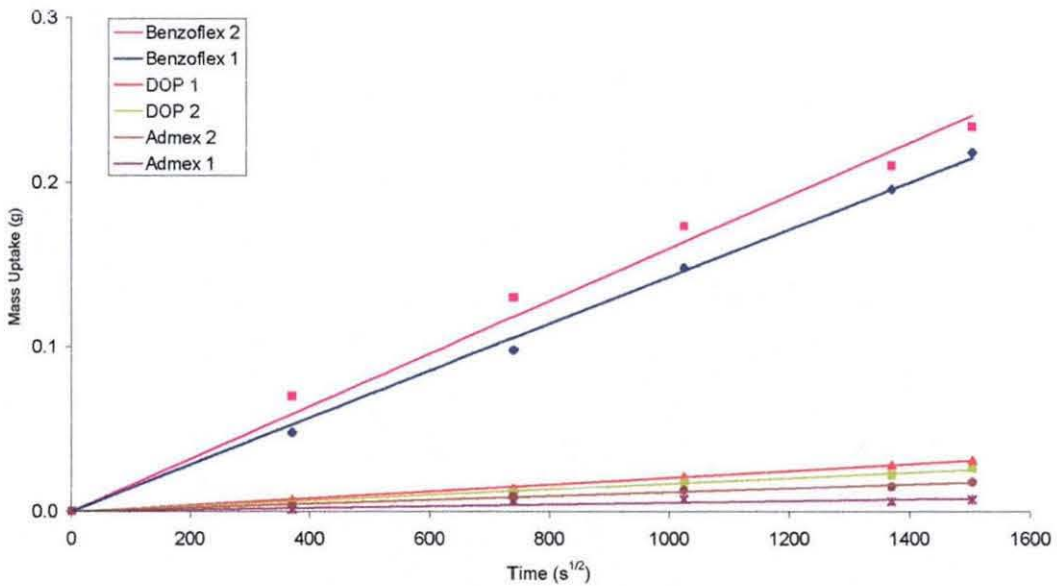
For both copolymers and homopolymers there appeared to be no distinctive trend to relate Shore hardness values to lap shear strength (Graphs 4.5.3.i & ii). The findings of Jacobson in Reference 139 confirm the affect of plasticiser concentration on hardness values. No references could be found in the literature that link lap shear strength of a substrate-interlayer system to original hardness of the interlayer.

4.6 Diffusion Testing

4.6.1 Introduction

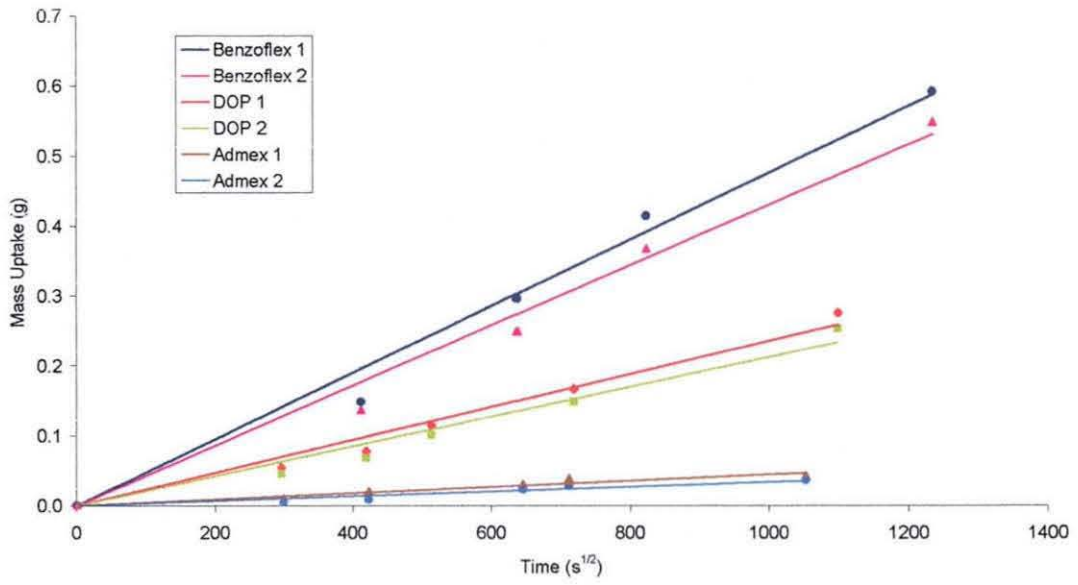
For an interface to be eliminated, material must move across from both sides to the other. In the context of this work, plasticisers were used to assist the process of mass transport and avoid deleterious degradation. It is therefore important to understand the rate at which the different plasticisers diffuse into the PVC substrates. This was achieved by using wipe and weigh diffusion testing.

4.6.2 Immersion Diffusion

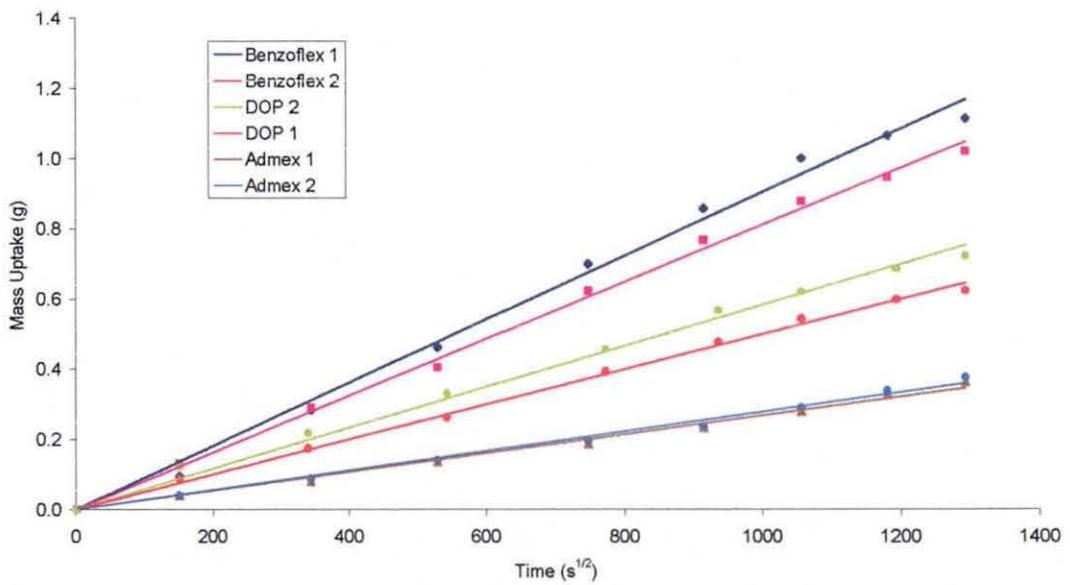


Graph 4.6.2.i: Mass uptake plots for all plasticisers into PVC at 50°C

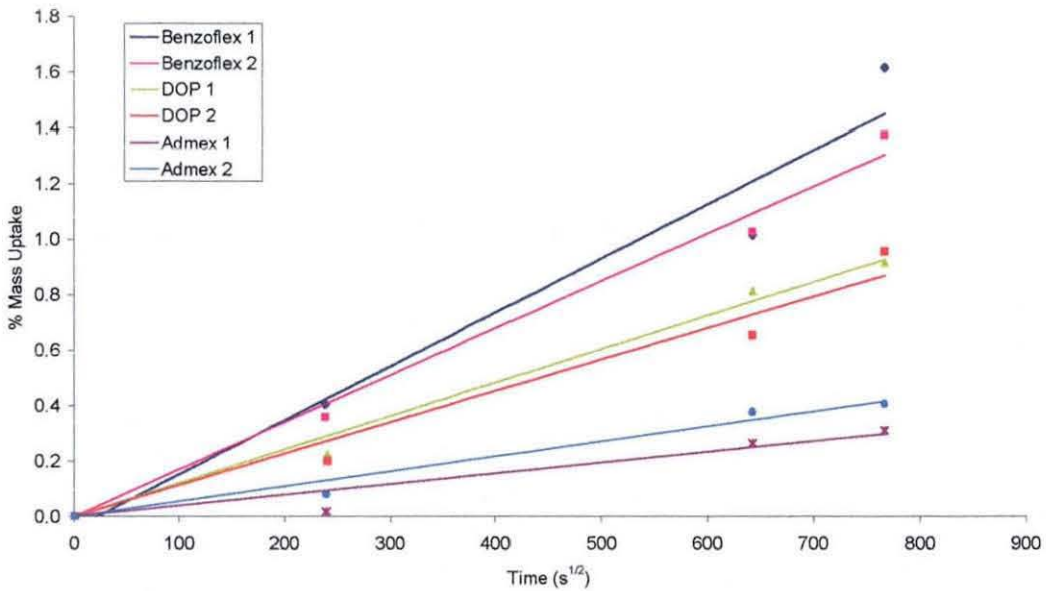
The rate of mass uptake at this temperature was very slow indeed, with prolonged testing required to generate a full set of results.



Graph 4.6.2.ii: Mass uptake plots for all plasticisers into PVC at 60°C



Graph 4.6.2.iii: Mass uptake plots for all plasticisers into PVC at 70°C



Graph 4.6.2.iv: Mass uptake plots for all plasticisers into PVC at 80°C

Due to the very long period of time required to generate a full set of results for the 50°C test, it was decided to estimate the equilibrium mass based on results from the 80°C test. However, it was important to determine the initial slope of the mass uptake plot at all temperatures. With all tests except those at 50°C, testing was continued until weighing was no longer possible due to sample disintegration.

These results indicate the efficiency of each plasticiser and when this was compared to the lap shear results it is clear that the fastest fusing plasticisers produced the highest lap shear strength. This infers that the plasticiser was key to obtaining a strong joint. The strongest joints fail with yielding around the wires which indicates that interdiffusion has occurred, this was only observed when plasticiser was present in the interlayer. It is anticipated that the use of an even more efficient plasticiser would result in a stronger bond, a fact known to be true since this forms the basis of solvent welding. However, this is to be avoided as the end use for these PVC systems is subject to stringent toxicity regulations.

The diffusion coefficient, D was determined by using the following equation:

$$D = \pi \left(\frac{mx}{4m_e} \right)^2 \quad [\text{Equation 17.}]$$

Where m_e is the equilibrium mass, m gradient of the mass uptake graph and x is the thickness of the sample.

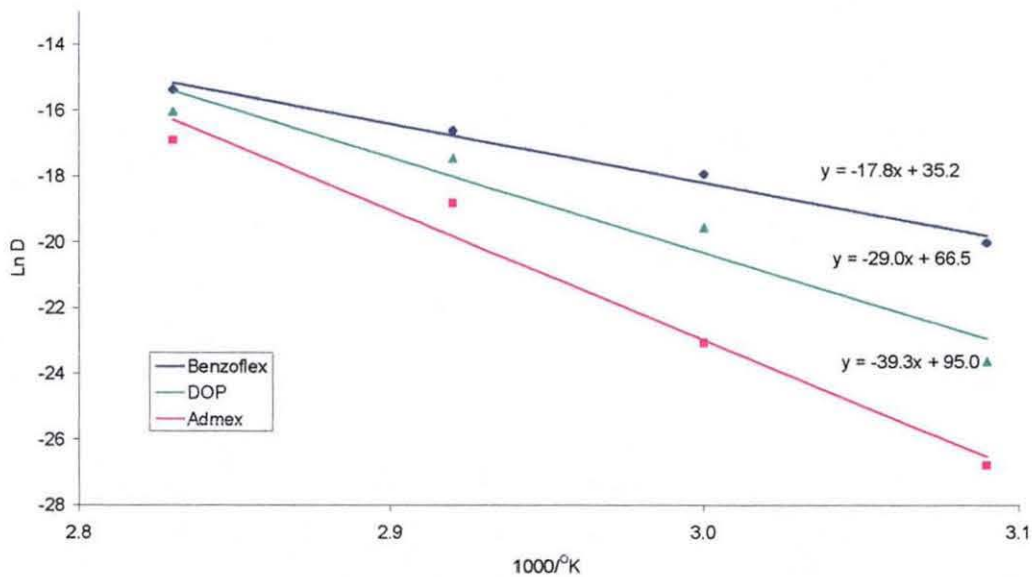
4.6.3 Activation Energy of Diffusion

It is possible to calculate the activation energy for diffusion using the equation:

$$D = D_0 \exp\left(\frac{-E_D}{RT}\right) \quad [\text{Equation 18.}]$$

Where E_D is the activation energy for diffusion, T is the absolute temperature and R is the universal gas constant (8.31). By plotting $\ln D$ versus T^{-1} , the gradient, m , of the plot will be:

$$m = \frac{-E_D}{R} \quad [\text{Equation 19.}]$$



Graph 4.6.3.i: Arrhenius plots for diffusion of plasticiser into PVC

Using this approach gave the following activation energies for the different plasticisers:

Benzoflex 2088: $147.9 \text{ kJ mol}^{-1}$

DOP: $241.0 \text{ kJ mol}^{-1}$

Admex 523: 326.6 kJ mol⁻¹

The energy available at room temperature may given by RT and assuming a temperature of 300K, this value is 2.5 KJmol⁻¹ which is considerably less than the activation energies of the diffusion process. The implications of these results are that diffusion will not occur, or will occur extremely slowly, at room temperature, therefore there would be virtually no change in the weld strength over a long period of time. As far as can be ascertained, this particular system has never before been treated in this way.

4.7 Atomic Force Microscopy

4.7.1 Introduction

Micro thermal atomic force microscopy (μ TA) is a relatively new technique allowing thermal properties of a sample to be examined on a microscopic scale. As the presence of degradation products in PVC leads to a change in the softening point of the specimen, a series of analyses should profile the extent of degradation away from a wire.

4.7.2 Topography Scan

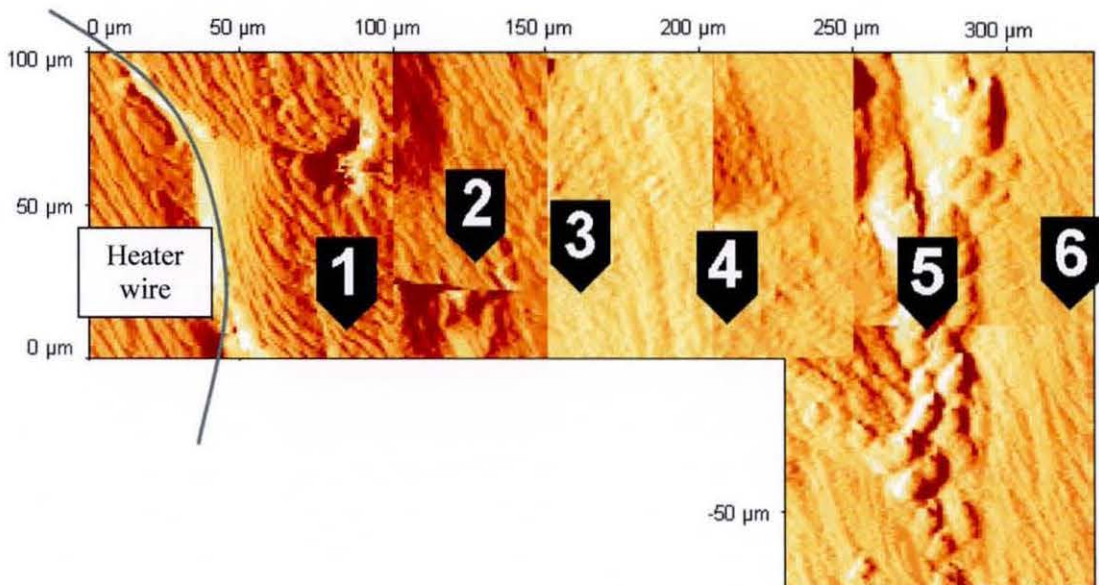
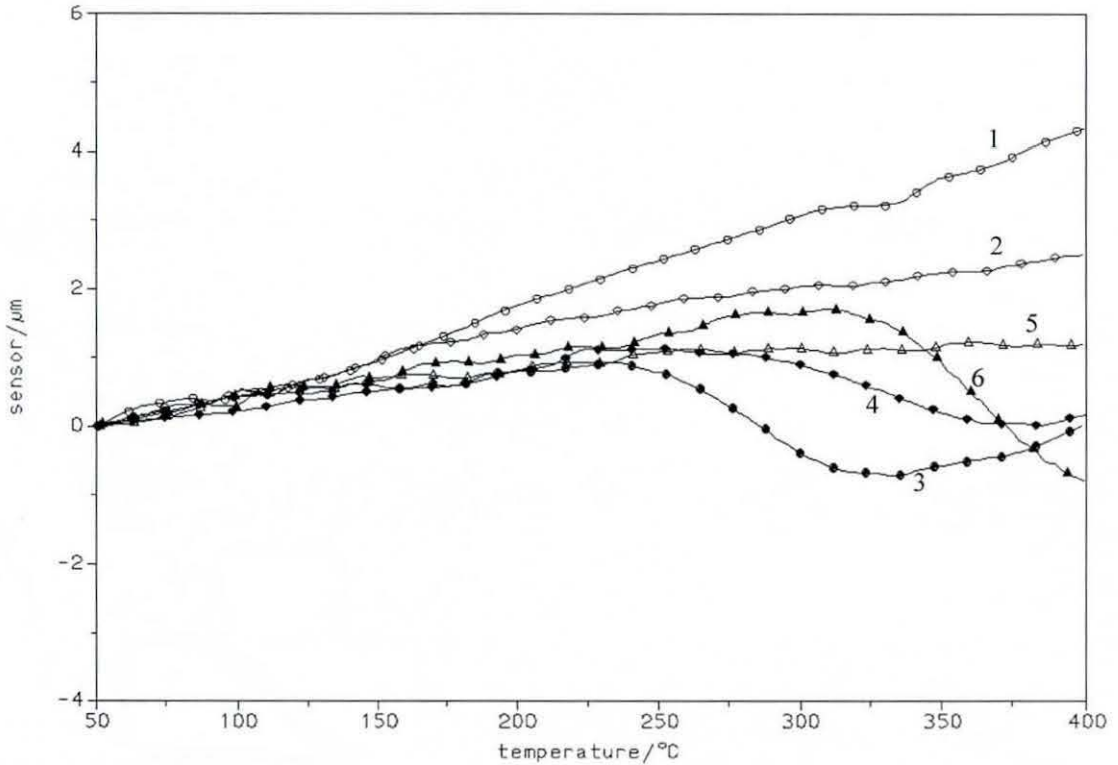


Figure 4.1: Composite topography image

Figure 4.1 shows a composite image of the specimen topography away from the heater wire. The presence of the wire and bulk of the material were expected, but the line of material along the interface (Point 5) was not. As can be seen from the μ TA results in Graph 4.7.3.i, the softening point of the PVC changed away from the wire but the material along the interface did not show a softening point.

4.7.3 μ TA Scans



Graph 4.7.3.i: μ TA results corresponding to marked points on Figure 4.1

The numbers next to the plot represent softening point data corresponding to the numbered areas in Figure 4.1. This chart shows how the position of the tip of the sensor moved as the temperature at its tip increased. A drop in the sensor reading indicates that it had softened the material and sunk into its surface. The upward trend at the beginning of the chart corresponds to thermal expansion of the material.

There was no explanation to account for the presence of the hard interface material as no interlayer was used and no compositional information is obtained from μ TA analysis. It was therefore decided to conduct laser induced mass analysis (LIMA) to obtain this information. A full presentation of the publication resulting (in part) from this work may be found in Appendix 2.

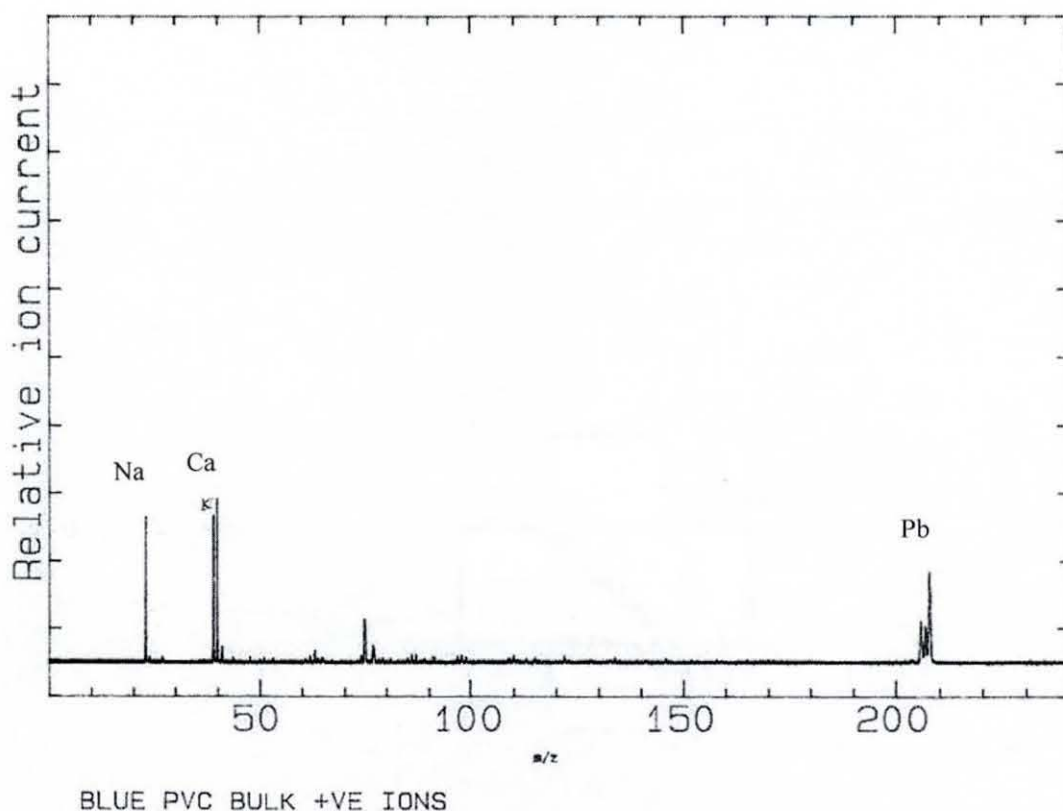
A second series of experiments was conducted to determine the sensitivity of the μ TA technique. Unfortunately, the μ TA was incapable of detecting low levels of degradation products and this line of inquiry was discontinued.

4.8 Laser Induced Mass Analysis

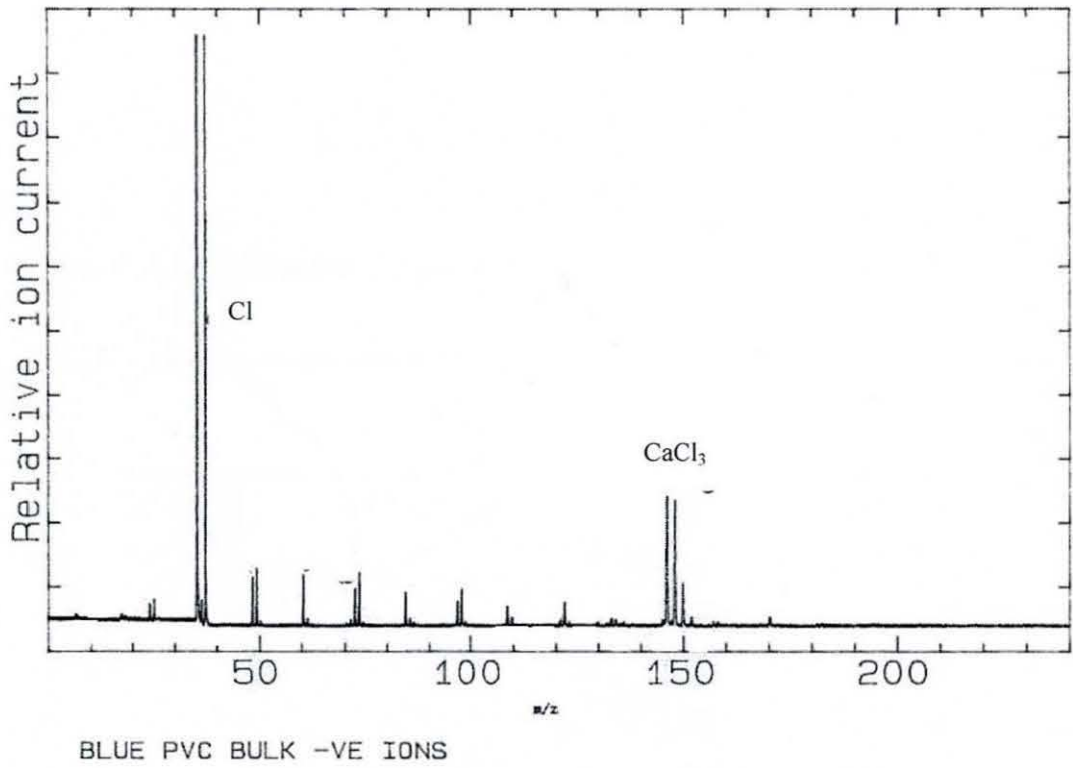
4.8.1 Introduction

This work was conducted to complement the μ TA results in the previous section. The composition of the hard material at the interface was determined to be degraded PVC. This was achieved by comparing scans from the bulk of both halves of the sample with scans taken from the edge of both halves. LIMA results took the form of both positive and negative spectra and while they are not quantitative, they do indicate the presence of a substance by the presence of a peak.

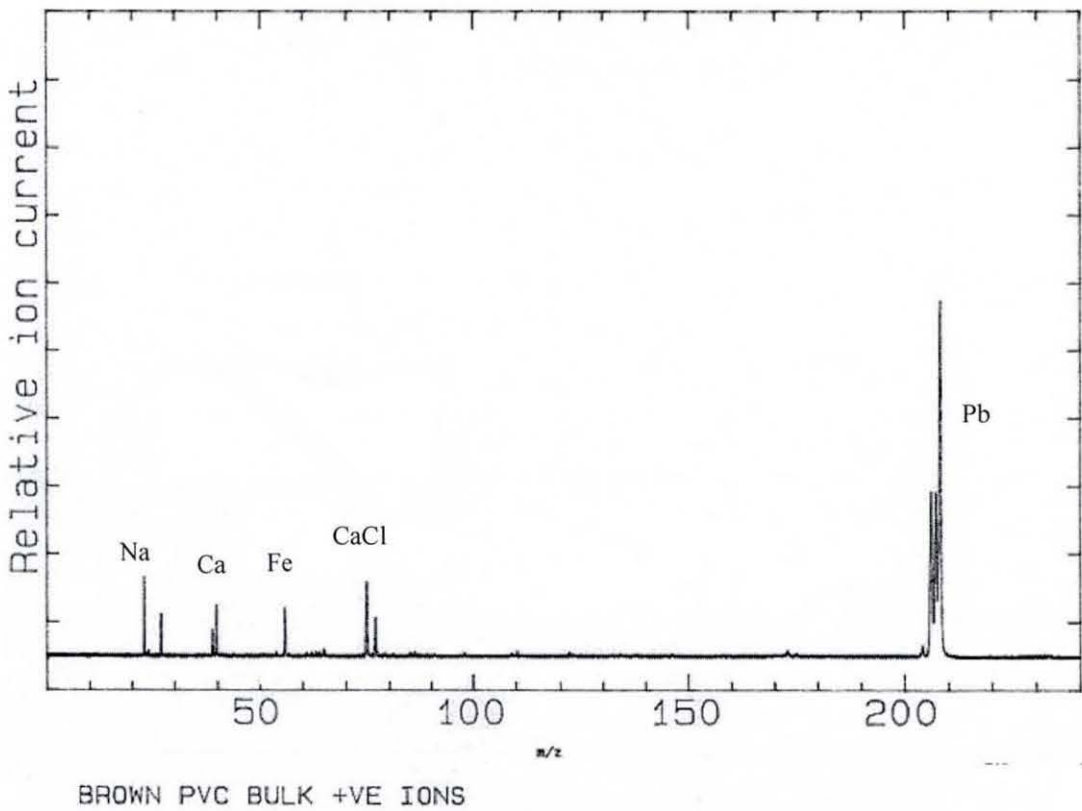
4.8.2 LIMA Spectra



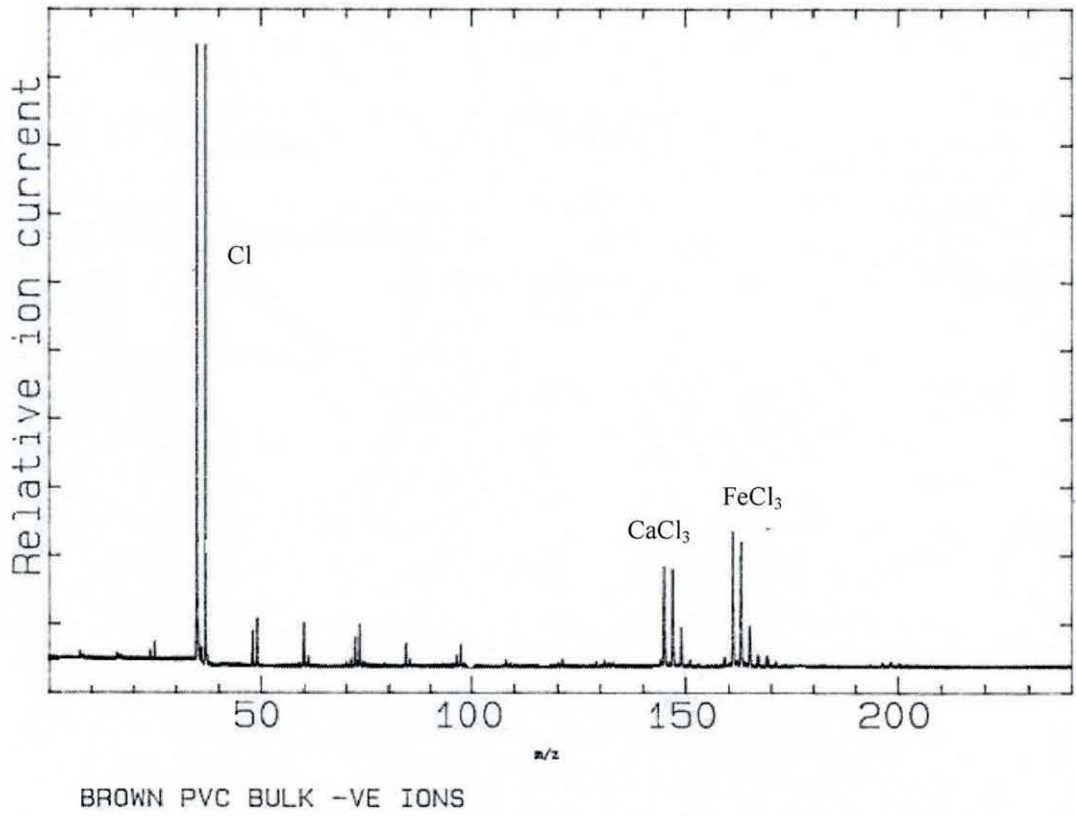
Graph 4.8.2.i: Blue bulk positive spectrum



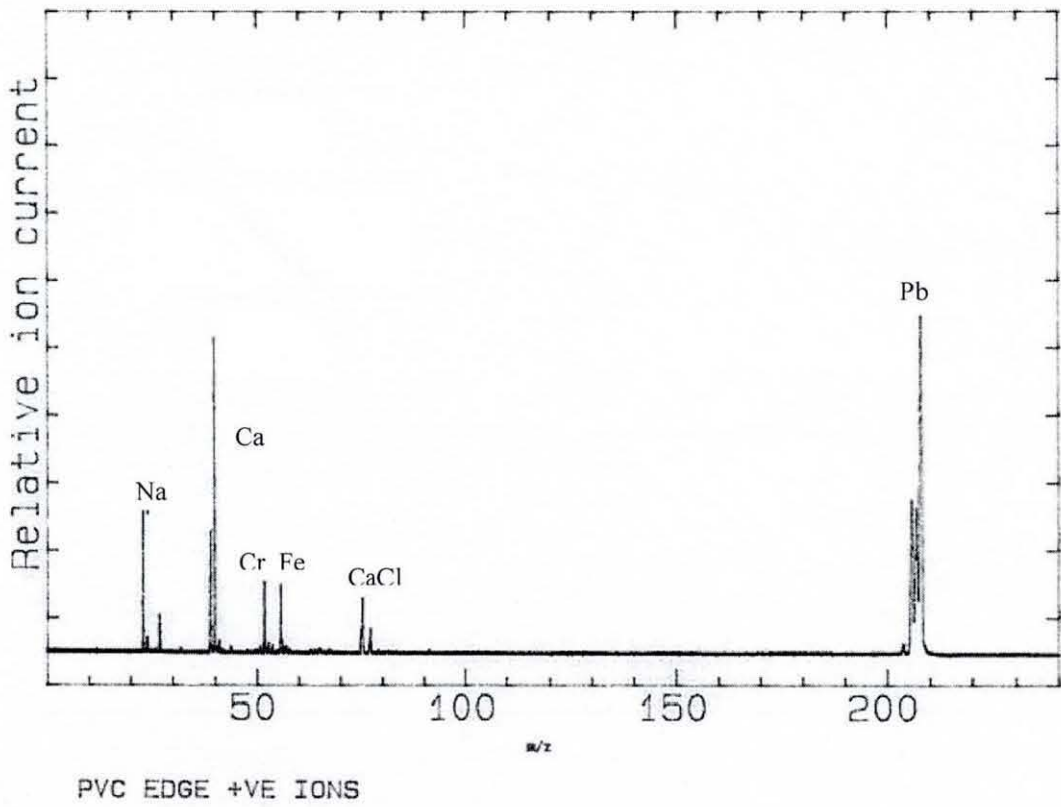
Graph 4.8.2.ii: Blue bulk negative spectrum



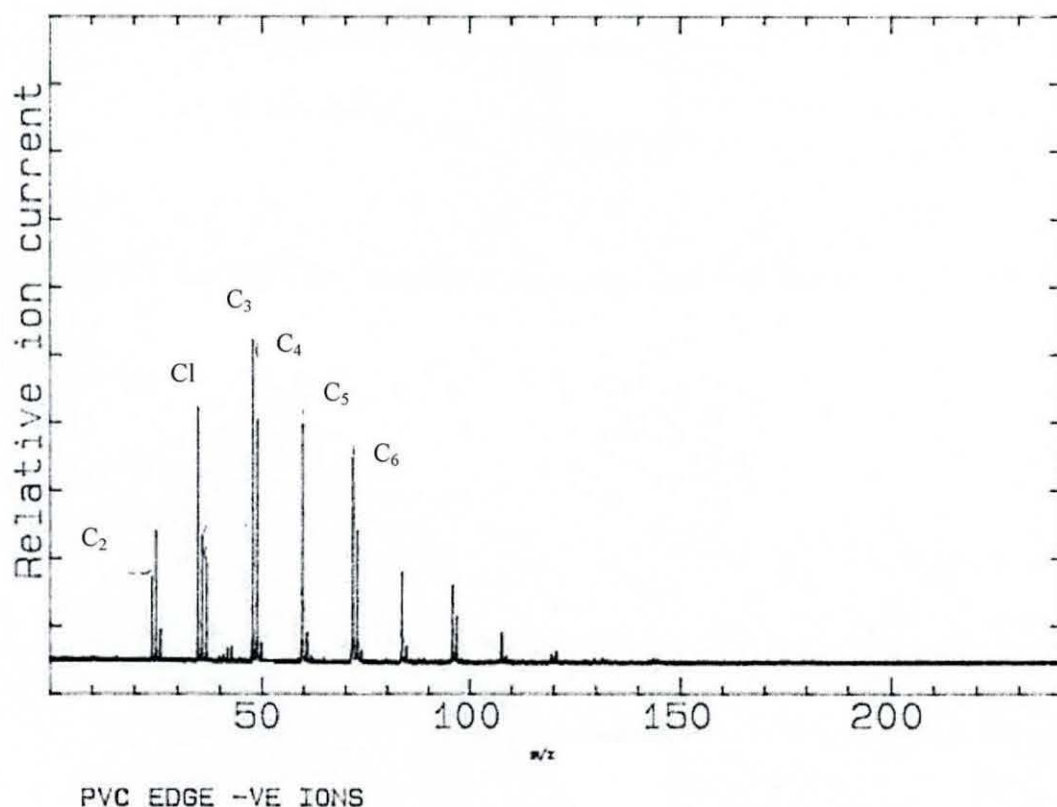
Graph 4.8.2.iii: Brown bulk positive spectrum



Graph 4.8.2.3.iv: Brown bulk negative spectrum



Graph 4.8.2.v: Edge positive spectrum



Graph 4.8.2.vi: Edge negative spectrum

In standard (or undegraded) PVC, the C_x peaks shown in Graph 4.8.2.vi are normally very much weaker when compared to the Cl peak. Therefore the very presence of C_2 to C_6 species in the edge spectra can be said to confirm the presence of PVC degradation products at the interface. The presence of degradation products away from the heat source (along the interface) may be due to the *Smarteat* process causing high frequency vibration between the components. All other species most likely arise from the additive package, the composition of which was not revealed.

4.9 Ultraviolet Fluorescence Microscopy

Samples were aged in an oven for various times and temperatures. Due to a very high level of background fluorescence, no results could be obtained from any samples.

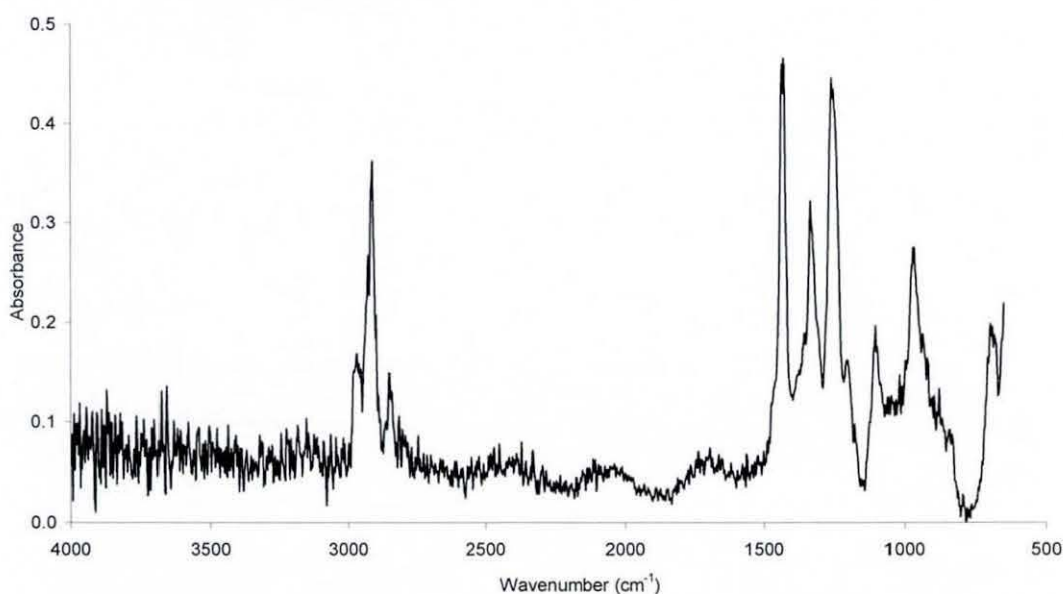
4.10 Microscopic Infrared Spectroscopy

4.10.1 Introduction

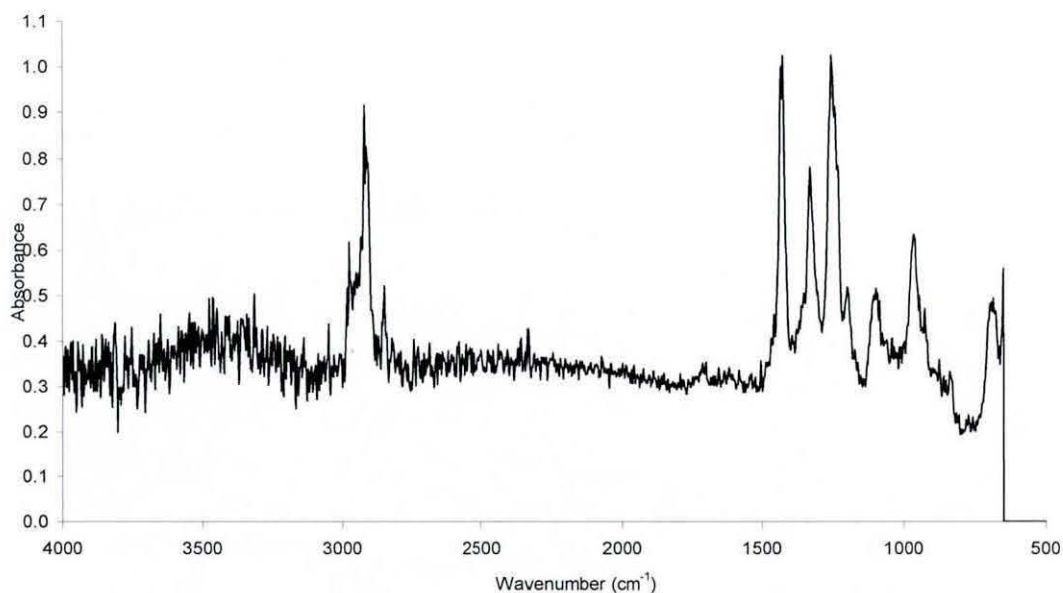
Microscopic IR spectroscopy was used to determine the extent of degradation around a heater wire. Control and sample scans are presented along with degradation profiles for various heating times and methods. The peak of main interest is the carbon-bromine peak found between 550 and 750cm^{-1} .

4.10.2 Infrared Spectra

The following spectra were taken from a sample welded using the isothermal *Smarteat* technique for 180 seconds. This welding time was used to determine the effect of excessive heating on a sample and because a sample with a larger amount of degradation readily indicated if the bromination process was successful. The spectra presented have had control and water vapour spectra subtracted from them. This was necessary to remove any peaks that were due to the PVC, leaving only those species present because of the bromination process.

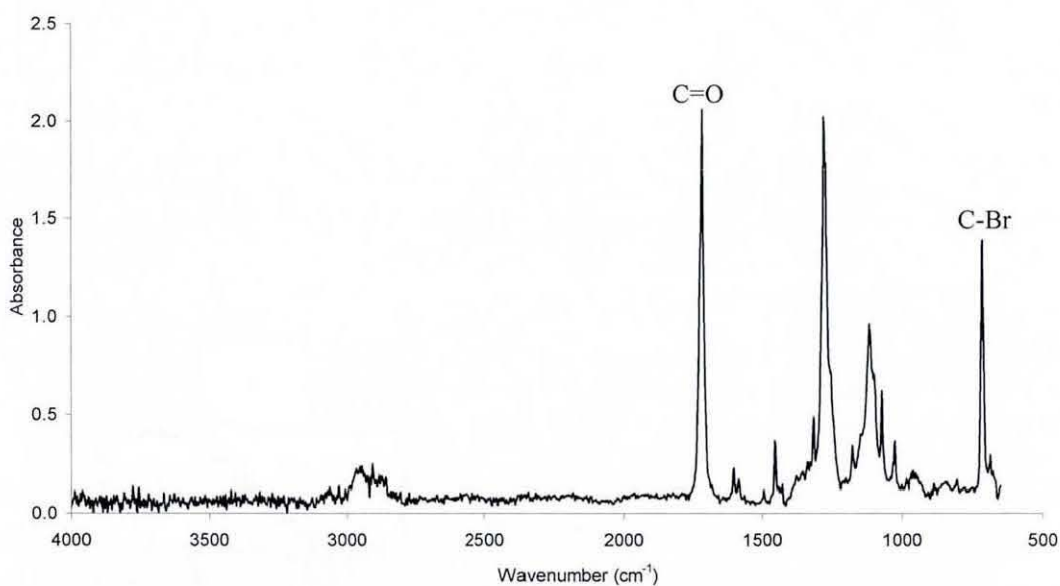


Graph 4.10.2.i: Bulk PVC pre-bromination, control spectrum

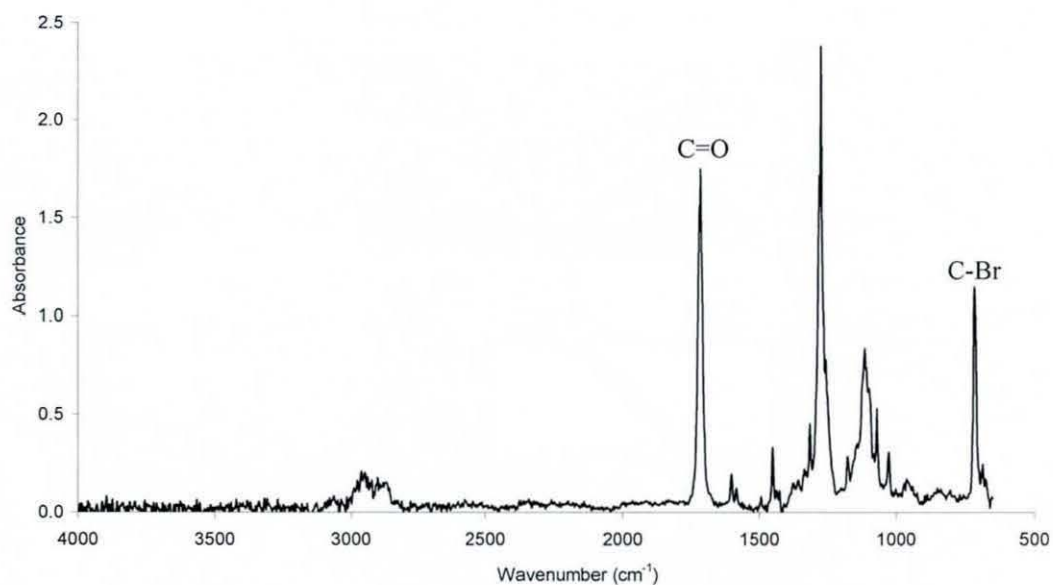


Graph 4.10.2.ii: Bulk PVC post-bromination, control spectrum

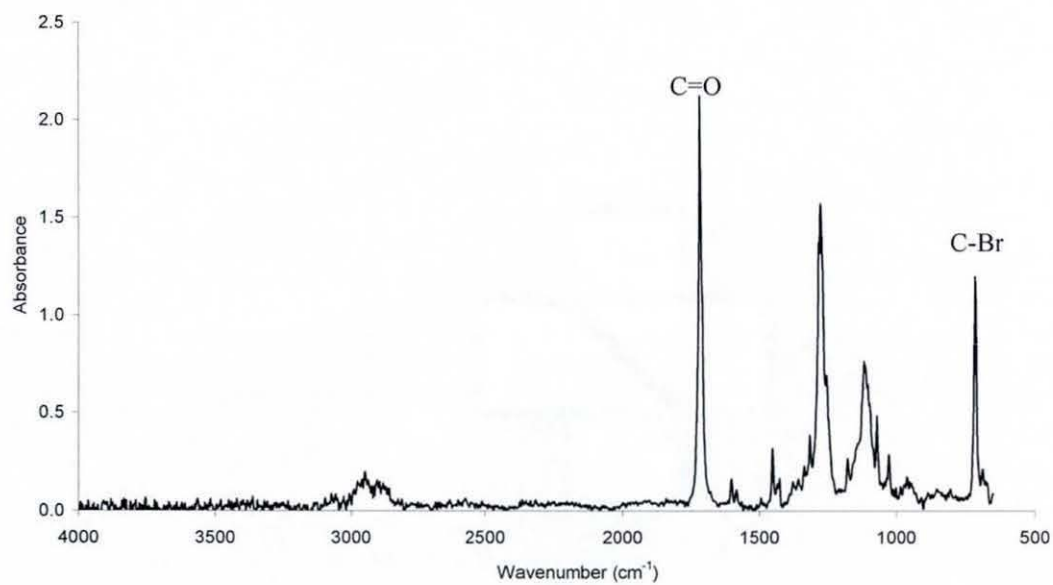
There is very little difference in the control spectra taken at distances away from the heater wire for both pre- and post-bromination and no bromine peak is present. This would indicate that any peaks found around the wire were not normally present in the PVC and are not due to interaction of bromine with undegraded PVC.



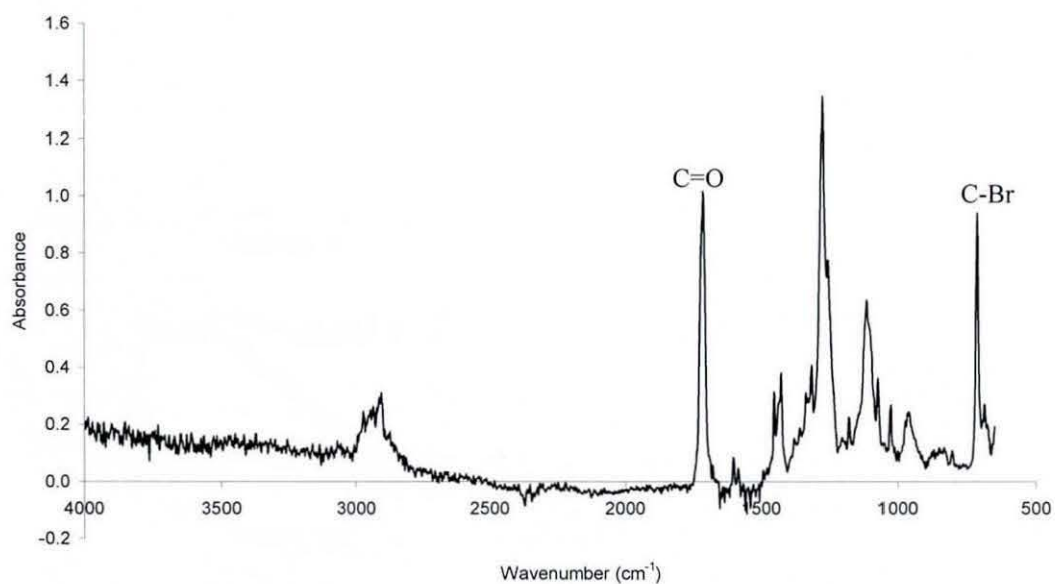
Graph 4.10.2.iii: Spectrum taken next to heater wire



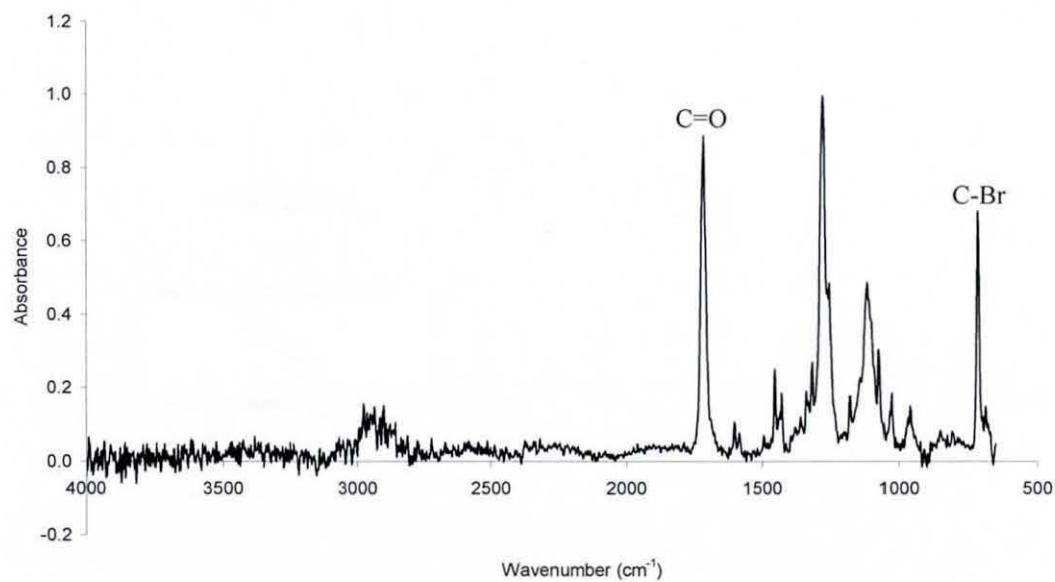
Graph 4.10.2.iv: Spectrum taken 0.09mm from heater wire



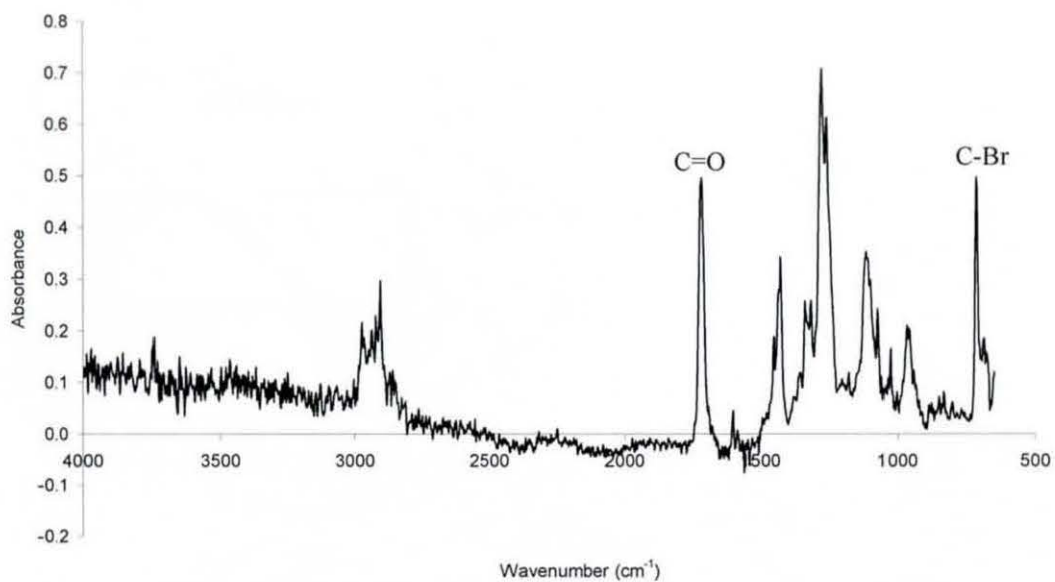
Graph 4.10.2.v: Spectrum taken 0.18mm from heater wire



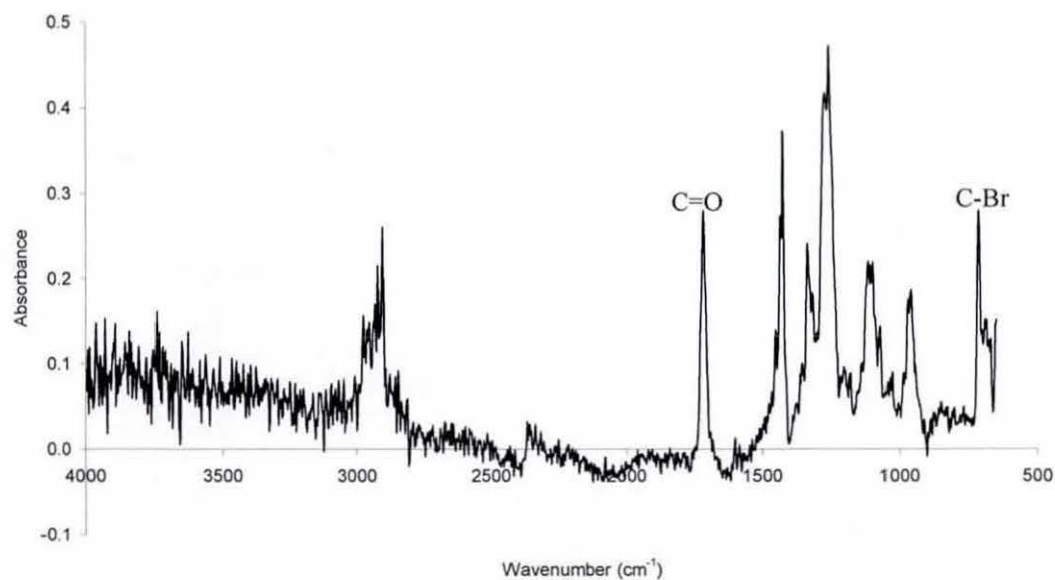
Graph 4.10.2.vi: Spectrum taken 0.27mm from heater wire



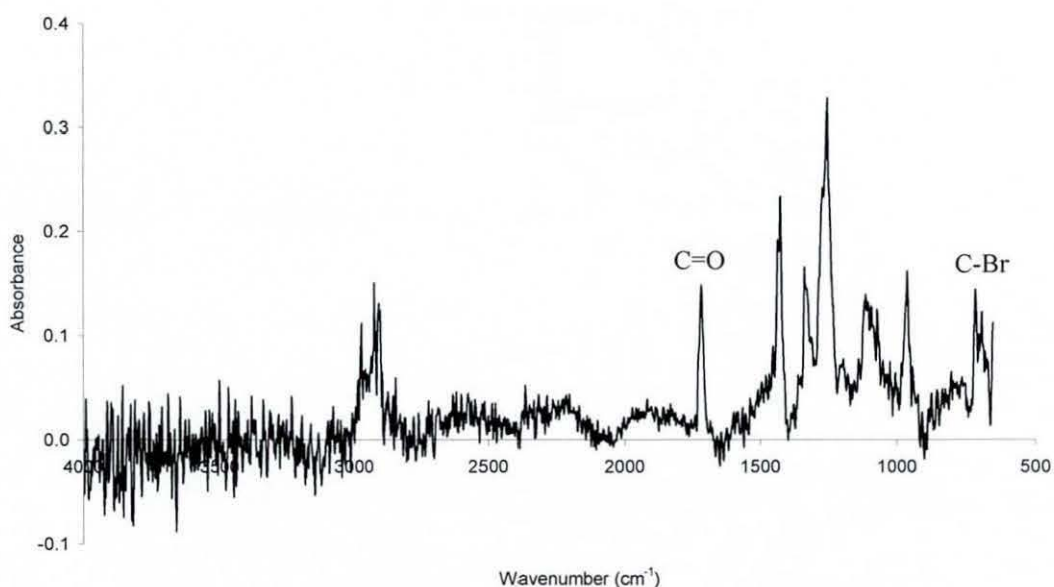
Graph 4.10.2.vii: Spectrum taken 0.36mm from heater wire



Graph 4.10.2.ix: Spectrum taken 0.45mm from heater wire



Graph 4.10.2.ix: Spectrum taken 0.54mm from heater wire

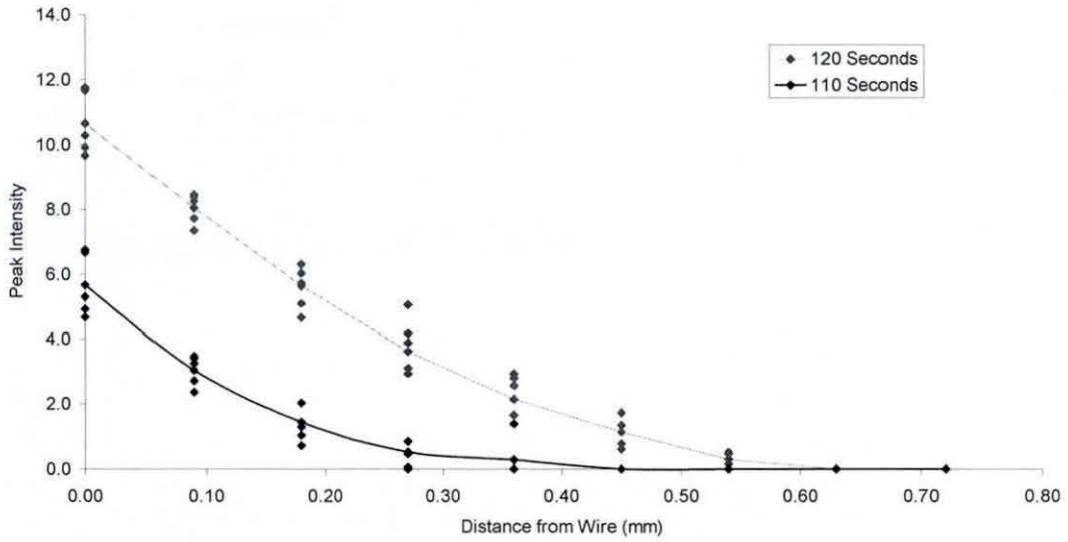


Graph 4.10.2.x: Spectrum taken 0.63mm from heater wire

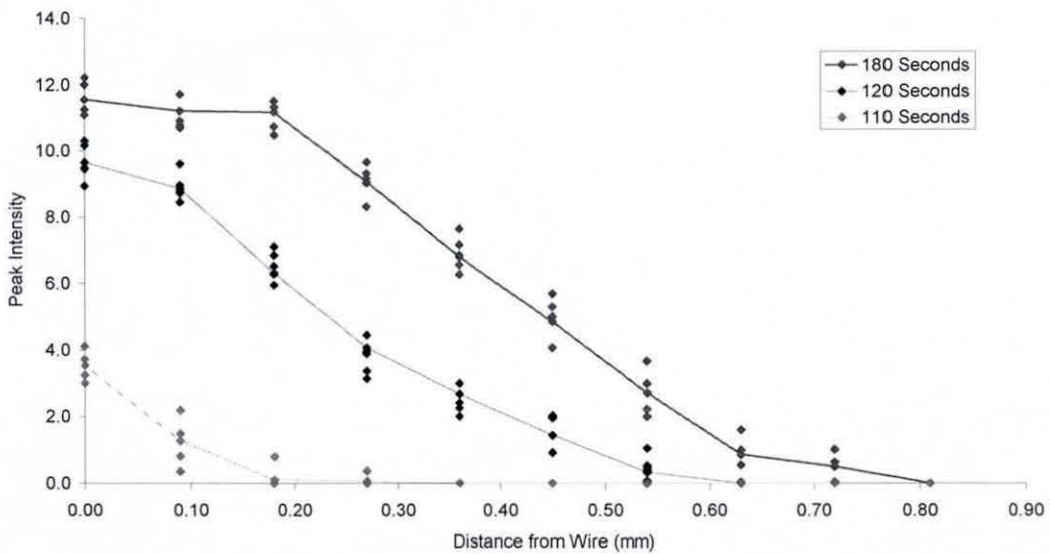
It can be clearly seen that the bromination procedure and subsequent infrared analysis was a success. The charts above show a clear difference between spectra taken in the bulk of the material where no significant degradation had occurred both pre- and post-bromination, and those taken around a heater wire. The spectra also show a reduction in the carbon-bromine and other associated peaks as distance from the wire increases. Since the additive package used in this commercial material was undoubtedly complex, those peaks that were not associated with the carbon-bromine bond were not considered. Their origin was unknown, as was their relation to the extent of degradation. The decrease in the intensity of the carbonyl peak was thought to be due to the interlayer and its concentration change away from the interface.

4.10.3 Degradation Profiles.

Due to a larger than expected scatter in the peak intensity data, it was decided to use “depth of penetration” rather than amount of degradation around the wire as an indicator. This method was more accurate because the position of each scan away from the wire was precisely measured using a graticule.



Graph 4.10.3.i: Profile of degradation around resistance heated samples (bromine peak)



Graph 4.10.3.ii: Profile of degradation around isothermally heated wire (bromine peak)

These profiles show that isothermal heating produced little difference in the amount of degradation seen around a wire, with the depth of penetration of degradation virtually the same for both processes. The shape of the curves was different,

however, with the isothermal data showing a tendency to form a plateau at distances close to the wire. This is thought to be due to heating of the surrounding polymer to the self-regulation temperature of the wire. As the resistance wire had no regulation properties, the temperature of the surrounding material continued to climb until the power supply was switched off. If it were possible to measure the temperature of the material surrounding an embedded wire on a micron scale, it is not an unreasonable assumption that the data would appear similar in shape to that of degradation.

These results have shown that while degradation is occurring, it is not on a scale that is visible to the naked eye in terms of discolouration and charring of the PVC. It can be seen from the micrograph 4.4.3.iv (sample isothermally welded for 180 seconds) that if the welding time were increased above 120 seconds, deleterious degradation does occur.

5.0 GENERAL DISCUSSION

5.1 Introduction

The objective of this research was to study the feasibility of thermally welding PVC. This has been accomplished using diffusion promoting interlayers specifically designed to promote interdiffusion between two compression moulded PVC plaques. The use of flat plaques rather than using pipe sections has allowed the completion of a large number of tensile tests (~700) without the difficulties associated with testing pipe sections. Conventional PVC pipes have never, to the authors knowledge, been tested in a way that allows the strength of a joint to be evaluated; conventional PVC water pipes are joined by a push-fit method with no adhesion taking place. The methods used to test PE pipes that have been thermally welded for many years¹⁹ were not transferable to PVC, which is relatively brittle in comparison. Furthermore by using actual pipe sections manufactured by Uponor Limited as a base material, the exact additive package has been studied.

5.2 Interlayers

The interlayers used in this research consisted of a PVC homopolymer, or copolymer with vinyl acetate and a plasticiser. In order to determine the optimum concentration of plasticiser, four different amounts were tested for each resin/plasticiser combination. The interlayers were solvent cast and met every functional requirement made of them. This method of production has proved very successful, other methods attempted (in-situ thermal fusing a plastisol), contributed to the thermal history of the interlayer, consuming a proportion of the stabiliser.

5.3 Welding

To supply heat to the system, two methods have been employed. The first, extensively used method was a heater element made from Nichrome wire through which a constant electrical current and voltage was passed, in much the same way as electrofusion is accomplished. The second, relatively new technique, known as *Smarteat*, used a continuously changing electromagnetic field to induce a current in a self regulating, composite metallic wire. This process has been shown to be

isothermal in nature when used in the system described above. Directly comparing the two methods in terms of ease of use, there is little between them. Advantages of *Smartheat* make themselves apparent with respect to the amount of degradation produced. Resistance welding produces an exponential increase in degradation as distance to the heater wire decreases, whereas the amount of produced by *Smartheat* is constant at distances close to the wire. Further away from the wire, the degradation profile is the same as for resistance heating.

5.4 Lap Shear Testing

Lap shear testing was the main performance indicator, and a direct measurement of the weld strength. It was carried out using a standard tensile tester with spacers to offset the specimens in the grips preventing off-axis loading. Lap shear results have shown that the development of strength increases with welding time, a large increase occurring as interdiffusion of the plaques began after approximately 90 seconds. The strength continued to increase after this time with resistance heating, reaching a maximum after 110 seconds. With isothermal welding, the peak strength was reached after 120 seconds in a similar pattern to resistance heating. The amount and type of plasticiser was also important, Benzoflex 2088 produced the highest strength and Admex 523 the lowest. Fracture was interfacial at low plasticiser concentrations and lap shear strengths, changing to part cohesive at higher strength and optimum plasticiser levels. At high plasticiser concentrations, fracture type was again interfacial. To the authors knowledge, this exact system has never been treated before in this manner. Although the lap shear test has been successfully used in a polymer adhesion study, which presented results supporting the suitability of the test method¹⁴⁹.

5.5 Hardness Testing

Vickers hardness testing has shown that it was possible to measure the depth of diffusion in a welded sample. Although this test is not widely used for polymers, it was found sufficiently reproducible for inclusion in this research. The nature of the indentation left in the sample made it possible for any orientation to be assessed, although no evidence of orientation was found in welded samples.

The change in the hardness profile across the interface with increased welding time has shown that the plasticiser moves away from the interface, with an accompanying increase in interfacial zone hardness and strength. At short welding times, the plasticiser was concentrated around the interface and produced a soft and relatively weak area, which lead to lower lap shear strengths. As welding time was increased, the surrounding plaque material was softened by plasticiser, and allowed interdiffusion to occur more readily.

Tests to evaluate orientation in pipe samples have shown that there was a measurable orientation in MoPVC pipes in some cases, but this was insufficiently greater than experimental error to warrant further investigation. This was due to the small (1:1.6) draw ratio of MoPVC pipes; the literature which led to this line of inquiry quoted results from materials with a much greater draw ratio (1:20). During diffusion depth analysis, no evidence of orientation at or near the interfacial zone was apparent. The hardness of the interlayers prior to welding gave results that were confirmed by the literature¹⁴⁹, but relationship was found between this property and the lap shear strength of the sample made with these interlayers.

5.6 Diffusion Testing

Diffusion testing has shown that the plasticiser that produced the highest lap shear strength had the lowest activation energy for diffusion. The strength produced by plasticisers was dependent on this value, with the lap shear ranking of the plasticisers identical in terms of activation energy increase. This result was to be expected since the mechanism responsible for any strength development was interdiffusion. It was expected that a more efficient plasticiser (i.e. one with a low activation energy) would result in higher lap shear strength, although toxicity issues may seriously limit the available plasticisers.

All the plasticisers tested had activation energies much greater than the energy available at room temperature. The practical result of this was that the lap shear strength of a welded component was unlikely to change with time, a result of considerable importance when the service life of pipe systems should be greater than 25 years. The activation energy for diffusion also had implications for storage of components and meant that, ignoring other factors, the interlayers may be stored in contact with the PVC pipe, (also preventing contamination), for long periods without

plasticiser migration. However, it should be noted that a degree of joint strength might develop between interlayer and pipe due to intimate contact.

The measured DOP diffusion coefficient agreed well with published values⁴, allowing for variation in formulation of PVC and DOP quality, no data could be found concerning the other two plasticisers.

5.7 Microscopy

Optical microscopy has shown how the interface develops over the welding time for both resistance and isothermal heating. Although some cohesion was developed at short welding times, the lap shear strength increased after 90 seconds of heating in both cases. There was little to tell the two systems apart, both showed a gradual reduction in the thickness of the interlayer over time until 120 seconds when the interlayer had fully diffused and was no longer visible as a separate phase. There was strong evidence to support the occurrence of interdiffusion. Micrographs were presented that clearly show whitened and yielded fracture surfaces between heater wires on high-strength samples.

5.8 Degradation Analysis

PVC degrades when it is heated and as the welding process supplied sufficient thermal energy to cause melting, at a temperature above that where degradation occurs, this was also studied. A number of different methods were assessed, including atomic force microscopy (AFM), fluorescence microscopy and spectroscopic techniques.

5.8.1 Atomic Force Microscopy and LIMA

AFM measured the change in softening point of the PVC, as it degraded, due to the formation of unsaturation and cross-linking. AFM was shown to be an extremely useful technique since it was able to produce a topographical image of the specimen then perform micro-thermal analysis on a few cubic microns of material at any desired point on the image. Although this work resulted in publication it was not sufficiently sensitive to quantify low levels of degradation and lacked compositional information. To overcome the latter disadvantage, laser induced mass analysis (LIMA) was used to provide compositional data. LIMA was selected because it did

not charge the sample, it detected all elements except hydrogen and most importantly, it could analyse a small area which was essential when attempting to monitor change of degradation with distance from the heat source. It was found that a high softening point material identified during AFM analysis was indeed degraded PVC but unfortunately the LIMA technique was not sufficiently sensitive to attempt profiling.

Due to the very recent development of the μ TA-AFM and the lack of interest in the LIMA technique, no published data could be found for comparison.

5.8.2 Fluorescence Microscopy

Fluorescence microscopy analysed degradation in terms of fluorescing carbon-carbon double bonds. These bonds fluoresce visible light when illuminated by ultraviolet radiation but unfortunately, the blue pigment in the PVC plaques also fluoresced and gave rise to a very large background fluorescence. Due to the large background fluorescence, no degradation could be detected, however, under correct conditions, this technique has been shown to be valid¹⁵⁰.

5.8.3 Infrared Spectroscopy

Infrared (IR) techniques are often used to obtain compositional and structural information from polymers. A standard IR spectroscope analyses several square centimetres of material, much greater than the resolution required by this research. It was therefore decided to make use of a little-used accessory for the IR, a specially constructed microscope. The use of an aperture and the visible light mode of the microscope made it possible to select a suitable area and analyse it using the IR mode. Carbon-carbon double bonds were rendered more visible to the IR spectroscope by adding a bromine molecule across the bonds using a novel vacuum derivatisation technique.

Results have shown that for both heating processes the intensity of the peak associated with carbon-bromine decreased exponentially away from the heater wire. In the case of isothermal heating, there was a region next to the heater wire corresponding to constant degradation. This is anticipated to be a product of the isothermal process; as the wire reached its isothermal temperature, so did the material surrounding it and the area at the isothermal temperature would grow larger as the welding time increased. Experimental results have shown that this was indeed the

case; there was a small plateau region for a welding time of 120 seconds, and a significantly larger region for those sample welded for 180 seconds.

Although no results on the exact equivalent of this work have been published, the derivatisation technique has been used previously on the study of polymer surfaces by XPS^{151, 152}, and FTIR has been used to study PVC degradation in-situ¹⁵³ and also by looking directly for the carbon-carbon double bond¹⁵⁴.

5.9 Summary

The table and passage below brings together all of the results and discussions presented above and attempts to present theory explaining the effects of the use of diffusion promoting interlayers.

Table 5.1 Properties of selected interlayers

Resin	K-value	Plasticiser	Activation Energy (kJ mol ⁻¹)	Optimum Concentration (wt.%)	Peak Lap Shear Strength (MPa)
GA9028	59	Benzoflex	147.9	23	6.0
GA9028	59	DOP	241.0	28	1.6
GA9028	59	Admex	326.6	38	1.5
K57	57	Benzoflex	147.9	27	4.2
K74	74	Benzoflex	147.9	40	3.2
K80	80	Benzoflex	147.9	> 60	3.0

From table 5.1 it is possible to identify the best interlayer and suggest reasons why this was the case.

Considering the effect of plasticiser type, the activation energy for diffusion had a strong influence on resultant lap shear strength with a clearly visible trend. As the welding time was the same for all of the samples above, the plasticiser with the lowest activation energy diffused further than a plasticiser with a higher activation energy, imparting a higher degree of chain mobility (plasticisation) than a plasticiser of lower activation energy. It was this property that was key to obtaining a strong joint. This also allowed a flatter plasticiser concentration profile across the interfacial zone.

Microhardness testing has shown that a large concentration around the interface leads to lower lap shear strengths, as is the case with welding times less than 90 seconds. The same effect is also achieved when welding at 120 seconds with a less efficient (greater activation energy) plasticiser. As the plasticiser requires a greater energy input to diffuse, it has less time to move away from the interface. This can be seen from the table above, where less efficient plasticisers require a greater initial concentration to achieve peak lap shear strength.

The presence of vinyl acetate in the interlayer resin also has some effect. Vinyl acetate is usually copolymerised with vinyl chloride as an internal plasticiser. The small amount of plasticisation imparted (in comparison with primary plasticisers) is often used by manufacturers as a processing aid to assist flow during production. In the context of this work, interlayers containing a copolymer have produced a higher lap shear strength than a homopolymer of a similar K-value. GA9028 has a K-value of 59 which, taken in isolation, should result in a slightly lower lap shear strength than a resin of K 57. However, the use of GA9028 resulted in a higher lap shear strength than a K 57 homopolymer, which can be attributed to an slight increase in the plasticisation of that interlayer, without the loss of strength that may have arisen from the use of a liquid.

In conclusion it can be said that the most important factor in the thermal welding of PVC using interlayers was correct plasticisation. The concept of using a diffusion promoting interlayer is sound but careful attention must be paid to the constitution of the interlayers used. The extent of plasticisation and hence diffusion (assuming welding variables are constant) must be balanced against the risk of producing an overly soft and hence weak interfacial zone.

6.0 CONCLUSIONS AND FURTHER WORK.

6.1 Conclusions

In summary, it can be said that a thermal welding process has been successfully used to weld PVC pipe materials. This statement is only valid if diffusion-promoting interlayers are used. These interlayers transfer heat to the substrate, melting in the process and allowing the plasticiser contained in them to diffuse into the PVC substrates. The type and concentration of plasticiser is crucial. Diffusion testing has shown that plasticisers with low activation energy produced higher lap shear strength than those of higher activation energy. The K-value of interlayers was the most important resin property, although the lap shear strength was further increased when this is combined with a small (10%) amount of acetate in a copolymer.

The amount of degradation was successfully and quantitatively measured by FTIR spectroscopy. In order to do this a novel bromine derivatisation technique had to be developed. By heating the sample and carrying out the reaction under vacuum to assure 100% concentration of bromine around the sample, carbon-carbon double bonds were made highly visible in the IR absorption spectrum. By using an IR microscope with a narrowed field of view, successive spectra were taken by moving the specimen under the microscope to produce a profile of the degree of degradation away from a heater wire. The advantage of this technique was that it might be used on virtually any PVC sample, whether specially prepared or taken from a component, with minimal preparation. To the author's knowledge this has never before been attempted and represents a significant advance in the field of infrared analysis.

Research carried out to assess the feasibility of thermally welding PVC has provided a detailed insight into the factors affecting this process. In addition, a method of detecting degradation in a complex commercial material while keeping the structure of the sample intact has been developed. The following conclusions may be drawn from this work:

The prime objective in this research was to determine the feasibility of thermally welding two uPVC substrates. The results presented in this thesis have shown that this objective has been achieved, providing that certain procedures are followed. In achieving the primary objective, it was necessary to offer solutions to other, equally

important problems, relating to more specific issues associated with thermally welding uPVC. These are addressed below.

The objective to devise a suitable method of using interlayers has been met, as has a means of measuring degradation, which was achieved by the use of FTIR profiling. The objective to optimise the composition of the interlayers has been substantially completed, by testing various compositions using lap shear strength as a performance measure, although further work would be beneficial to future development.

More specific conclusions arising from the work done in meeting these overall objectives are given in the following pages.

6.1.1 The use of diffusion-promoting interlayers makes the thermal welding of PVC possible without causing deleterious degradation. The composition of interlayers must be optimised to achieve maximum weld strength.

6.1.2 Fast fusing plasticisers lead to higher weld strength than slower fusing plasticisers. Slower fusing plasticisers require a higher concentration to achieve a peak weld strength. For example, plasticiser with an activation energy of diffusion of $147.9 \text{ kJ mol}^{-1}$ reaches peak weld strength at 20 to 25 wt.% compared with 40 to 45 wt.% for a plasticiser of activation energy of $326.6 \text{ kJ mol}^{-1}$.

6.1.3 Vinyl chloride/vinyl acetate copolymer resins result in higher weld strength than a PVC homopolymer of the same K-value. The inclusion of an amount of acetate increases the plasticisation effect of the interlayer but without reducing interlayer strength, as would normally result when using an increased concentration of plasticiser.

6.1.4 The optimum welding time for a resistance welded component is 110 to 120 seconds. For an isothermally welded component, a peak strength is not observed until after a welding time of 120 seconds.

6.1.5 A study into the activation energy of diffusion has concluded that further diffusion of plasticisers at room temperature is unlikely to occur to any significant degree.

6.1.6 Movement of plasticiser and associated softening of surrounding material in welded specimens containing an interlayer may be measured by Vickers hardness

testing. This technique has been shown to have sufficient resolution and repeatability to justify its use.

6.1.7 Degradation of welded PVC components may be monitored using microthermal atomic force microscopy. However, this technique may only be used in situations where a large degree of degradation is apparent. LIMA may be used to confirm the presence of conjugated carbon-carbon double bonds.

6.1.8 The amount of degradation around a heater element embedded in PVC may be profiled with increasing distance from the wire using microscopic IR analysis. This technique is sufficiently sensitive to distinguish between an isothermal process and a constantly increasing heat source.

6.2 Further Work

Given scope for further studies into the thermal welding of PVC, areas that are considered relevant with respect to this study are as follows:

6.2.1 Factors relevant to the *Smartheat* process, such as wire temperature and wire spacing could further optimise the process.

6.2.2 The effect of an even faster fusing plasticiser could determine if there is an optimum activation energy for diffusion. This should be considered with respect to possible service life since no reduction of weld strength can be tolerated.

6.2.3 The next logical stage in this research is to transfer the knowledge gained using made using flat plaques to actual pipe sections. There are currently no base data with which to compare thermally welded PVC components with, in the correct geometry.

6.2.4 The application of the vacuum bromine derivatisation technique could be further studied to identify additional materials and applications for which it may be used.

7.0 REFERENCES.

1. Oxford English Dictionary. University Press, Oxford, (2000).
2. M. Kaufmann. The History of PVC, Elsevier, London. (1969).
3. M. Kaufmann. *Plasts. & Polym.* **37, (12)**, 243, (1969).
4. W.V. Titow. PVC Technology, Elsevier, London (1984).
5. W.S. Penn. PVC Technology, Applied Science, Essex (1971).
6. J. Brydson. Pge. 319-321 *Plastics Materials*, 7th Edition, Butterworth Heinemann, London, 1999.
7. M. Gilbert, D.A. Hemsley, A. Miadonye. *Plast. & Rubb. Proc. & Appl.*, **3, (4)**, 343-351, (1983).
8. M. Gilbert. *Plast. & Rubb. Int.*, **10, (3)**, 16-19, (1985).
9. T. Hattori, K Tanaka, M Matsuo. *Polym. Eng. & Sci.* **12**, 199, (1972).
10. Y. Shinagawa. *Plast. Ind. News*, **65**, May 1973.
11. M.W. Allsopp. *J. Macromol. Sci. - Chem.*, **A11, (7)**, 1223-1234, (1977).
12. M.W. Allsopp. Pge 183-215, *Manufacture and Processing of PVC*, ed. R.M. Burgess, Applied Science Publishers, London, 1982
13. M. Gilbert, J.A. Covas, D.E. Marshall. *Plast. & Rubb. Proc. & Appl.*, **9, (2)**, 107-116, (1988)
14. Reference 3, page 99 in W.V. Titow. PVC Technology, Elsevier, London (1984).
15. C. Baker, W.F. Maddens. *J. Polym. Sci., Polym. Phys.*, **15**, 1041, (1977)
16. I.L. Gomez. *Engineering with Rigid PVC*. Applied Science, Essex. (1965).
17. Private conversation with IPTME Technical Staff.
18. A.J. Ganzeman. *Plast. Rubb. Proc. Appl.*, **4, (2)**, 127, (1984).
19. J. Bowman. *Polym. Eng. & Sci.* **37, (4)**, 674, (1997)
20. Private communication with Uponor Limited.

21. J.M. Stuart. "Fusion Welding of Polyethylene Pipe Using an Inductive Heating Method," Proc. The Use of Plastics and Rubber in Water and Effluents, p. 31.1 The Plastics and Rubber Institute, London, (February 1982).
22. T. Tight. "Smart Heat Induction Fusion Joining of Polyethylene Gas Pipes – Results of GRI Sponsored Project," Proc. Plastic Pipes VIII, paper no. E1/3, The Plastics and Rubber Institute, London (September 1992).
23. Private communication with Uponor Limited.
24. ASTM D 907-82.
25. E.M. Petrie. Handbook of plastics and elastomers, Applied Science. (1976).
26. N.S. Korenevskaya. J. Polym. Sci., **8**, 1372, (1968).
27. R.P. Wool, K.M. O'Conner. J. Polym. Sci., Polym. Lett. **20**, 7, (1982).
28. R.P. Wool, K.M. O'Conner. J. Appl. Phys. **52**, 5953, (1981).
29. K.M. Foster. Macromol., **24**, 1397, (1991).
30. J.L. Willett, Macromol., **26**, 5336, (1993).
31. I. Sutherland & R.J. Heath. Prog, Rubb & Plast. Tech., **14**, (3), 151, (1998).
32. W.C. Abrahms. Polymer. **19**, 291 (1978).
33. A.J. Kinlock. J. Mat. Sci., **15**, 2141, (1980).
34. T. Young. Trans. Royal Chemical Society, **95**, 65 (1805).
35. R.J. Good. J. Colloid Interface Sci., **52**, (2), 308-313. (1975).
36. D. Li, M, Xie, A.W. Neumann. Colloid Polymer Science, **271**, 573-580, (1993).
37. D.G. Rance in "Industrial Adhesion Problems" Ed. D.M. Brewis, D. Briggs. Orbital (1985), p.50.
38. J.R. Huntsberger. Journal of Paint Technology, **39**, 199 (1967).
39. J.R. Huntsberger. Int. J. Adh. & Adh., **2**, 13, (1982).
40. H. Ottewill in "Wetting Spreading and Adhesion, Ed. J.F. Padday, Academic Press, London. (1978).
41. D.G. Rance in "Industrial Adhesion Problems" Ed. D.M. Brewis, D. Briggs. Orbital (1985), p.54.

42. Dupre "Théorie Mécanique de la Chaleur." Trans. "Thermodynamic Theory." Guarthier-Villars, Paris. (1869)
43. H.W. Fox. *J. Colloid Sci.*, **5**, 514-231. (1950).
44. R.J. Good, L.A. Girafalco. *J. Phys. Chem.*, **64**, 561-564, (1960).
45. R. J. Good, L.A. Girafalco. *J. Phys. Chem.*, **43**, 1, (1964).
46. L.A. Girafalco, R. J. Good. *J. Phys. Chem.*, **61**, 94, (1957)
47. Sutherland. "Contact Angles, Wettability and Surface Energy" notes.
48. M. Fowkes. *J. Chem. Phys.*, **67**, 2538, (1963).
49. M. Fowkes. *J. Chem. Phys.*, **66**, 1863, (1962).
50. D.K. Owens. *J. App. Polym. Sci.*, **14**, 1725-1730, (1970).
51. D.K. Owens. *J. App. Polym. Sci.*, **13**, 1741-1747, (1969).
52. S. Wu. *J. Macromol. Sci. Part C*, **10**, 1, (1974).
53. S. Wu. *J. Polym. Sci. Part C*, **34**, 19, (1971).
54. F.M. Fowkes. *J. Adhesion*, **4**, 155, (1972)
55. R.S. Drago, G.C. Vogel, T.E. Needham. *J. Amer. Chem. Soc.*, **93**, 6014, (1971)
56. R.S. Drago, L.B. Parr, C.S. Chamberlain. *J. Amer. Chem. Soc.*, **99**, 3203, (1977)
57. P.G. de Gennes. *J. Chem. Phys.*, **55**, (2), 572-579, (1971)
58. M. Doi. *J. Chem. Soc., Faraday Trans.*, **2**, 1789, (1978)
59. R.P. Wool, Y.H. Kim. *Macromol.*, **16**, 1115-1120, (1983)
60. J. Klein, *Macromol.*, **11**, 582, (1978)
61. P.G. de Gennes, *J. Chem. Phys.*, **72**, (9), 4756-4763, (1980)
62. S.S. Voyutskii. *Autohesion and Adhesion of Polymers*. Wiley-Interscience, New York, (1963)
63. S. Prager, D. Adolf, M. Tirrel. *J. Chem. Phys.*, **75**, (10), 5194, (1981)
64. R.P. Wool. *Polymer Interfaces; Structure and Strength*. Hanser, (1995).
65. R.P. Wool, K.M. O'conner. *J. App. Phys.*, **52**, 5953, 1981.

66. D. B. Kline, R. P. Wool. *Polymer Engineering and Science*, **28**, (1), 52-57 (1988)
67. J. N. Anand. *Adhesion*, **1**, 39, (1969)
68. R.P. Wool. *New Trends in Physics and Physical Chemistry*. Plenum Press, New York, (1989).
69. S. Mazur, S. Reich. *J. Phys. Chem.*, **90**, 1365, (1986).
70. M. McLeish. *Polymer*, **30**, 1651, (1989).
71. J. Creton. *Macromolecules*, **25**, 3075, (1992).
72. ASTM D883 Plastics Nomenclature.
73. H. Barron. *Plastics*, **7**, 449, (1943)
74. Kirkpatrick. *J. Appl. Phys.*, **11**, 255, (1940)
75. A.K. Doolittle. *Plasticiser Technology*, Reinhold, Munich, (1954).
76. D.L. Buszard in *PVC Technology*, Ed. W.S. Penn, Elsevier, London, (1984).
77. J.K. Sears & J.R. Darby. *The Technology of Plasticisers*. Wiley & Son, New York, (1982)
78. C.J. Hawick. *Plastics Additives*. Chapman & Hall, London, (1998).
79. Harold A. Sarvetnick. *Plastisols and Organosols*. Van Nostrand Reinhold, London, (1972). Pge. 80.
80. A.W. Birley, B. Howarth, J. Batchelor. *Physics of Plastics, Processing, Properties and Materials Engineering*. Hanser, Munich, (1992).
81. J.K. Sears, J.R. Darby. *The Technology of Plasticisers*. Wiley & Son, New York, (1982).
82. Harold A. Sarvetnick. *Plastisols and Organosols*. Van Nostrand Reinhold, London, (1972). Pge. 82.
83. R. Gächter, H. Müller. *Plastics Additives Handbook*. Hanser, Munich, (1987).
84. Velsicol Chemical Corporation, MSDS for "Benzoflex 2088."
85. U. Jacobson. *Brit. Plasts.*, **32**, (4), 152, (1969).
86. D.L. Tabb. *Macromol*, **8**, (6), 929, (1975).

87. G. Pezzin. *J. Appl. Polym. Sci.*, **11**, 2533, (1967).
88. N. Kinjo. *Polym. J.*, **4**, (2), 143, (1973).
89. L.M. Robeson. *J. Polym. Sci. B*, **7**, 59, (1969).
90. L.M. Robeson. *Polym. Eng. Sci.*, **9**, 277, (1969).
91. G. Pezzin. *J. Appl. Polym. Sci.*, **16**, 1839, (1972).
92. P. Radiotis, G.R. Brown. *J. Macromol. Sci. – Pure App. Chem.*, **A34**, (5), 734-735, (1997).
93. P. Ayery. *J. Polym. Sci., Macromol. Rev.*, **8**, 1, (1974).
94. Z. Mayer. *J. Macromol. Sci.*, **C10**, 263, (1964)
95. T. Hjertburg, A. Wendel. *Polymer*, **23**, 1641, (1982).
96. Ivan, J.p Kennedy, T Kelen. *J. Polym. Sci. Polym. Chem.*, **21**, 2177, (1983)
97. K.B. Abbas, E.M. Sorvik. *J. Appl. Polym. Sci.*, **19**, 2177, (1983)
98. F. Tudos, T. Kelen, T.T. Nagy, B. Turcsanyi. *Pure Appl. Chem.*, **38**, 201, (1974).
99. G.R. Brown. *J. App. Polym. Sci.*, **46**, 179-187, (1992).
100. B. Ivan, *J. Polym. Sci. Polym. Chem.*, **21**, 2177, (1983).
101. K.B. Abbas. *J. Appl. Polym. Sci.*, **19**, 2991, (1975).
102. T. Kelen. *Pure Appl. Chem.*, **38**, 201 (1974).
103. H. Braun. *Macromol. Chem.*, **99**, 59, (1966).
104. J.L. Millan, G. Martinez, C. Mijangosc. *J. Phys. Chem.*, **180**, 2937, (1979).
105. J.L. Millan G. Martinez, C. Mijangosc. *J. Phys Chem.*, **185**, 1277, (1984).
106. D.E. Winkler. *J. Polym. Sci.*, **35**, 3, (1959).
107. B. Ivan. *Polymer Durability. Chapter 2, pge. 19, Amer. Chem. Soc.*, (1996).
108. N. Bensemra. *Polym. Degra. Stab.*, **28**, 173, (1990).
109. T. Hjertberg, E.M. Sorvik. *Polymer*, **24**, (6), 673, (1983).
110. T. Hjertberg, E.M. Sorvik. *Polymer*, **24**, (6), 685, (1983).
111. T. Hjertberg, M. Rogested. *Macromol.*, **26**, (1), 60-64, (1990).

112. K.S. Minsker, V.V. Listsky, V.V. Petrov. *J. Macromol. Sci. – Rev. Macromol. Chem.*, **C20**, (2), 243, (1981).
113. G. Martinez, J. Millan, C. Mijangos. *Polym. Bull.*, **5**, (7), 407, (1981).
114. G. Martinez, J. Millan, C. Mijangos. *J. Appl. Polym. Sci.*, **28**, (1), 33, (1983).
115. G. Martinez, J. Millan, C. Mijangos. *J. Appl. Polym. Sci.*, **29**, (1), 1735, (1984).
116. G. Martinez, J. Millan, C. Mijangos. *Eur. Polym. J.*, **21**, 387, (1985).
117. G. Martinez, J. Millan, C. Mijangos. *J. Polym. Bull.*, **13**, 151, (1985).
118. A.R. Amer. *J. Macromol. Chem.*, (ref 12 *Macromol* **26**, 60, 1993).
119. G. Martinez, J. Millan, C. Mijangos. *Polym. Degra. Stab.*, **40**, 1 (1993).
120. E.D. Owen in *Degradation and Stabilisation of PVC*, ed. E.D. Owen. Elsevier, London, (1984).
121. D. Bailey. *Macromol.*, **11**, (2), 312, (1972).
122. M.Y. Tsai, J. Morton, R.B. Krieger. *Journal of Advanced Materials*, **27**, (3), 28, (April 1996).
123. F.J. Balta-Calleja. *Journal of Materials Science*, **15**, 765-772, (1980)
124. J. Tabor. *The Hardness of Metals*. Oxford University Press,. Oxford, (1951).
125. R. Rueda. "The influence of Processing Conditions on the Micro-hardness and Structure of Injection Moulded Polyethylene" Draft copy, supplied by Uponor Ltd.
126. P. Eyerer. *Kunststoffe*, **62**, (5), 19, (1972).
127. J. Bowman, M. Bevis. *Plastics and Rubber: Materials and Applications*, pg. 177, September (1976).
128. F.J. Balta-Calleja. *Colloid and Polymer Science*, **254**, 258-266, (1976).
129. J. Bowman, M. Bevis. *Colloid and Polymer Science*, **255**, 954-966, (1977).
130. J. Bednarz, *Werkstofftechnik*. **4**, 195, (1970).
131. J.I. Goldstien. *Scanning Electron Microscopy and X-ray Microanalysis*, Plenum Press, New York, (1981).

132. J. Brown, C. Vickerman. *Surf. Interface Analysis*, **8**, (2), 75, (1984).
133. J. Brown, C. Vickerman. *Surf. Interface Analysis*, **6**, (1), 1, (1984).
134. *Practical Surface Analysis By Auger and X-ray Photoelectron Spectroscopy*.
Ed. D. Briggs & M.P. Seah, Wiley, Chichester, (1983).
135. N.S. Clarke. *Chemistry in Britain*, pg. 484, May 1989.
136. J. Haslam, H.A. Willis, D.C.M Squirrell. *Identification and Analysis of
Plastics*, Heyden, London, (1980).
137. D.H. Williams and Ian Fleming. *Spectroscopic Methods in Organic
Chemistry*, McGraw Hill, London, (1989).
138. R.A. Dickie, J.S. Hammond, J.E. deVries, J.W. Holubka. *Anal. Chem.*, **54**,
2045, (1982).
139. D.K. Bowen. *Microscopy of Materials: Modern imaging Techniques Using
Electron, X-Ray and Ion Beams*. Macmillan, London, (1975).
140. B.P. Richards. *Microscopy Handbook Number 25*, Oxford University Press,
Oxford, (1992).
141. E.A. Nash, G. Nicholls. *Nature* **237**, 510 (1972).
142. C.F Binnig,. Quate, Ch. Gerber. *Phys. Rev. Lett.*, **56**, 930, (1986).
143. L.T. Williams. *Science.*, 243, 1568 (1989).
144. Y. Martin, C.C. Williams, H.K. Wickramasinghe. *J. Appl. Phys.*, **61**, 4723,
(1987).
145. Digital Instruments trade brochure.
146. D.M Price, M. Reading, A. Caswell, A. Hammiche, H.M. Pollock.
Microscopy & Analysis, **65**, (5), 17, (1998).
147. M.Y. Tsai, J. Morton, R.B. Krieger, D.W. Oplinger. *J. Adv. Mats.* 28-35,
April 1996.
148. D. K. Hall, Ph.D. Thesis, Loughborough University, 1994.
149. U. Jacobson. *British Plastics*, pge. 152-156, April 1959.

150. D.A. Hemsley, R.P. Higgs, A. Miadonye. *Polym. Comm.* **24**, (4), 103-106, (1983).
151. I. Mathieson. Ph.D. Thesis, Loughborough University, 1995.
152. R.A. Dickie, J.S. Hammond, J.E. deVries, J.W. Holubka. *Anal. Chem.*, **54**, 2045-2049, (1982).
153. M. Celina, D.K. Ottensen, K.T. Gillen, R.L. Clough. *Poly. Degra. & Stab.*, **58**, 15-31, (1997).
154. M. Beltran, A. Marcilla. *Eur. Polym. J.*, **33**, (7), 1135-1142, (1997).
155. G. Kämpf. *Characterisation of Plastics by Physical Methods; Experimental Techniques and Practical Application*. Hanser, Munich, (1986).

APPENDICES**Appendix 1 Detailed Interlayer Compositions****1.1 Copolymers**

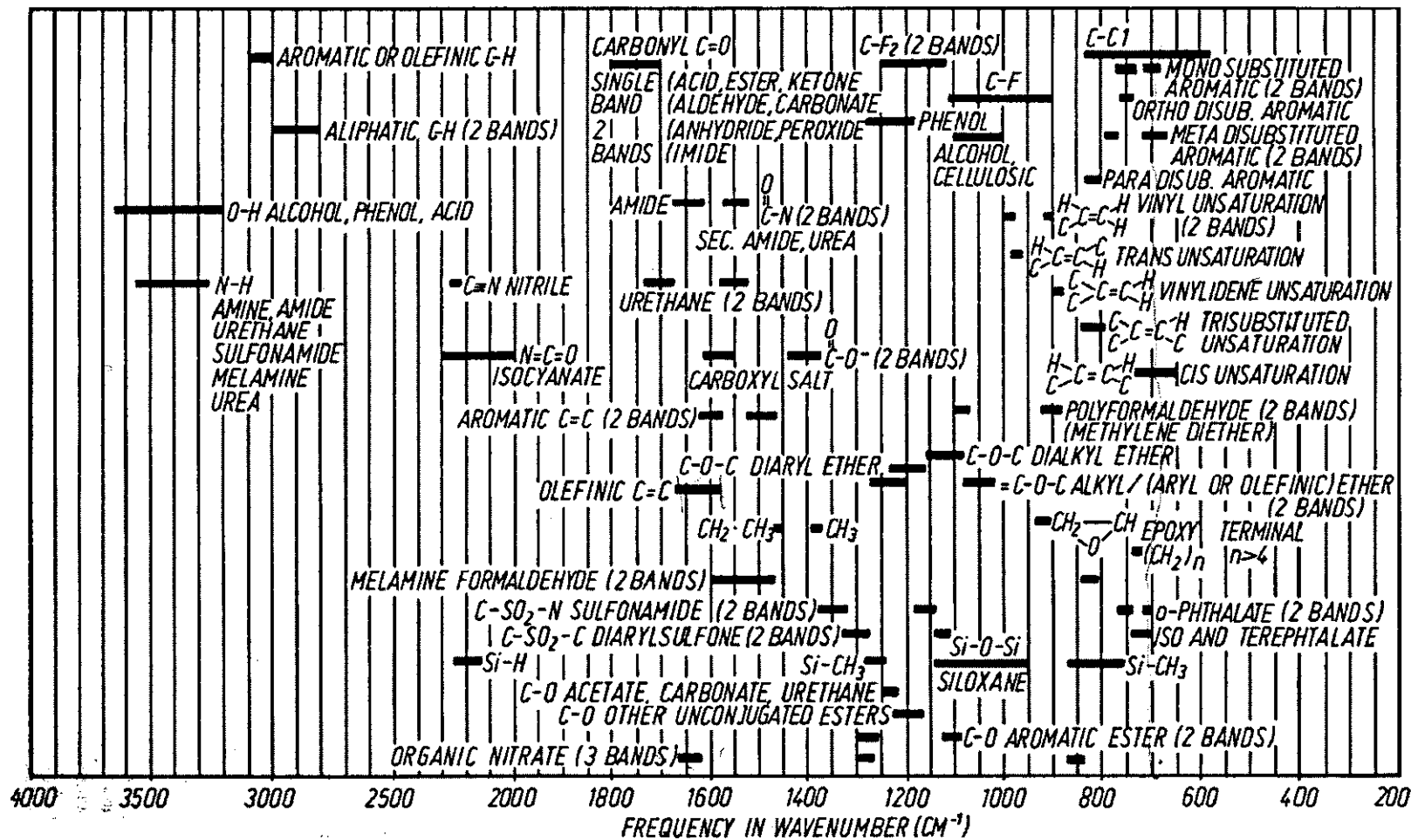
Interlayer	Resin		Plasticiser	
	Type	Amount (g)	Type	Amount (ml)
6/0A	GA 6015	25	None	0
6/20A	GA 6015	20	Admex 523	5
6/40A	GA 6015	15	Admex 523	10
6/60/A	GA 6015	10	Admex 523	15
7/0/A	GA 7701H	25	None	0
7/20A	GA 7701H	20	Admex 523	5
7/40A	GA 7701H	15	Admex 523	10
7/60A	GA 7701H	10	Admex 523	15
9/0A	GA 9028	25	None	0
9/20A	GA 9028	20	Admex 523	5
9/40A	GA 9028	15	Admex 523	10
9/60A	GA 9028	10	Admex 523	15
6/0B	GA 6015	25	None	0
6/20B	GA 6015	20	Benzoflex 2088	5
6/40B	GA 6015	15	Benzoflex 2088	10
6/60B	GA 6015	10	Benzoflex 2088	15
7/0/B	GA 7701H	25	None	0
7/20B	GA 7701H	20	Benzoflex 2088	5
7/40B	GA 7701H	15	Benzoflex 2088	10
7/60B	GA 7701H	10	Benzoflex 2088	15
9/0B	GA 9028	25	None	0
9/20B	GA 9028	20	Benzoflex 2088	5
9/40B	GA 9028	15	Benzoflex 2088	10
9/60B	GA 9028	10	Benzoflex 2088	15
6/0D	GA 6015	25	None	0
6/20D	GA 6015	20	D-2(ethyl hexyl) phthalate	5
6/40D	GA 6015	15	D-2(ethyl hexyl) phthalate	10
6/60D	GA 6015	10	D-2(ethyl hexyl) phthalate	15
7/0D	GA 7701H	25	None	0
7/20D	GA 7701H	20	D-2(ethyl hexyl) phthalate	5
7/40D	GA 7701H	15	D-2(ethyl hexyl) phthalate	10
7/60D	GA 7701H	10	D-2(ethyl hexyl) phthalate	15
9/0D	GA 9028	25	None	0
9/20D	GA 9028	20	D-2(ethyl hexyl) phthalate	5
9/40D	GA 9028	15	D-2(ethyl hexyl) phthalate	10
9/60D	GA 9028	10	D-2(ethyl hexyl) phthalate	15

Stabiliser was added at 0.4 pph.

1.2 Homopolymers

Interlayer	Resin		Plasticiser	
	Type	Amount (g)	Type	Amount (ml)
57/0B	K57	25	Benzoflex 2088	0
57/20B	K57	20	Benzoflex 2088	5
57/40B	K57	15	Benzoflex 2088	10
57/60B	K57	10	Benzoflex 2088	15
60/0B	K60	25	Benzoflex 2088	0
60/20B	K60	20	Benzoflex 2088	5
60/40B	K60	15	Benzoflex 2088	10
60/60B	K60	10	Benzoflex 2088	15
74/0B	K74	25	Benzoflex 2088	0
74/20B	K74	20	Benzoflex 2088	5
74/40B	K74	15	Benzoflex 2088	10
74/60B	K74	10	Benzoflex 2088	15
80/0B	K80	25	Benzoflex 2088	0
80/20B	K80	20	Benzoflex 2088	5
80/40B	K80	15	Benzoflex 2088	10
80/60B	K80	10	Benzoflex 2088	15

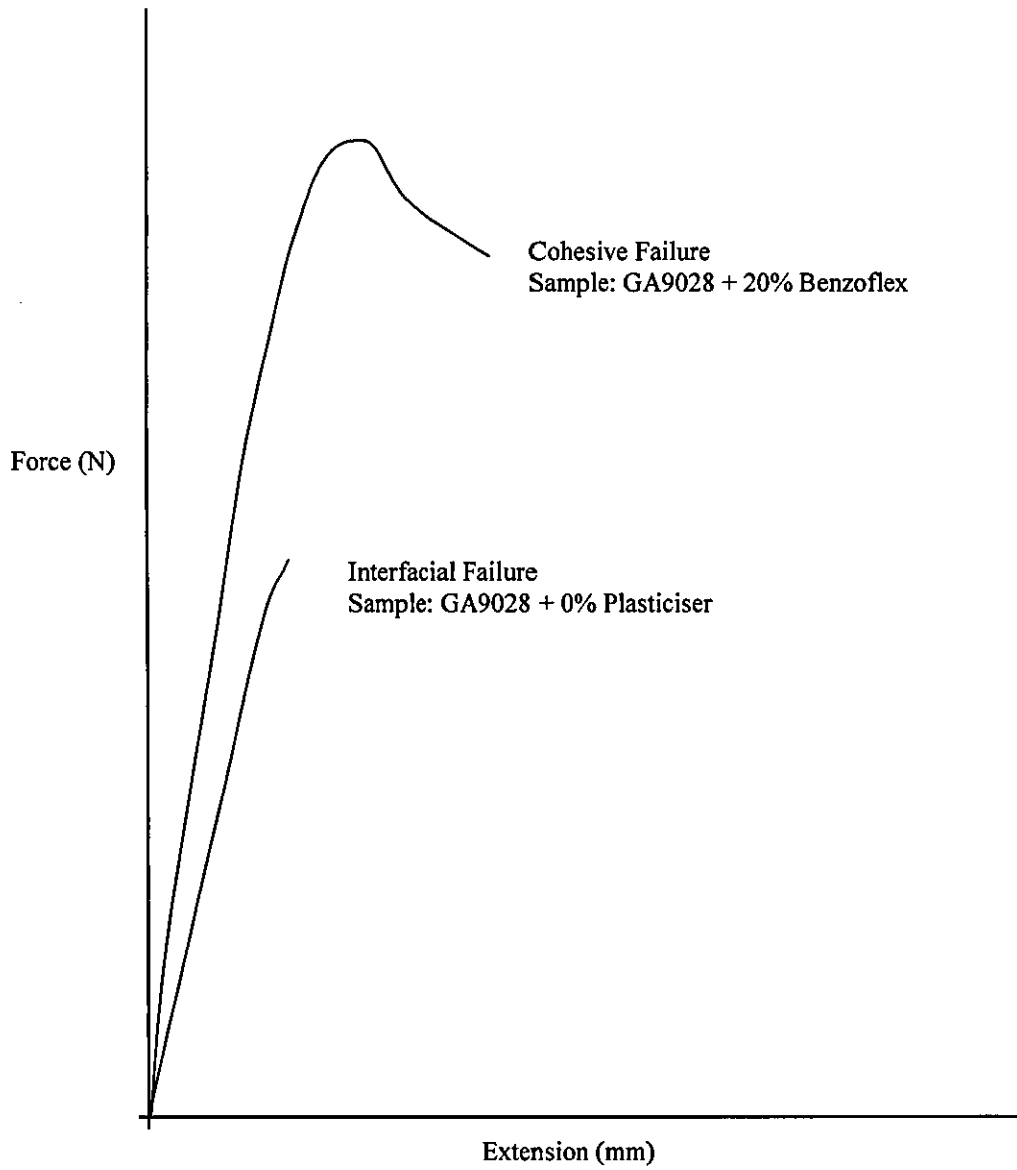
Stabiliser was added at 0.4 pph.



Appendix 2 Infra-red Spectra Frequency-Structure Correlation Chart (after¹⁵⁵)

Appendix 3 Selected Lap Shear Data and Treatment of Results

3.1 Typical Force-Extension Plots



3.2 Lap Shear Data

GA 6015 with Benzoflex 2088

Sample	Wt.% Benzoflex	Force (N)	S.A. (mm ²)	Stress (MPa)	Average
6015 + 0%	0	1227	1075	1.14	
	0	1700	1175	1.45	
	0	1299	1075	1.21	
	0	1451	1075	1.35	
	0	1527	1075	1.42	
	0	1236	1075	1.15	
	0	1279	1075	1.19	
	0	1494	1075	1.39	
	0	1387	1075	1.29	1.29
6015 + 20%	20	3635	888	4.09	
	20	3952	888	4.45	
	20	4165	888	4.69	
	20	3765	888	4.24	
	20	4058	888	4.57	
	20	4094	888	4.61	
	20	4120	888	4.64	
	20	3765	888	4.24	
	20	3952	888	4.45	4.44
6015 + 40%	40	2876	765	3.76	
	40	3215	888	3.62	
	40	2798	698	4.01	
	40	2975	888	3.35	
	40	3765	888	4.24	
	40	3152	888	3.55	
	40	3516	888	3.96	
	40	3161	888	3.56	
	40	3330	888	3.75	3.76
6015 + 60%	60	1847	1075	2.81	
	60	2357	1075	3.18	
	60	2457	1075	3.44	
	60	1936	1075	2.79	
	60	2059	1075	2.98	
	60	2415	1075	3.29	
	60	3419	1075	3.18	
	60	3204	1075	2.98	
	60	3300	1075	3.07	3.08

GA 6015 with DOP

Sample	Wt.% DOP	Force (N)	S.A. (mm ²)	Stress (MPa)	Average
6015 + 0%	0	1227	1075	1.14	
	0	1700	1175	1.45	
	0	1299	1075	1.21	
	0	1451	1075	1.35	
	0	1527	1075	1.42	
	0	1236	1075	1.15	
	0	1279	1075	1.19	
	0	1494	1075	1.39	
	0	1387	1075	1.29	1.29
6015 + 20%	20	2213	936	2.36	
	20	2581	936	2.76	
	20	2370	960	2.47	
	20	2415	936	2.58	
	20	2480	936	2.65	
	20	2546	936	2.72	
	20	2518	936	2.69	
	20	2331	936	2.49	
	20	2415	936	2.58	2.59
6015 + 40%	40	2311	1008	2.29	
	40	2386	888	2.69	
	40	2798	975	2.87	
	40	2105	888	2.37	
	40	2149	888	2.42	
	40	2256	888	2.54	
	40	2158	888	2.43	
	40	2335	888	2.63	
	40	2264	888	2.55	2.53
6015 + 60%	60	2064	1025	2.01	
	60	2282	1008	2.26	
	60	2625	1008	2.60	
	60	2197	1008	2.18	
	60	2510	1008	2.49	
	60	2661	1008	2.64	
	60	2591	1008	2.57	
	60	2197	1008	2.18	
	60	2389	1008	2.37	2.37

GA 6015 with Admex 523

Sample	Wt.% Admex	Force (N)	S.A. (mm ²)	Stress (MPa)	Average
6015 + 0%	0	1227	1075	1.14	
	0	1700	1175	1.45	
	0	1299	1075	1.21	
	0	1451	1075	1.35	
	0	1527	1075	1.42	
	0	1236	1075	1.15	
	0	1279	1075	1.19	
	0	1494	1075	1.39	
	0	1387	1075	1.29	1.29
6015 + 20%	20	798	848	1.80	
	20	777	1248	1.61	
	20	798	1000	2.00	
	20	945	1075	1.80	
	20	735	1115	2.00	
	20	735	1225	1.90	
	20	2021	1225	1.65	
	20	2511	1225	2.05	
	20	2266	1225	1.85	1.85
6015 + 40%	40	945	2500	2.46	
	40	903	978	2.44	
	40	924	214	1.90	
	40	770	1297	2.10	
	40	858	1916	2.13	
	40	770	1922	2.30	
	40	4651	1922	2.42	
	40	3882	1922	2.02	
	40	4267	1922	2.22	2.22
6015 + 60%	60	726	1567	2.16	
	60	770	1319	1.71	
	60	726	1321	1.82	
	60	836	2090	2.20	
	60	836	686	1.89	
	60	814	2151	2.38	
	60	4582	2151	2.13	
	60	4151	2151	1.93	
	60	4410	2151	2.05	2.03

GA7701H with Benzoflex 2088

Sample	Wt.% Benzoflex	Force (N)	S.A. (mm ²)	Stress (MPa)	Average
7701 + 0 %	0	1521	1050	1.45	
	0	674	1175	0.57	
	0	1267	1175	1.08	
	0	1116	1175	0.95	
	0	1563	1175	1.33	
	0	1410	1175	1.20	
	0	799	1175	0.68	
	0	1504	1175	1.28	
	0	764	1175	0.65	1.10
7701 + 20%	20	3371	690	4.72	
	20	2811	828	4.09	
	20	3500	966	4.35	
	20	1463	920	3.93	
	20	1131	748	3.20	
	20	3275	920	3.56	
	20	3864	920	4.20	
	20	3790	920	4.12	
	20	3772	920	4.10	4.03
7701 + 40 %	40	3677	924	3.98	
	40	4130	902	4.58	
	40	3538	924	3.83	
	40	2618	924	3.32	
	40	3625	924	3.92	
	40	3283	924	3.55	
	40	3382	924	3.66	
	40	3751	924	4.06	
	40	3557	924	3.85	3.86
7701 + 60%	60	2883	902	3.20	
	60	3188	880	3.62	
	60	1688	924	2.18	
	60	1588	858	2.38	
	60	2764	924	2.99	
	60	2584	924	2.80	
	60	2458	924	2.66	
	60	2827	924	3.06	
	60	2652	924	2.87	2.86

GA7701H with DOP

Sample	Wt.% DOP	Force (N)	S.A. (mm ²)	Stress (MPa)	Average
7701+0%	0	1521	1050	1.45	
	0	674	1175	0.57	
	0	1267	1175	1.08	
	0	1116	1175	0.95	
	0	1563	1175	1.33	
	0	1410	1175	1.20	
	0	799	1175	0.68	
	0	1504	1175	1.28	
	0	764	1175	0.65	1.02
7701+20%	20	2456	1175	2.09	
	20	2512	1150	2.18	
	20	3726	1150	3.24	
	20	2829	1150	2.46	
	20	2990	1150	2.60	
	20	2990	1150	2.60	
	20	2346	1150	2.04	
	20	3220	1150	2.80	
	20	3335	1150	2.90	2.55
7701+40%	40	3313	925	3.58	
	40	2542	850	2.99	
	40	1670	825	2.65	
	40	1947	825	2.36	
	40	2822	825	3.42	
	40	2813	825	3.41	
	40	2516	825	3.05	
	40	2549	825	3.09	
	40	2516	825	3.05	3.07
7701+60%	60	1298	975	1.33	
	60	200	1025	0.20	
	60	637	825	0.77	
	60	536	975	0.55	
	60	1209	975	1.24	
	60	956	975	0.98	
	60	624	975	0.64	
	60	1014	975	1.04	
	60	829	975	0.85	0.84

GA7701H with Admex 523

Sample	Wt.% Admex	Force (N)	S.A. (mm ²)	Stress (MPa)	Average
7701 + 0 %	0	1521	1050	1.45	
	0	674	1175	0.57	
	0	1267	1175	1.08	
	0	1116	1175	0.95	
	0	1563	1175	1.33	
	0	1293	1175	1.20	
	0	799	1175	0.68	
	0	1504	1175	1.28	
	0	764	1175	0.65	1.10
	7701 + 20%	20	698	1366	2.96
20		720	1030	1.96	
20		788	1251	2.28	
20		743	1289	2.49	
20		765	1156	2.12	
20		720	1350	2.67	
20		3524	1350	2.61	
20		2984	1350	2.21	
20		3240	1350	2.40	2.41
7701 + 40 %		40	788	3151	4.00
	40	698	2338	3.35	
	40	698	2758	3.95	
	40	743	2548	3.43	
	40	720	2984	4.14	
	40	765	3005	3.93	
	40	10818	3005	3.60	
	40	12050	3005	4.01	
	40	11419	3005	3.80	3.80
	7701 + 60%	60	832.5	877	2.67
60		832.5	1060	3.02	
60		877.5	359	2.51	
60		922.5	412	1.97	
60		900	912	2.14	
60		945	942	2.40	
60		2025	942	2.15	
60		2496	942	2.65	
60		2402	942	2.55	2.45

GA9028 with Benzoflex 2088

Sample	Wt.% Benzoflex	Force (N)	S.A. (mm ²)	Stress (MPa)	Average
9028 + 0%	0	486	1175	0.42	
	0	1074	1175	0.91	
	0	600	675	0.89	
	0	646	1175	0.55	
	0	799	1175	0.68	
	0	846	1175	0.72	
	0	658	1175	0.56	
	0	870	1175	0.74	
	0	752	1175	0.64	0.68
9028 + 20%	20	4262	897	5.31	
	20	5138	851	6.04	
	20	5000	851	5.88	
	20	5472	874	6.26	
	20	4852	851	5.70	
	20	5218	851	6.13	
	20	5183	851	6.09	
	20	4842	851	5.69	
	20	5012	851	5.89	5.89
9028 + 40%	40	3168	770	4.34	
	40	1917	836	4.84	
	40	2114	880	3.75	
	40	2030	946	3.56	
	40	1567	924	4.20	
	40	1868	748	4.01	
	40	2932	748	3.92	
	40	3231	748	4.32	
	40	3082	748	4.12	4.12
9028 + 60%	60	2428	836	2.90	
	60	1703	858	1.98	
	60	2802	924	3.03	
	60	2355	836	2.82	
	60	2457	880	2.79	
	60	2125	880	2.41	
	60	2235	880	2.54	
	60	2297	880	2.61	
	60	2517	880	2.86	2.66

GA9028 with DOP

Sample	Wt.% DOP	Force (N)	S.A. (mm ²)	Stress (MPa)	Average
9028 + 0%	0	486	1175	0.42	
	0	1074	1175	0.91	
	0	600	675	0.89	
	0	646	1175	0.55	
	0	799	1175	0.68	
	0	846	1175	0.72	
	0	658	1175	0.56	
	0	870	1175	0.74	
	0	752	1175	0.64	0.68
9028 + 20%	20	1479	800	1.85	
	20	1088	675	1.61	
	20	721	675	1.47	
	20	851	675	1.26	
	20	1067	675	1.58	
	20	965	675	1.43	
	20	1100	675	1.63	
	20	965	675	1.43	
	20	1033	675	1.53	1.53
9028 + 40%	40	1327	900	1.47	
	40	1480	1000	1.48	
	40	698	800	1.69	
	40	1476	900	1.64	
	40	1395	900	1.55	
	40	1080	900	1.20	
	40	1485	900	1.65	
	40	1530	900	1.70	
	40	1449	900	1.61	1.55
9028 + 60%	60	1152	1050	1.10	
	60	2029	1100	1.64	
	60	1131	1025	1.10	
	60	1639	1100	1.49	
	60	1562	1100	1.42	
	60	1320	1100	1.20	
	60	1573	1100	1.43	
	60	1353	1100	1.23	
	60	1463	1100	1.33	1.33

GA9028 with Admex 523

Sample	Wt.% Admex	Force (N)	S.A. (mm ²)	Stress (MPa)	Average
9028 + 0%	0	486	1175	0.42	
	0	1074	1175	0.91	
	0	600	675	0.89	
	0	646	1175	0.55	
	0	799	1175	0.68	
	0	846	1175	0.72	
	0	658	1175	0.56	
	0	870	1175	0.74	
	0	752	1175	0.64	0.68
9028 + 20%	20	855	713	0.83	
	20	900	638	1.22	
	20	878	473	1.11	
	20	968	2102	1.30	
	20	1058	1930	1.38	
	20	1058	1846	1.29	
	20	2104	1846	1.14	
	20	2289	1846	1.24	
	20	2197	1846	1.19	1.19
9028 + 40%	40	945	450	1.60	
	40	945	351	1.90	
	40	945	404	1.50	
	40	833	1334	1.60	
	40	698	1506	1.77	
	40	788	1189	1.90	
	40	1795	1189	1.51	
	40	2271	1189	1.91	
	40	2033	1189	1.71	1.71
9028 + 60%	60	832.5	864	1.04	
	60	855	762	0.89	
	60	855	679	0.79	
	60	832	905	1.09	
	60	832	435	0.52	
	60	855	835	0.98	
	60	911	835	1.09	
	60	576	835	0.69	
	60	744	835	0.89	0.89

According to ASTM D 3163 - 96, the lap shears strength is "failing stress as pounds-force per square inch of shear area (or megapascals)."

The lap shear strength is therefore :

$$\sigma_{lapshear} (MPa) = \frac{force(N)}{SA(mm^2)}$$

Appendix 4

Research Papers Resulting from this Work

1. Micro-thermal Analysis: A New Form of Analytical Microscopy. *Microscopy & Analysis*, May 1998.

MICRO-THERMAL ANALYSIS: A NEW FORM OF ANALYTICAL MICROSCOPY

D M Price¹, M Reading¹, A Caswell¹, A Hammiche² and H M Pollock². ¹ IPTME, Loughborough University, Loughborough, UK ² School of Physics & Chemistry, Lancaster University, Lancaster, UK

Keywords: Scanning probe microscopy, thermal analysis, packaging materials, polymer welding.

Introduction

Thermal methods have been for many years amongst the most widely used techniques for characterising morphology of, in particular, complex polymeric systems. The recent introduction of modulated temperature differential scanning calorimetry (MTDSC) [1-4] has considerably increased the ability of DSC to identify and quantify polymer phases and interphases making it, perhaps, the most powerful general method for these tasks. However, conventional thermal methods give no information about how these phases are distributed in space. For this microscopy must be used. Electron & optical microscopy - and also existing forms of analytical microscopy (IR, Raman, SIMS *etc.*) - can be successful in mapping the spatial distribution of phases. However, none of these techniques has achieved the status of a reliable, general, and simple-to-use tool for this application due to a variety of factors including resolution, specificity, difficulties in sample preparation and the amount of time required to acquire high resolution images. We are developing a novel form of analytical thermal microscopy, as an additional complementary method to these existing microscopies, with potential advantages for characterising the morphology of polymer composites and blends. Furthermore, a variety of other materials including pharmaceuticals, foods and even biological specimens could be analysed using this new technique.

Background

The most popular thermal method is differential scanning calorimetry (DSC) which measures the heat flow into or out of a sample subjected to a temperature ramp. In this way transition temperatures can be found and the enthalpies and heat capacity changes associated with them can be measured. Reading and co-workers introduced a few years ago a temperature modulation combined with a Fourier analysis of the resulting data [1-4]. This new technique is called modu-

Duncan Price & Mike Reading are members of the Advanced Thermal Methods Group, IPTME, Loughborough University. They have an interest in the development of new thermal analysis techniques, in particular: modulated temperature and controlled rate thermal analysis. Andrew Caswell is a postgraduate student in the same department. Azzedine Hammiche and Hubert Pollock are based at the School of Physics & Chemistry, Lancaster University where they are active in the development of scanning probe microscopy.

lated temperature DSC or MTDSC. This has the effect of significantly improving sensitivity and resolution for some transitions while also enabling their "reversing" or "non-reversing" character to be probed. Stated simply, multi-component polymer systems will exhibit the corresponding number of glass transitions, while crystalline systems will give melting endotherms. Observing and quantifying these transitions enables the sample's morphology to be characterised.

Another popular thermal method is thermo-mechanical analysis (TMA) where a probe is placed on a sample with a given force then, as the temperature is ramped, changes in dimension (such as accompany softening during melting) can be detected. In this way, thermal expansion coefficients and transition temperatures can be determined. For both of these techniques the sample is typically tens of milligrams or even, in the case of TMA, larger.

The starting point for Micro-Thermal Analysis (Micro-TA) is an atomic force microscope where the probe tip has been replaced with an ultra miniature resistive heater that also serves as a temperature sensor. This type of probe was first described by Dinwiddie *et al.* who used it purely in an isothermal mode to simultaneously map topography and thermal conductivity [5]. We, in parallel with others [6,7] added a temperature modulation to improve the ability of sub-surface

Scanning Thermal Microscopy (SThM) to discriminate between detail seen at different depths. We then introduced the facility to position the tip on any feature in an image and then scan temperature - thus making possible, for the first time, localised thermal measurements - transforming thermal microscopy into a form of analytical microscopy [8].

In the SThM mode, three images are produced simultaneously as illustrated in figure 1. This shows a metal wire embedded in a polymer - although there is some topographic contrast at the interface between the wire and the substrate, the contrast is markedly different on the DC and AC thermal images. The DC image represents a convolution of the sample's thermal conductivity with its topography. Previously we have referred to the AC image as the "thermal diffusivity" image. However recent modelling studies have suggested that the contrast mechanism is more dependant on other factors so it is more correct to refer to it simply as the "AC thermal image". We will be publishing more on our theoretical work in the future.

Figure 2 shows typical results for a melting transition: the signals measured are deflection of the cantilever carrying the heated probe (equivalent to Micro-TMA [9]) and the DC power, AC amplitude and AC phase for the calorimetric measurement, called micro-Modulated Temperature Differential Thermal Analysis (micro-MTDTA) signals. We use the term "micro-MTDTA" rather than "micro-MTDSC" to indicate we are not yet claiming quantitative calorimetric measurements. Consequently, we do not relate the strengths of the signals directly to enthalpies for transitions (the capability to do this is the subject of ongoing work). However, often simply measuring the temperature of a transition is sufficient to identify a component and, in this case, all three signals clearly show the melting transition. We have also used a force modulation to provide two additional signals, the AC amplitude and phase for the position sensor (this is a micro-

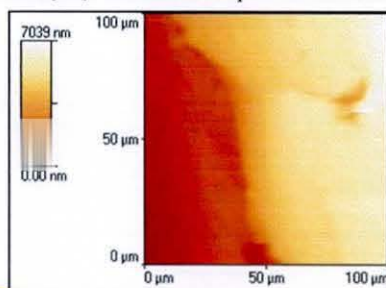


Fig 1a

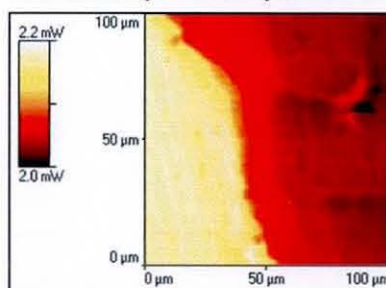


Fig 1b

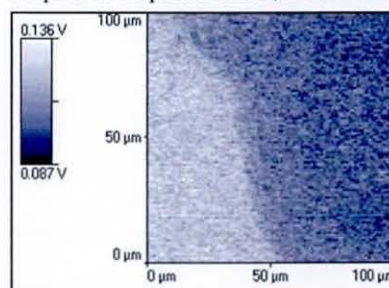


Fig 1c

Figure 1. (a) topographic, (b) DC thermal and (c) AC thermal (2 kHz) images of a wire embedded in a polymer substrate.

equivalent to dynamic mechanical analysis), but this is not currently routinely available [10].

Micro-TA has been used in a preliminary study of phase separation of polymer blends and of crystallinity variations of different branched polyethylenes [11]. To further illustrate the use of this approach we shall use two examples: the first is a packaging film of the type used to make toothpaste tubes. This is made up of several layers of polyethylene. A thin layer of poly(ethylene-vinyl alcohol) copolymer (EVOH) is incorporated in order to provide adequate gas and flavour barrier performance. Different grades of polyethylene (PE) such as low density polyethylene (LDPE), medium density polyethylene (MDPE) & high density polyethylene (HDPE) are also used in the final construction. The type of polyethylene used in films is well known to affect their properties, however identification of the grade of polymer, particularly for commercial films, remains difficult. Bulk analytical techniques such as nuclear magnetic resonance spectroscopy (NMR), and differential scanning calorimetry (DSC) - whilst very sensitive to structure - are only able to give a specimen-averaged picture of the properties of the sample. More elaborate chromatographic techniques such as temperature rising elution fractionation (TREF) can, in favourable cases, separate the constituents of a multi-component film but afford no information regarding the original location of each fraction [12]. Infra-red microscopy is able to give more localised information of spectral properties, but (in this instance) it is not easy to distinguish between different grades of polyethylene.

The second example is a welded-joint produced by heating a wire embedded in the polymer just below the surface of one side of the joint. The temperature rise at the interface is sufficient to soften and fuse the two surfaces together. However, too much heat can cause cross-linking and thermal degradation of the polymer. In this case, we would like to study the morphology of the sample across the weld region - an application ideally suited to thermal measurements on this scale.

Experimental

The instrument used for this work was a TA Instruments μ TA 2990 Micro-Thermal Analyser based on the TopoMetrix Explorer TMX2100 scanning probe microscope. In this work, we will concentrate on Micro-Thermomechanical measurements (Micro-TMA, see above); in this mode, the displacement of the tip is measured as it is heated in contact with the sample - as the temperature is raised a point is reached where the sample softens under the applied load causing a downwards deflection of the cantilever. At the end of the experiment, the probe is heated to the maximum scanned temperature and raised clear of the surface. Imaging of the sample after micro-TA shows cratered areas where the tests were carried out. Because of small thermal mass of the probe, high heating rates (typically 10°C/s or more) can be used. The low thermal conductivity of polymer samples means that only a small region ($10\ \mu\text{m}^3$) is examined.

The packaging film was prepared cutting $20\ \mu\text{m}$ thick slivers of material using a microtome which were then mounted on a metal stub so that

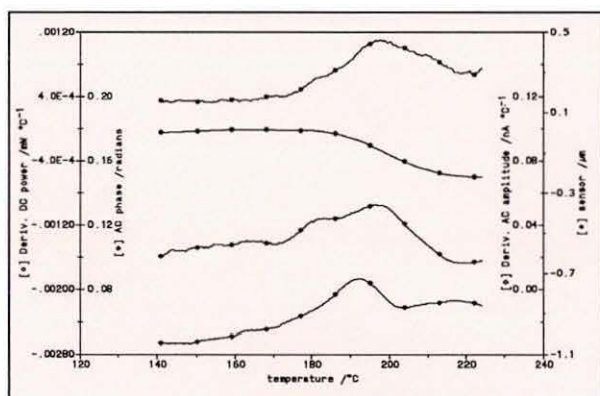


Fig 2

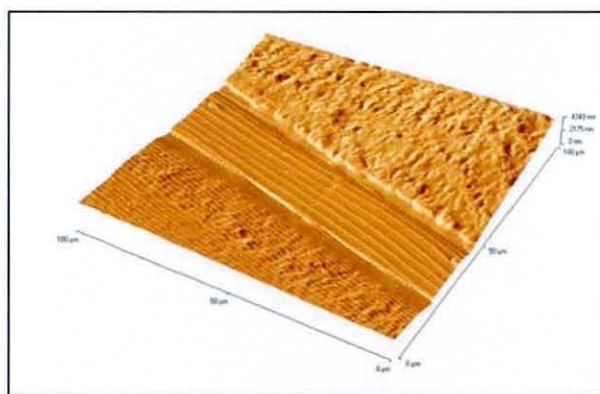


Fig 3

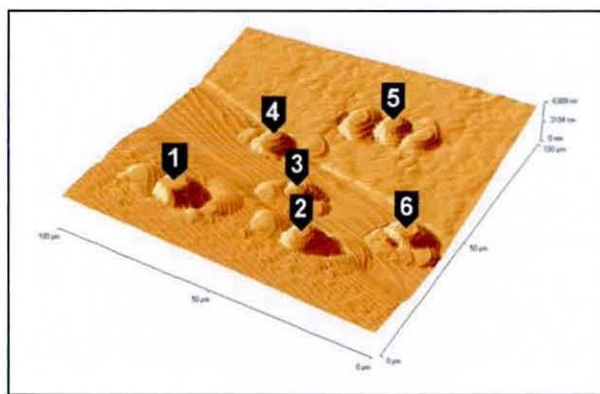


Fig 4

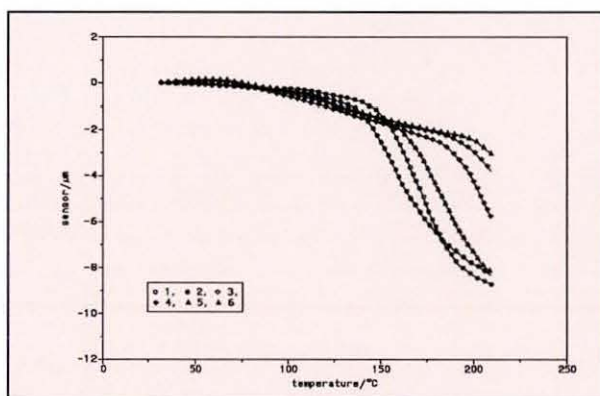


Fig 5

Figure 2. Typical Micro-Thermal Analysis results for the melting of a polymer.

Figure 3. Three-dimensional image of barrier layer region of film before Micro-Thermal Analysis.

Figure 4. Three-dimensional image of barrier layer region of film after Micro-Thermal Analysis - labels refer to sequence of scans.

Figure 5. Micro-TMA plots for the scan locations shown in figure 4.

a cross-section could be presented to the microscope for imaging and subsequent thermal analysis. The welded joint was simply cut open using a saw and carefully polished to the required smoothness.

Results & Discussion

Packaging Film

Figure 3 shows a three dimensional representation of the gas barrier layer in the packaging film - it is clear from the topography that there is a central layer of polymer flanked by two outer layers with possibly an intermediate tie layer. Micro-TMA was carried out at six selected positions across the sample. The effect of tests are clearly seen in figure 4 which illustrates the damage craters (approximately 20 μm by 10 μm) caused by the test. The regions affected by the measurements appear large because the molten polymer flows away from the probe to cover the adjacent area. We estimate that the area characterised by the onset of probe penetration to be of the order of a few square microns. Plots of sensor response (obtained from the photodetector feedback circuit in the microscope head) versus temperature are shown in figure 5, these correspond to the locations indicated in the earlier figure. The softening temperatures are indicative of the polymer present in the film: curves 1 & 5 are typical of HDPE, curves 3 & 6 correspond to the EVOH layer, curve 2 (the tie layer) has a lower softening point than HDPE and is probably MDPE, curve 4 is located on the EVOH/tie layer interface and the thermal response is a combination of both. The entire sequence of tests took less than four minutes. This example shows that it is quite possible to quickly correlate the composition of a complex structure with its thermal behaviour.

Weld joint

The topography, thermal conductivity and modulated temperature images of the region around the heater wire were shown in figure 1. In order to examine a wider area using the microscope, the sample was moved under the head after each set of images (before and after Micro-TMA) and thermal scans had been collected. The resulting images were then overlaid to produce the composite map shown in figure 6. The heater wire can be clearly seen on the left of the image and the weld line runs vertically down the right of the image. As in the previous example, Micro-TMA was carried out in order to measure the softening temperature of the polymer (figure 7). As expected, the curves corresponding to positions closest to the source of heat show that the polymer had been cross-linked to such an extent that its softening point is above 400°C. As one moves further away from the heater, the softening temperature drops (curve 3) then rises again. Polymer lying on the weld line has a softening temperature above 400°C. Why this should occur is not clear - we speculate that mechanical vibration brought about by AC heating of the wire may provide a localised source of heat along the weld line itself. Further work is required to measure the softening temperatures of polymer with known thermal history so that we can determine the actual processing conditions seen by the sample.

Conclusions

The above examples illustrate some of the practical potential of the technique - we have concen-

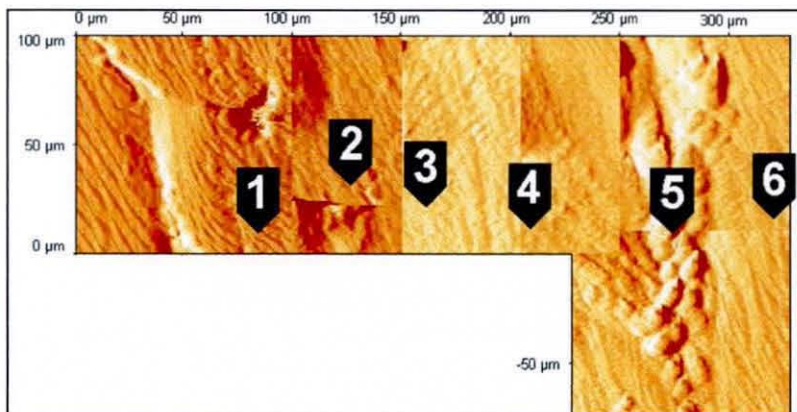


Figure 6. Composite shaded topographic image of weld joint - Micro-TMA scan positions shown.

trated here on the examination of articles in cross-section using Micro-TMA: other applications include the characterisation of polymer surfaces such as coatings and printed material. Future developments will include the exploitation of the frequency dependence of the AC thermal imaging technique to derive depth specific information about the sample. It is possible to use the thermal probe as a very sensitive infrared detector so as to achieve IR microscopy at very high resolution \bar{n} well below the diffraction limit of conventional IR microscopes [13]. There is also the potential to perform localised pyrolysis-mass spectrometry using the probe to volatilise specified areas of the sample. High-resolution thermal probes are currently under development in order to enhance the spatial resolution of the technique. By combining scanning probe microscopy with thermal methods it is now possible to visualise and characterise a material, in the future it will be possible to analyse it too.

References

1. Reading, M. Modulated differential scanning calorimetry - a new way forward in materials characterisation. *Trends Poly. Sci.*, 1, 248-253, 1993
2. Song, M. *et al.* Modulated differential scanning calorimetry: IV. Miscibility and glass transition behaviour in poly(methyl methacrylate) and poly epichlorohydrin blends. *Polymer* 37, 5661-5665, 1996
3. Hourston, D. J. *et al.* Modulated differential scanning calorimetry: VI. Thermal characterisation of multi-component polymers and interfaces. *Polymer*, 38, 1-7, 1997
4. Song, M. *et al.* Modulated differential scanning calorimetry: VIII. Interface development between films

of poly(epichlorohydrin) and poly(vinyl acetate), *Polymer* 38, 503-7, 1997

5. Dinwiddie, R. B. *et al.* Thermal conductivity contrast imaging with a scanning thermal microscope. Tong, T. W. (editor), *Thermal Conductivity 22*, Technomics, Lancaster PA, p. 668-677, 1994

6. Hammiche, A. *et al.* Scanning thermal microscopy: sub-surface imaging, thermal mapping of polymer blends, localised calorimetry', *J. Vac. Sci. Technol. B: Microelectronics and Nanostructures*, 14, 1486-1491, 1996

7. Balk, L. J., *et al.* Nanoscopic detection of the thermal conductivity of compound semiconductor materials by enhanced scanning thermal microscopy, 9th Conf. on Microscopy of Semiconducting Materials, Oxford 1995

8. Hammiche, A. *et al.* Localised thermal analysis using a miniaturised resistive probe. *Rev. Sci. Instr.*, 67, 4268-4274, 1996

9. Oulevey, F. *et al.* Phase transitions in polymers: towards dynamic mechanical analysis with submicron spatial resolution. In: *Surfaces and interfaces of polymers and composites* (European Conference on Macromolecular Physics vol. 21B, Lausanne, 1-6 June 1997), Pick, R. & Thomas, G., eds., European Physical Society 1997, pp. 155-156

10. Reading, M. *et al.* Thermal analysis for the 21st century. *American Laboratory*, 30(1), 13-17, 1998

11. Pollock, H. M. *et al.* Interfaces in polymeric systems as studied by C.A.S.M. - a new combination of Calorimetric Analysis with Scanning Microscopy, *J. Adhesion*, 67, 193-205, 1998

12. Keeting, M. *et al.* Thermal fractionation of ethylene polymers in packaging applications. *Thermochim. Acta*, 284, 47-56, 1996

13. Hammiche, A. *et al.* submitted to *Applied Spectroscopy*, 1998

Author's details (correspondence): Duncan Price, IPTME, Loughborough University, Loughborough, Leics. LE11 3TU UK. Tel: +44 (0)1509 223332. email: d.m.price@lboro.ac.uk

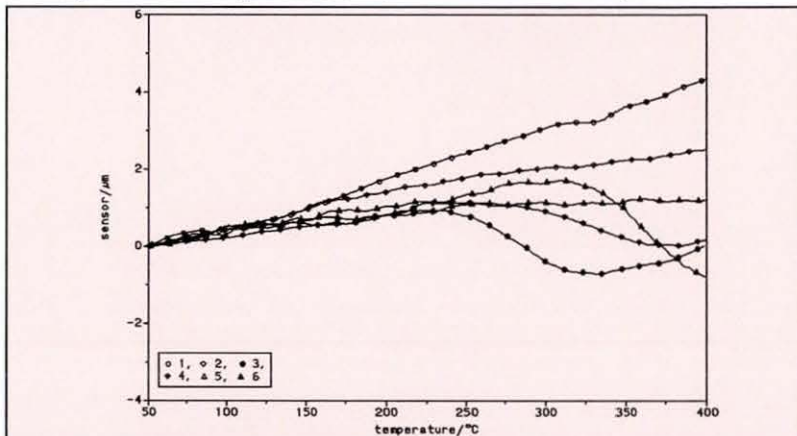


Figure 7. Micro-TMA plots for the scan locations shown in figure 6.

tr Spine

